



Cyprus
University of
Technology

Faculty of
Engineering
and Technology

Doctoral Dissertation

**NUMERICAL MARINE DYNAMICS MODELING OF
THE LEVANTINE AND CYPRUS SEA**

Andreas Nikolaidis

Limassol, December 2019

CYPRUS UNIVERSITY OF TECHNOLOGY
FACULTY OF ENGINEERING AND TECHNOLOGY
DEPARTMENT OF CIVIL ENGINEERING AND GEOMATICS

Doctoral Dissertation

NUMERICAL MARINE DYNAMICS MODELING OF THE LEVANTINE AND
CYPRUS SEA

Andreas Nikolaidis

Limassol, December 2019

Approval Form

Doctoral Dissertation

NUMERICAL MARINE DYNAMICS MODELING OF THE LEVANTINE AND CYPRUS SEA

Andreas Nikolaidis

Supervisor: Faculty of Engineering and Technology, Dr. Evangelos Akylas Department
of Civil Engineering & Geomatics, *Cyprus University of Technology*

Signature:

Member of the committee: Dr. Phaedon Kyriakidis, Department of Civil Engi-
neering & Geomatics, *Cyprus University of Technology*

Signature:

Member of the committee: Dr. Dimitra Kitsiou, Department of Marine Sciences,
University of the Aegean

Signature:

Cyprus University of Technology

Limassol, December 2019

Copyrights

Copyright © 2019 Andreas Nikolaidis

All rights reserved.

The approval of the dissertation by the Department of Civil Engineering and Geomatics does not imply necessarily the approval by the Department of the views of the writer.

AUTHOR'S PUBLICATIONS DURING THIS RESEARCH

Journal Publications

1. Samuel-Rhoads Y., Zodiatis G., **Nikolaidis A.**, Hayes D., Georgiou G., Konnaris G., Nikolaides M.: (2013) Climate Change Impacts on Sea Surface Temperature in the Eastern Mediterranean, Levantine Basin. Proceedings of SPIE - The International Society for Optical Engineering 08/2013; 8795. DOI:10.1117/12.2028329
2. Jimenez C., Hadjioannou L., Petrou A., **Nikolaidis A.**, Evriviadou M., Lange A.M.: (2014) Mortality of the scleractinian coral *Cladocora caespitosa* during a warming event in the Levantine Sea (Cyprus). Regional Environmental Change 12/2014; DOI:10.1007/s10113-014-0729-2
3. Zodiatis G., Galanis G., **Nikolaidis A.**, Kalogeri Ch., Hayes D., Georgiou G.C., Chu P.C., Kallos G.: (2014) Wave energy potential in the Eastern Mediterranean Levantine Basin. An integrated 10- year study. Renewable Energy 09/2014; 69:311. DOI:10.1016/j.renene.2014.03.051
4. **Nikolaidis A.**, Georgiou G.C., Hadjimitsis D., Akylas E.: (2014) Filling in missing sea-surface temperature satellite data over the Eastern Mediterranean Sea using the DINEOF algorithm. Open Geosciences 03/2014; 6(1):27-41. DOI:10.2478/s13533-012-0148-1
5. Zodiatis G., Galanis G., Kallos G., **Nikolaidis A.**, Kalogeri Ch., Liakatas A., Stylianou S.: (2015) The impact of sea surface currents in wave power potential modeling. Ocean Dynamics 10/2015; 65(11). DOI:10.1007/s10236-015-0880-4
6. Zodiatis G., Dominicis M. D., Perivoliotis L., Radhakrishnan H., Georgoudis E., Sotillo M., Lardner R., Krokos G., Bruciaferri D., Clementi E., Guarnieri A., Ribotti A., Drago A., Bourma E., Padorno E., Daniel P., Gonzalez G., Chazot C., Gouriou V., Kremer X., Sofianos S., Tintore J., Garreau P., Pinardi N., Coppini G., Lecci R., Pisano A., Sorgente R., Fazioli L., Soloviev D., Stylianou S., **Nikolaidis A.**, Panayidou X., Karaolia A., Gauci A., Marcati A., Caiazza L., and Mancini M. (2016). The Mediterranean decision support system for marine safety

dedicated to oil slicks predictions. *Deep Sea Research Part II: Topical Studies in Oceanography*, 133, 4-20. DOI:10.1016/j.dsr2.2016.07.014

7. Nikolaidis, G., Karaolia, A., Matsikaris, A., **Nikolaidis, A.**, Nicolaidis, M., and Georgiou, G. C. (2019). Blue energy potential analysis in the Mediterranean. *Frontiers in Energy Research*, 7(62), 12. DOI:10.3389/fenrg.2019.00062

Conference Proceedings

1. **Nikolaidis A.**, Georgiou G., Hadjimitsis D., Akylas E.: (2013) Applying DINEOF Algorithm On Cloudy Sea-Surface Temperature Satellite Data Over The Eastern Mediterranean Sea. Proc. SPIE 8795, First International Conference on Remote Sensing and Geoinformation of the Environment (RSCy2013), 87950L (August 5, 2013);, Paphos, Cyprus; 08/2013
2. Zodiatis G., Galanis G., Kalogeri Ch., **Nikolaidis A.**, Hayes D., Georgiou G., Chu P.C., Kallos G.: (2013) Monitor and Forecasting the wave energy potential in the eastern Mediterranean sea. Fluxes and Structures in Fluids, Saint Petersburg, Russia; 01/2013
3. Zodiatis G, Galanis G., Hayes D., **Nikolaidis A.**, Georgiou G., Stylianou S., Kallos G., Kalogeri C., Chu P.C., Charalambous A., Savvidou K., Kountouriotis Z., Michaelides S: (2013) Estimation and monitoring of the wave energy potential in Cyprus. 4th International Meeting on Meteorology and Climatology of the Mediterranean, Roussillon, France; 01/2013
4. Radhakrishnan H., Moulitsas I., Syrakos A., Zodiatis G., **Nikolaidis A.**, Hayes D., Georgiou G.C.: (2013) Performance Improvements of the CYCOFOS Flow Model. EGU General Assembly Conference Abstracts; 01/2013
5. Jimenez C., Petrou A., Evrivadou M., **Nikolaidis A.**, Hadjioanou L., Lange M.: (2013) Coral Mass Mortality Associated to the Summer 2012 Seawater Temperature Anomalies in the Levantine Sea (Cyprus).EGU General Assembly Conference Abstracts; 04/2013.
6. **Nikolaidis A.**, Stylianou S., Georgiou G., Hajimitsis D., Akylas E.: (2014) Using Data INterpolating Empirical Orthogonal Functions (DINEOF) Algorithm for filling the missing data of AVHRR satellite images.. EastMed Symposium 2014, Limassol, Cyprus; 11/2014
7. Zodiatis G., Radhakrishnan H., Galanis G., **Nikolaidis A.**: (2014) Downscaling My-Ocean: The CYCOFOS new forecasting systems at regional and sub-regional scales. EuroGoos; 11/2014

8. **Nikolaidis A.**, Stylianou S., Georgiou G., Hadjimitsis D., Akylas E.: (2014) New tool-box in ArcGIS for the reconstruction of missing satellite data using DINEOF algorithm: A case study of reconstruction of Chlorophyll-A gaps over the Mediterranean Sea. Second International Conference on Remote Sensing and Geoinformation of the Environment (RSCy2014); 08/2014
9. **Nikolaidis A.**, Stylianou S., Georgiou G., Hajimitsis D., Gravanis E., Akylas E.: (2015) Reconstruction and downscaling of Eastern Mediterranean OSCAR satellite surface current data using DINEOF. EGU General Assembly 2015, Vienna, Austria; 04/2015
10. Zodiatis G., De Dominicis M., Perivoliotis L., Radhakrishnan H., Lardner R., Pinardi N., Coppini G., Soloviev D., Tintore J., Sotillo M., Drago A., Stylianou S., **Nikolaidis A.**, Alves T., and Kokinou E. (2016) Modeling oil spills in the Med-Sea as a mean of early response in cases of oil leakages, EGU General Assembly Conference Abstracts, EPSC2016–14 174; 04/2016.
11. Miliou, A., Quintana, B., Kokinou, X., Alves, Tiago, **Nikolaidis, A.** and Georgiou, G. (2018) Enhancing critical thinking of students on marine pollution through scientific based scenarios. Presented at: 6th Conference on Hazardous-Industrial Waste Management, Chania, Crete; 09/2018.
12. **Nikolaidis A.**, Stylianou S, Georgiou G., Hadjimitsis D., and Akylas E., “Application of ROMS-AGRIF over Levantine and Cyprus seas.,” in EGU General Assembly Conference Abstracts, vol. 21, 2019, p. 13 889.

To Marios

ACKNOWLEDGEMENTS

Over some years, it has been my fortune to meet many nice people who have provided me with their time, knowledge, support, companionship and patience. This thesis is a complex result of a long process involving chaotic brainstorming, discussions, feedback and motivations from these people.

First of all, I would like to express my gratitude and thanks to my supervisor, Professor Evangelos Akylas, for guiding me to do this research. He has not only given me with brilliant ideas, deep thought, fresh innovation, critical feedback, but he also offered me full support and strong motivation. His sense of humour and nice communication made doing research with him attractive and pleasant. Without these contributions from him, I would never have come to this stage.

I would also thank my advisors Professor George Georgiou and Professor Diofantos Hajimitsis for their continuous financial, scientific and moral support. I express my special gratitude to Professor Georgiou, also Director of the Oceanography Center of the University of Cyprus, who was the inspirer of this effort.

I am also very grateful to all the personnel of the Department of Civil Engineer and Geomatics of the Cyprus Technical University who supported me in all aspects and for creating pleasant and wonderful working environment.

I am thanking also all my colleagues of the Oceanographic Center of the University of Cyprus, for their good willing and cooperation. In particular, I would like to thank Dr. George Zodiatis, for his support that allowed me to work and do research in Cyprus, throughout the last decade.

I am deeply indebted to my wife Stavroula, for her continuous patience, support and enthusiasm.

Last but not least, my gratitude and great appreciation set out to my son Marios, who inspired me and to whom I dedicate this work.

TABLE OF CONTENTS

Acknowledgments	v
List of Tables	x
List of Figures	xi
Chapter 1: Objectives and Dissertation Outline	1
1.1 Introduction	1
1.2 Outline	3
1.3 Objectives	5
1.4 Innovations	6
Chapter 2: Introduction and Background	7
2.1 Definition of Operational Oceanography	7
2.2 Physical aspects	9
2.2.1 Physical principles on the marine environment	10
2.3 General sea circulation	14
2.3.1 Sea circulation theories	17
2.4 Spatial and Temporal scales	18
2.5 Morphology and circulation of the Mediterranean Sea	20
2.5.1 Morphology	20
2.5.2 Circulation	22

Chapter 3: Numerical marine dynamics modeling	27
3.1 Introduction	27
3.2 Marine dynamics models: A critical review	29
3.2.1 Model categories	30
3.2.2 Horizontal coordinates and grids	31
3.2.3 Regarding the CFL criterion	32
3.3 Cyprus–Levantine numerical marine dynamics model implementation	33
3.3.1 Model overview	33
3.3.2 Horizontal curvilinear coordinates	34
3.3.3 Vertical stretched sigma–coordinates	36
3.3.4 Time stepping	38
3.3.5 The AGRIF nesting capability	39
3.3.6 Preprocessing	41
Chapter 4: ROMS-AGRIF numerical ocean model application over Eastern Mediterranean and Levantine Sea.	45
4.1 Introduction	45
4.2 Methodology	46
4.2.1 The CYCOFOS model	46
4.2.2 The ROMS model	47
4.2.3 ROMS model setup and compilation	50
4.3 Results and comparison	50
4.3.1 CYCOFOS and ROMS-AGRIF	50
4.3.2 ARGO Floats profiles vs Model results	51
4.4 Discussion and conclusions	53

Chapter 5: Applying a DINEOF Algorithm On Cloudy Sea-Surface Temperature Satellite Data Over The Eastern Mediterranean Sea	57
5.1 Introduction	57
5.2 Description	59
5.3 PCA-SVD-EOF	59
5.4 The algorithm	61
5.5 Application	62
5.6 Validation of the Results and discussion	65
5.7 Conclusions	69
Chapter 6: Implementation of DINEOF ArcGIS Toolbox: Case study of reconstruction of Chlorophyll-a missing data over the Mediterranean using MyOcean satellite data products.	72
6.1 Introduction	72
6.2 Methodology	73
6.3 Implementation	74
6.4 Installation and execution	76
6.5 Conclusions	80
Chapter 7: Conclusions and recommendations for future work	82
7.1 ROMS-AGRIF application	82
7.2 DINEOF operational implementations	82
7.3 DINEOF application on chlorophyll-a data	83
7.4 Future work	84
Appendix A: Cyprus – Levantine numerical marine dynamics model configuration	86
A.1 Introduction	86

A.1.1	param.h configuration file	86
Appendix B: Post-processing	98
B.1	Introduction	98
B.1.1	Sigma- to zeta- coordinates transformation codes	98
References	108

LIST OF TABLES

2.1	Global sea currents	17
3.1	z -, ρ -, σ - and hybrid vertical coordinate models	30
3.2	Variables used in the description of the numerical model.	34
3.3	Bathymetry data 2-D variables used by ROMS-AGRIF model.	43

LIST OF FIGURES

2.1	Ekman layer vector velocities in the Northern hemisphere. The total transport direction is perpendicular to the wind direction. (Source: Talley 2011)	15
2.2	Upwelling and downwelling due to the Ekman transport. (Source: Tillingier and Gordon 2010)	16
2.3	Thermohaline circulation: The largest volume flows in Antarctica over a period of about 600 years (Toggweiler and Samuels 1998).	18
2.4	Spatial and temporal scales in marine sciences.(Based on Kantha and Clayson 2000).	19
2.5	Bathymetry and Topography of the Mediterranean Sea in resolution of 100 <i>m</i> (Source: Ryan, Carbotte, Coplan, O’Hara, Melkonian, Arko, Weis- sel, Ferrini, Goodwillie, and Nitsche 2009).	21
2.6	Vertical distribution of Mediterranean water masses. (Source: UNEP/MAP 2012).	24
3.1	Numerical model’s variable placement over an Arakawa- <i>C</i> grid.	36
3.2	ROMS-AGRIF model implementation.	41
4.1	ROMS-AGRIF and CYCOFOS model bathymetries and their longitudinal differences (bottom right). On the top right is shown the ROMS vertical coordinate levels in S-coordinates and their analogy at the maximum depths. On the top left, the rectangular shows the internal higher resolution nested grid.	48
4.2	ROMS-AGRIF and CYCOFOS potential temperature results for the December 31st, 2018, at surface, 300 and 1500 m.	49
4.3	ROMS-AGRIF and CYCOFOS salinity results for the December 31st, 2018, at surface, 300 and 1500 m.	51
4.4	ROMS-AGRIF and CYCOFOS current magnitude and direction results for the December 31st, 2018, at surface, 300 and 1500 m.	52

4.5	ROMS-AGRIF and CYCOFOS potential temperature results for the January 5th, 2019, at 1500 m.	52
4.6	ROMS-AGRIF and CYCOFOS salinity results for the January 5th, 2019, at 650 m.	53
4.7	ROMS-AGRIF and CYCOFOS surface current magnitude and direction results for the January 5th, 2019.	53
4.8	Surface Temperature and Salinity ‘Goodness of Fit’ (GoF) statistical tests (Holst, 2012) for the period December 29th, 2018 until January 6th, 2019.	54
4.9	ARGO floats (in-situ), CYCOFOS and ROMS-AGRIF vertical temperature and salinity profile comparison.	55
4.10	Location of ARGO float on December 31st, 2018 (left). Float, CYCOFOS and ROMS-AGRIF T-S diagram (right) for the same date and area.	55
4.11	Location of ARGO float on January 5th, 2019 (left). Float, CYCOFOS and ROMS-AGRIF T-S diagram (right) for the same date and area.	55
5.1	DINEOF algorithm iterative scheme (based on Alvera-Azcárate et al., 2011).	63
5.2	A typical example of cloud-covered area during the data collection (left), and its recovered information (right) over the area of application.	65
5.3	Original and reconstructed SST data for the Eastern Mediterranean, for the period from 9/1/2013 to 12/1/2013.	66
5.4	Outline of the validation procedure for an arbitrary time-step of Eastern Mediterranean SST data.	67
6.1	Chlorophyll-a L3 MODIS Aqua data coverage of Mediterranean sea from December 21st,2013 to January 5th,2014.(16 time-steps).	73
6.2	Schematic DINEOF toolbox flowchart.	75
6.3	Left: DINEOF toolbox user interface options. Right: Configuration file contents example. Lines beginning with the (!) symbol, are considered as comments.	76
6.4	Installation process of the toolbox. There is an option of selection of the destination folder, according to the user’s choice. A new icon will appeared on desktop after the task finished.	77

6.5	DINEOF toolbar in ArcMap. Button icons description (from left to the right): Main process button, distance measure button, information button, copy and paste buttons, zoom and pan buttons, view entire region button. .	77
6.6	DINEOF toolbox interface initial appearance (left). Example of input file selection in the application's interface (right).	77
6.7	Input data appearance after the file selection. Empty (blank) space denotes the missing data.	78
6.8	DINEOF application appearance during execution. A new window indicates the process.	79
6.9	Application results: Under the Table of Contents section, all time steps included as separated layers.	79
6.10	Spatial Analyst's Boundary Clean algorithm application on the DINEOF results.	80
6.11	Filling 16 time steps of chlorophyll-a concentration over Mediterranean sea, after DINEOF and Boundary Clean algorithm application.	80

LIST OF SYMBOLS

- κ diffusivity
- ν horizontal viscosity
- Ω angular velocity of Earth [$7.29 \cdot 10^{-5} s^{-1}$]
- $\Omega(x, y, s, t)$ vertical velocity in stretched vertical coordinates
- $\phi(x, y, z, t)$ dynamic pressure [$\phi = (P/\rho_0)$]
- $\rho_0 + \rho(x, y, z, t)$ total *in-situ* density
- τ, τ_x, τ_y wind stress [$m \cdot s^{-1}$]
- \vec{u} velocity vector [$(u = u_x, v = u_y, w = u_z)$]
- $\zeta(x, y, z)$ surface elevation [m]
- C Courant number
- D_u, D_v, D_T, D_S diffusive terms
- f Coriolis parameter [$2\Omega \cdot \sin(\text{latitude})$]
- F_u, F_v, F_T, F_S forcing terms
- g gravity acceleration [$9.81 m \cdot s^{-1}$]
- h bottom depth [m]
- H_z vertical gradient in s coordinates [$(H_z = \partial z / \partial s)$]
- L length [m]

L^2 surface [m^2]

L^3 volume [m^3]

LT^{-1} velocity [$m \cdot s^{-1}$]

M mass [kg]

$m(\xi, \eta)$ scale factor on $\Delta\xi$ differential distance

$ML^{-1}T^{-2}$ pressure [Pa]

ML^{-3} density [$kg \cdot m^{-3}$]

MLT^{-2} force [N]

MT^{-2} stress [$N \cdot m^{-1}$]

$n(\xi, \eta)$ scale factor on $\Delta\eta$ differential distance

R_0 Rossby radius of deformation

$S(x, y, z, t)$ salinity

T time [s]

t time unit

$T(x, y, z, t)$ potential temperature

z vertical coordinate

ABSTRACT

Operational Oceanography is one of the most interesting branches of the science of Oceanography, relatively new and under rapid development during the last decades, with numerical modeling as one of the most important, fascinating and challenging products. A number of numerical models have been developed in order to anticipate the difficulties in gathering *in-situ* data and they are evolving continuously with the aid of the technological improvements in the fields of computers and of satellites. However, among the many required improvements there are two of great importance:

- alternative numerical oceanographic, and specifically, *marine dynamics* simulations of the circulation of the eastern Mediterranean and particularly of the Levantine Sea. The expected advance with this kind of model is higher and more accurate details in the obtained results. While such a model has been adopted effectively in various places of the globe, it has never been applied over the specific area of Levantine so far.
- data and numerical methods that should improve the satellite products, such sea surface height, temperature, salinity and chlorophyll-*a*. Application algorithms, like DINEOF, are used to eliminate missing data caused by cloud interference and thus to enrich the information that will drive the numerical models. This algorithm is applied for the first time to satellite data over the Eastern Mediterranean.

This thesis attempts a presentation on the particular features that describe the development and implementation of a new marine dynamics numerical model. Initially there is a description of the general ocean circulation, with reference to mechanisms and related theories. Emphasis is given on the description of the basic physical principles and on the general wind generated and thermohaline circulation in the planet. A summary of the Mediterranean physiography and the prevailing opinions of the emerging circulation will be shown. Finally, reference is made to the effect of different meteorological conditions on submeso-scale phenomena, with particular reference to the eastern Mediterranean and Levantine region, focusing on the area around Cyprus.

CHAPTER 1

OBJECTIVES AND DISSERTATION OUTLINE

In this chapter is presented the structure outline and the innovations introduced by this doctoral dissertation.

1.1 Introduction

The Mediterranean Sea is a water system in which parameters interact over various temporal and spatial scales (basin, sub-basin and average mesoscale) to form an extremely complex and variable circulation (Horton, Clifford, Schmitz, and Kantha 1997). It is one of the few places in the world where deep transfer and formation of water masses takes place. Because of these phenomena, it can be used for the research of the interaction between physical and other dynamic processes of the environment.

The Mediterranean is also an important marginal basin connected with the North Atlantic. The Atlantic produces very salty waters, the outflow of which through the Strait of Gibraltar, is likely to support the deep circulation of the North Atlantic. Incoming sea water masses are changing because of increased evaporation of the basin, and are cooled during their 100–year trip before they return to the ocean. (El-Geziry and Bryden 2010)

Research results presented by Zodiatis, Hayes, Gertman, Poulain, Menna, and Nikolaidis 2013, showed that the main characteristic of the circulation in the Eastern Mediterranean Levantine Basin is a general cyclonic flow following more or less the coastline, with several persistent eddies in the open sea. The interaction between all of these dynamical features produces a complicated flow pattern with strong spatial variability on a synoptic, seasonal and inter-annual scales. It was found that for the period 1995–2012, three dominating flow features exist in the South Eastern Levantine Basin: The two warm core eddies, i.e. the Cyprus and Shikmona, and the open sea flow jet of the Mid Mediterranean. This research preformed, based on the Cyprus Basin Oceanography (CYBO) cruises, along with Argo float drifters, satellite and glider collected data. The Cyprus

warm core eddy appeared to be the most influential flow feature in the area, with significant fluctuations in time and space. All these phenomena, are studied by the science of **oceanography**, and their dynamic behavior and evolution is related to the *operational* oceanography.

During the last decade the branch of **operational oceanography** has grown steadily. Particularly for the region of Eastern Mediterranean and Cyprus, progress of the relevant research has resulted in numerous scientific findings.

Recently, it has been shown that:

- In the Mediterranean, during periods of low wind speeds the impact of sea surface currents, of the significant wave height and of the mean wave period in the wave energy potential, is limited. Gradients in the sea currents speed seem to be correlated with rapid changes in the wave power potential values (Zodiatis, Galanis, Kallos, Nikolaidis, Kalogeri, Liakatas, and Stylianos 2015).
- A ten-year numerical simulation (2001--2010) at a very high spatial resolution ($1/60^\circ$) of the wave activity in the Mediterranean driven by reanalyzed hydrological and with assimilated satellite and meteorological data, shown that the regions with increased values of wave energy potential are mainly the western and southern coastlines of Cyprus island, the sea area of Lebanon and Israel, as well as the coastline of Egypt especially around Alexandria.

Over these areas, relatively low but also stable, and hence exploitable, wave energy potential was revealed. However, non-trivial impact of infrequent values was also recorded. Especially the area of Eratosthenes sea mountain seems to be a point of exceptional interest with increased power potential of even 500% more than the average of the Levantine Basin having at the same time critical geographical advantages (Zodiatis, Galanis, Nikolaidis, Kalogeri, Hayes, Georgiou, Chu, and Kallos 2014).

Furthermore, the regional numerical simulations of the sea over the last decade were mainly based on **NEMO** (Nucleus for European Modelling of the Ocean, Madec 2015)

and **POM** (Princeton Ocean Model, Blumberg and Mellor 1987). In this thesis, an approach to a numerical simulation using **ROMS** (Regional Ocean Model, Shchepetkin and McWilliams 2005) over the Levantine basin and Cyprus **will be implemented for the first time**.

It is a common, in places where the interest is very high, the scientific application growth to be analogous. While the POM and NEMO are very well known and respective applications, ROMS provides even better results describing the physical status and circulation evolution of the Levantine and Cyprus sea.

All of the above studies, performed with highly sophisticated scientific methods (most of them characterized as '*state-of-the-art*') share a common problem. A disadvantage, which is a common occurrence on observations originating from satellite data: **Missing data due to cloudy atmospheric conditions**. A method to overcome this disadvantage is described in this thesis, based on the **DINEOF** (Data Interpolating Empirical Orthogonal Functions), a technique to reconstruct missing data in satellite images.

The outcome of the use of the DINEOF with respect to the ROMS model results, is showing the improvements achieved with the application of the specific algorithm over the geophysical data.

1.2 Outline

Chapter 2 provides brief physical aspects, that support the theoretical background including the known circulation theories for the global ocean and for the Mediterranean, with reference to the spatial and temporal scaling. A presentation on the particular features that contribute to the current state of the ocean circulation, with reference to mechanisms and related theories. Emphasis is given on the description of the basic physical principles and on the general wind induced and thermohaline circulation of the planet. The importance of using the numerical simulations is indicated. A summary of the Mediterranean physiography and the prevailing opinions of the emerging circulation is shown, with particular reference to the eastern Mediterranean and Levantine region, focusing on the area around Cyprus.

In Chapter 3 a definition of the marine dynamics modeling is introduced followed by the its operational description of over the Levantine and Cyprus Sea. A case study of this model is contained in Chapter 4.

Chapter 4 provides a description of ROMS-AGRIF version 3.1.1 (2014) that has been applied for the first time on Eastern Mediterranean and, specifically, over the Levantine and Cyprus Seas. Initial and boundary conditions from Marine Copernicus Portal data and surface fluxes from NOAA Global Forecast System were used. The grid, with horizontal resolution of 5.5 km x 4.6 km and with an internal nested grid of 1.8km, at 30 vertical, terrain following, s-levels, has been created based on EMODNET Bathymetry portal data (tile 241). All data used are open source. The model run in operational prognostic mode, producing results every six hours, for a period of ten days, with daily averages included. Comparisons of the results with the CYCOFOS system (Cyprus Coastal Ocean Forecasting and Observing System, Zodiatis, Lardner, Georgiou, Demirov, Manzella, and Pinardi 2003; Zodiatis, Lardner, Hayes, and Georgiou 2006; Zodiatis, Lardner, Hayes, Georgiou, Sofianos, Skliris, and Lascaratos 2008) and with ARGOS float profiles showed compliance and very high accuracy.

Chapter 5 provides a description of the Data Interpolating Empirical Orthogonal Functions method, which is a special technique based on Empirical Orthogonal Functions and developed to reconstruct missing data from satellite images, especially useful for filling in missing data from geophysical fields. It is presented the implementation of the method and its ability to reconstruct the sea-surface temperature fields over the Eastern Mediterranean basin, and specifically in the Levantine Sea. L3 type Satellite Sea-surface Temperature data has been used and reprocessed in order to recover missing information from cloudy images. Data reconstruction with this method proved to be extremely effective, even when using a relatively small number of time steps, and markedly accelerated the procedure. A detailed comparison with the two oceanographic models proves the accuracy of the method and the validity of the reconstructed fields.

Chapter 6 describes a new DINEOF ArcGIS® Toolbox impementation. Implementation of DINEOF method in a GIS system provides a more complete, integrated approach,

permitting the expansion of the applicability of an effective and computationally affordable solution, on the problem of data reconstruction, for missing data from geophysical fields, such as chlorophyll-a, sea surface temperatures or salinities and geophysical fields derived from satellite data. The inclusion of many statistical tools within the GIS, multiply the effectiveness, providing interoperability with other sources in the same application environment. This is especially useful in studies where various different kinds of data, have to be examined. A case-study of filling the chlorophyll-a missing data in the Mediterranean Sea area, for a 18-day period is analyzed, as an example for the effectiveness and simplicity of the usage of this toolbox. The specific study focuses to chlorophyll-a MODIS satellite data collected by CNR-ISAC (Italian National Research Council, Institute of Atmospheric Sciences and Climate), from the respective products of Copernicus organization, that provides free online access to Level 3, with 1 km resolution. In particular, all the daily products with an initial level of only 27% data coverage were successfully reconstructed. Finally Chapter 7 presents conclusions and recommendations for future extensions of this research. Two additional appendices provide the marine dynamics model pre-processing configuration structure rules and improved post-processing vertical scale transformation codes. These codes are essential for the model's implementation over the specific area of interest.

1.3 Objectives

Taking into account all the above subjects, the objectives of this doctoral dissertation are:

1. the implementation and validation of a new marine dynamics model that will provide improved results for the Levantine and Cyprus sea,
2. an in-depth description and implementation of the DINEOF algorithm, that will improve the quality of satellite geophysical data and
3. the preparation of a complete new web service that will be used for the dissemination of the reconstructed data to the scientific community and to the public.

1.4 Innovations

The following items were developed for the first time during the research process :

- Application and testing of the ROMS–AGRIF marine dynamics numerical model over Levantine and Cyprus Sea, including improved pre– and post–processing algorithms for regridding algorithms.
- Application of the DINEOF algorithm over eastern Mediterranean and Black Sea, for sea surface height and temperature and chlorophyll-*a* satellite products, including special pre- and post-processing codes.
- Implementation¹ of a web service (through Github open source site) for the presentation and the dissemination of the sea surface reconstructed satellite data, both in graphics and in binary (netCDF) format.

Also there were code improvements in pre- and post–processing and the ability of inclusion of a new Fortran compiler, which improves the execution time of the model. Pre–processing improvements were implementations of new download and re–gridding python based codes. Post–processing improvements focused on the development of new vertical coordinates transformation codes, using the NOAA Ferret application and mapping routines in python programming language.

¹This service is available at <https://emed-bsea-sst.github.io/Data/>

CHAPTER 2

INTRODUCTION AND BACKGROUND

In this Chapter a brief introduction to operational oceanography is presented. The physical aspects and accompanying equations of the marine environment are demonstrated followed by a general circulation description with the spatial and temporal scales that cover the relevant phenomena. Finally a description of the morphology and of the circulation of the Mediterranean sea is given.

2.1 Definition of Operational Oceanography

Operational Oceanography is one of the branches of the science of Physical Oceanography, which focuses in the physical motions and properties of the sea water. According to the European component of the Global Ocean Observing System (EuroGOOS), operational oceanography can be defined as the activity of systematic and long-term routine measurements of the seas and oceans and atmosphere, and their rapid interpretation and dissemination.

Operational oceanography techniques can provide estimates of essential ocean variables (e.g. sea level, temperature and currents) which can be used to improve safety of life at sea, help create wealth, and assist in the security and protection of the marine environment.

Examples of operational oceanography products include warnings (of coastal floods, ice and storm damage, harmful algal blooms and contaminants, etc.), electronic charts, optimum routes for ships, prediction of seasonal or annual primary productivity, ocean currents, ocean climate variability etc. These products and forecasts usually are distributed to industrial users, government agencies, and regulatory authorities (Schiller and Brassington 2011, EuroGOOS, the European Global Ocean Observing System 2019).

According to Schiller et al. (2018), operational oceanography is like weather forecasting for the ocean, it provides estimates of ocean variables (temperature, currents, surface

height, etc.) for the past, present, and future. There is a systematic focus on sustained operational ocean observing systems, estimates of the current state of the sea, short-range predictions and ocean reanalyses.

Pinardi and Coppini, (2010) state that operational oceanography is the branch of ocean science that routinely generates high quality observational and model data for both fundamental studies and practical applications.

Operational Oceanography procedures first require the rapid transmission of observational data to data assimilation centres. Powerful computers using numerical forecasting models process the data. The results, complimented by acquired observational, partner and third organization data, are used to generate data products. Examples of data products include warnings (of coastal floods, ice and storm damage, harmful algal blooms and contaminants, etc.), electronic charts, optimum routes for ships, prediction of seasonal or annual primary productivity, ocean currents, ocean climate variability etc. The final products are distributed rapidly to industrial users, government agencies, and regulatory authorities.

Nittis and Chronis (2005) suggest that operational oceanography is the development of methods and systems for continuous **monitoring, forecasting** and **information** on the **conditions** which predominate in the marine environment.

The term *conditions* includes meteorological conditions, currents, wave, hydrological characteristics and the biochemical parameters that determine the health of an ecosystem. The term *monitoring* is also more encompassing than the concept of measurement-observation and relates to the numerical simulation using measurements (diagnosis – now-cast). The term *forecast* refers to the description of the future conditions using appropriate numerical models. The term *information* refers to production and dissemination products tailored to the needs of the end user on a continuous basis or for specific periods.

In simple terms, operational oceanography will enable us to forecast the sea state in the same way that meteorologists forecast the atmosphere. Operational oceanography is expected to describe and forecast the global ocean conditions in real time and at any moment from satellites, *in situ* observations and with the aid of numerical modeling.

2.2 Physical aspects

Examination of Physics of the marine environment requires, in addition to good knowledge of the basic principles of Newtonian mechanics, the use of Thermodynamics and Fluid mechanics. While the Newtonian mechanics are able to explain the dynamics of one or small number of solid bodies, they are insufficient when it comes to the description of fluids. The cause of this deficiency is not that they are not applicable, but that they are not practical for the temporal and spatial range of such phenomena. When a particle concentration is considered like a fluid, it means that they are not considered physically as a gathering of individual particles with interactions between them, but as a single mass, which is likely deformed, with a number of molecules, moving in conflicting directions with each other. The description of this system by simple Newtonian mechanics would require knowledge of the position and the kinetic state of an enormous number of molecules and solve an even greater number of complex equations. This may theoretically be possible, but it is practically impossible on the space-time reference scales. Therefore, due to the great number of particles contained in a marine environment fluid, it is only practical to adequately describe the system only with the use of Thermodynamics and Continuum Mechanics. For a brief description of the relevant principles (Zervakis 2007):

The *first law of thermodynamics* is that the change in internal energy of a thermodynamic system is equal to the heat exchanges and work with its environment.

The *second law of thermodynamics* states that the entropy of an isolated system never decreases. If the transition of a system from one state to another is slow and without friction, then the entropy of the system remains constant, and the transition is reversible (reversible process). In case of abrupt changes and friction, the entropy of a system always tends to increase.

2.2.1 Physical principles on the marine environment

The 300 year old Newton's Laws, as they were adapted during the 18th century by Euler and Bernoulli, are the governing motion rules of the marine environment. Notably the second law, "force equals the product of mass by acceleration" in fluids is interpreted as "force per unit mass equals acceleration" (Dyke 2001).

Newton's second law in terms of dimensions states that acceleration is LT^{-2} and force per unit mass is $MLT^{-2} \times M^{-1} = LT^{-2}$. More specifically, in the marine sciences (e.g. Oceanography and Meteorology), we take into account three (3) forms of acceleration because we study the movements in the Earth's non-inertial reference system (Dyke 2001).

- The first is the acceleration of the fluid $\partial\vec{u}/\partial t$. This is proportional to the particle acceleration of the Newtonian Mechanics. This acceleration is sometimes referred to as **point acceleration**. The acceleration dimension is LT^{-2} .
- The second form of acceleration, $\Omega \times \vec{u}$ is apparent and is observed due to the Earth's rotation. The effect of this acceleration on sea currents is equal to f times the current velocity, where $f = 2\Omega \sin(\text{latitude})$ is called **Coriolis parameter** and $\Omega = 7.29 \cdot 10^{-5} s^{-1}$ is Earth's angular velocity. It is the most important for the study of the medium and large scale sea and atmospheric flows, known as **Coriolis acceleration**.
- Finally, the **advective** acceleration $(\vec{u} \cdot \nabla)\vec{u}$ is present even when there is a constant current flow. The natural "feeling" that describes this form of acceleration is what a person feels when he steps in a corner. According to Dyke (2001), it is mistakenly referred to as "centrifugal force", while the right term is "centripetal acceleration".

The following basic principles are used to study and understand sea currents:

- (a) The material or substantial derivative is the sum of the terms of acceleration and horizontal transport (Zervakis 2005; Talley 2011). Horizontal transfer terms appear only when Eulerian motions are being studied. In Lagrangian motions, only the temporal derivative appears, since the terms of the horizontal transport are contained in

the movement of the particle. The material or substantial derivative is defined as

$$\frac{D\vec{u}}{Dt} = \frac{\partial\vec{u}}{\partial t} + \vec{u} \cdot \nabla\vec{u} \quad (2.1)$$

The term D/Dt is physically the time rate of change following a moving fluid element; the term $\partial/\partial t$ is the *local derivative*, which is physically the time rate of change at a fixed point and the term $(\vec{u} \cdot \nabla)$ is the *convective derivative*, which is physically the time rate of change due to the movement of the fluid element from one location to another in the flow field where the flow properties are spatially different. The substantial derivative applies to any flow-field variable (Anderson and Wendt 1995).

The material derivative of the velocity of flow, under the influence of the Coriolis force, equalizes the rate of change in pressure relative to the density, plus some form of viscous or shear stress.

The equation describing this principle is an expression of **Newton's second law** on fluid movements, known as the **Navier-Stokes equation**, which in the case of the rotating earth reference system becomes (Zervakis 2005):

$$\frac{D\vec{u}}{Dt} + f\hat{k} \times \vec{u} = -\frac{1}{\rho}\vec{\nabla}p - g\hat{k} + \nu\nabla^2\vec{u} \quad (2.2)$$

where the centrifugal acceleration is included in the corrected value of g . The ν quantity is the kinematic viscosity of the fluid, defined as the ratio of molecular diffusion (or dynamic viscosity) over density ($\nu = \mu/\rho$).

(b) The **principle of conservation of mass** applies (Talley 2011)

$$\frac{D\rho}{Dt} + \rho\left(\frac{\partial u}{\partial x} + \frac{\partial v}{\partial y} + \frac{\partial w}{\partial z}\right) = 0 \quad (2.3)$$

(c) The pressure variation in the depth is equal to the product of the density times the

gravitational acceleration (**hydrostatic balance**):

$$\frac{\partial p}{\partial z} = -\rho g \quad (2.4)$$

The negative sign is a convention which is meaningful when the depth is measured (increases) from the surface to the bottom.

- (d) The **equation of state** of the sea, where the density varies with temperature increase and / or salinity decrease

$$\rho = \rho(S, T, P) \quad (2.5)$$

- (e) The principle of **geostrophy**, resulting from the equation (2.1) accepting as significant only the terms of the Coriolis and pressure gradient,

$$f\hat{k} \times \vec{u} = \frac{\nabla p}{\rho_0} \quad (2.6)$$

which applies to cases (Stewart 2008) where

- the Coriolis force should be taken into account in relation to the inertial reference system. That is when, the Rossby *radius of deformation* ($R_0 = U/fL$) is small.
 - in **barotropic** flows where isobars and isopycns are parallel, and **baroclinic** flows where the isobars intersect isopycns.
 - is applied in cases where the time scales being examined are greater than one (1) day and the vertical mixing is small, in stratified fluid, even if the Rossby radius is large. In these cases, we refer to **quasi-geostrophy**.
- (f) Ekman transport, with upwelling and downwelling phenomena (Dyke 2001).

Specifically, Swedish postgraduate student Walfrid Ekman, in his doctoral dissertation, explained and described Norwegian Fridtjof Nansen's observation, that the icebergs do not travel parallel and in the same direction as the wind, but almost

perpendicular to it, towards the right side of the wind. Ekman's hypothesis of the problem were:

- Stable wind exerts a stress τ on the sea surface, and only the steady state is examined (thus $\partial/\partial t = 0$)
- Horizontal and vertical uniformity, that is $\partial/\partial x = \partial/\partial y = \partial/\partial z = 0$. Due to the vertical uniformity, the viscosity (either molecular, ν , or turbulent, k) is constant with depth.

The momentum conservation equations in the two horizontal axes are:

$$\begin{aligned} -fv &= v \frac{\partial^2 u}{\partial z^2} \\ +fu &= v \frac{\partial^2 v}{\partial z^2} \end{aligned} \quad (2.7)$$

Equation 2.7 (Zervakis 2007, Talley 2011) is solved by expressing vectors of velocity and wind stress as complex numbers, where the x component is the real part and y is the imaginary part of the complex variable. The vector velocity \mathbf{u} , where $\mathbf{u} = u + iv$ and of the vector stress of the wind τ , where $\tau = \tau_x + i\tau_y$ is used. By multiplying the second part of the system of equations (2.7) with the *imaginary* unit, and adding these equations, the following differential equation is obtained

$$\frac{\partial^2 \vec{u}}{\partial z^2} - i \frac{f}{v} \vec{u} = 0 \quad (2.8)$$

The boundary conditions of (2.8) on the surface ($z = 0$), are $v(\partial \vec{u} / \partial z) = \vec{\tau} / \rho$, and at a depth where the effect of the wind is not directly felt $v(\partial \vec{u} / \partial z) = 0$. The complete solution of the equation (2.8) is (Zervakis 2005)

$$\begin{aligned} \vec{u}(z) &= \frac{\vec{\tau}}{\rho} \sqrt{\frac{1}{2fv}} (1 - i) e^{\sqrt{\frac{f}{2v}}(1+i)z} = \\ &= \frac{\vec{\tau}}{\rho} \sqrt{\frac{1}{2fv}} (1 - i) e^{\frac{\sqrt{2f/v}}{2}z} \left\{ \cos\left(\frac{\sqrt{2f/v}}{2}z\right) + i \sin\left(\frac{\sqrt{2f/v}}{2}z\right) \right\} \end{aligned} \quad (2.9)$$

which represents a velocity vector in the direction of 45° to the right of the surface

wind. As the depth increases, velocity vector rotates to the right, while its magnitude decreases exponentially with the depth. Because of the resulting geometric shape, the solution is called the *Ekman spiral* (Figure 2.1). Vertical integration of equation (2.8) by applying boundary conditions gives

$$\vec{u} = -i \frac{v}{f\rho} \vec{\tau} = \frac{\vec{\tau} \times \hat{k}}{f\rho} \quad (2.10)$$

Equation (2.10) is the total *wind induced Ekman transport of water*, resulting in a vector always perpendicular (and to the right in the Northern hemisphere) at the surface wind. This movement of the surface layer of the sea to the right (left-) of wind, as a result of the rotation of the Earth, is the basis of dynamic oceanography. Also was the starting point of various explanations for the description and interpretation of the sea circulation by Stommel and Munk in the years immediately following the World War II.

- (g) The dynamic sea mass vorticity is equal to the sum of the planetary vorticity¹. The relative vorticity of the height of the water column is a conservative (irrotational) quantity. The planetary vorticity increases from the equator toward the poles. The water mass relative vorticity increases either when the water is under the influence of forces that cause it to move with cyclonic flow (anti-clockwise), or when a stratified water column is forced to "stretch", as for example in a forced flow to deeper areas.

2.3 General sea circulation

The sea currents flow horizontally and vertically. Typical speeds occurring in the horizontal flow are in the range of $0.01 - 1 \text{ m s}^{-1}$. The velocities observed in the vertical flow in a stratified water column are much smaller, of the order of 0.001 m s^{-1} .

There are two physical mechanisms forcing the creation of non-tidal, sea currents:

¹The 'absolute' vorticity $\frac{\partial v}{\partial x} - \frac{\partial u}{\partial y} + f$ is the sum of 'relative' vorticity, caused by the relative to the rotating planet motion and of the 'planetary' vorticity, f , caused by the rotation of the planet (Marshall and Plumb 2008).

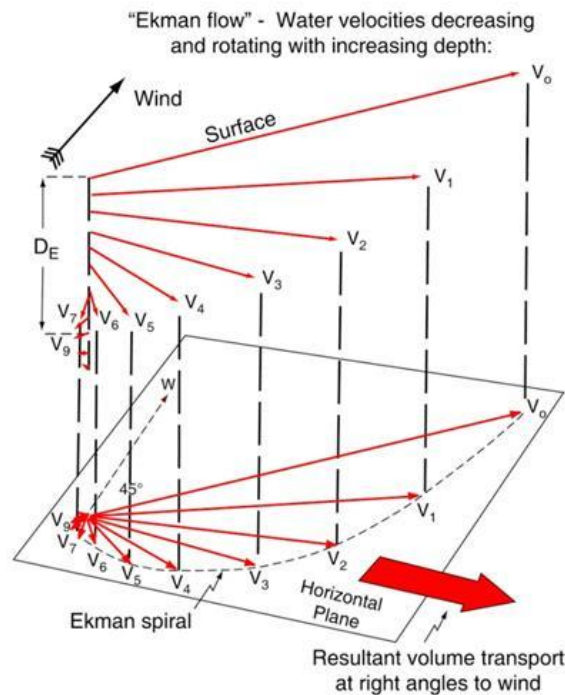


Figure 2.1: Ekman layer vector velocities in the Northern hemisphere. The total transport direction is perpendicular to the wind direction. (Source: Talley 2011)

- the wind, who generates a stress to the surface of the sea and
- buoyancy flows (thermal and through water masses with different densities) presented in the sea–atmosphere interface, altering the density of the surface layer.

The wind generated currents category, is known as *wind induced circulation*, and the buoyancy flows category is addressed as *thermohaline circulation*. (Figure 2.3)

The wind induced circulation is much more intense, but covers only the upper layers of the water column up to one thousand (1000 m) meters. The much slower thermohaline circulation in places reaches to the sea bottom and is inseparable from the water column overturn, contributing to the creation of the sea masses.

The surface wind stress creates a pattern of motion, which acts on the first 50 meters of the surface and up to a depth of 200-250 meters. This motion, known as **Ekman transport**, occurs in a direction perpendicular to the wind direction, to the right in the Northern hemisphere and to the left in the Southern. As the wind blows in variable directions, Ekman transport creates upwelling and downwelling of surface water (Figure 2.2).

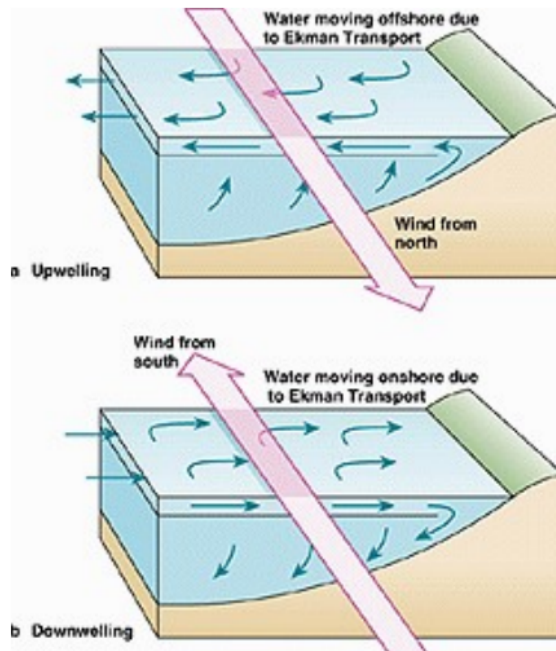


Figure 2.2: Upwelling and downwelling due to the Ekman transport. (Source: Tillinger and Gordon 2010)

The surface layers have a lower density than deeper. Because of the Ekman transport, the rearrangement of the water column causes the creation of "valleys" in the upwelling regions and "hills" in the downwelling areas at sea level. Although the amplitude of the change does not exceed 1.5 m, it is sufficient to create a horizontal pressure gradient with respect to the geostrophic balance, indicating the start of the wind induced circulation. As a general rule, the sea currents are mainly geostrophic, which means that the horizontal pressure gradient balances the Coriolis force.

The wind induced circulation is characterized by the presence of large scale cyclonic and anti-cyclonic motion of sea masses, such as subtropical and polar currents.

As the surface water becomes gradually denser due to heat loss or the increase of salinity, it is immersed in the lower layers. If the column stratification is weak and the buoyancy loss sufficient, it is possible to reach the bottom. Such behavior occurs in the North Atlantic (North Atlantic Deep Water masses) and around the Antarctic (Antarctic Bottom Water). Table 2.1 shows the velocities of the most well known global sea currents. (The Sv (sverdrup) unit, named after the Norwegian oceanographer and meteorologist Harald Ulrik Sverdrup (1888 —1957), is defined as $1 Sv = 10^{-6} m^3 s^{-1}$.)

The thermohaline circulation is the mechanism that imposes the influence of the sea

Table 2.1: Global sea currents

Name	Magnitude(Speed) – Area
Gulf Stream	0.3 ms^{-1} near Florida, 70-100 cms^{-1} near Cape Hatteras
Kurishio	0.5 ms^{-1} in North Pacific Ocean
Agulhas	100 cms^{-1} , around North Africa
Antarctic Circumpolar Current	0.001 Sv , from west to east around Antarctica through Drake Passage

in the atmosphere at 100 – 1000-year time scale. The main existing theories for the sea circulation (Talley 2011, Tillinger and Gordon 2010) were created during the late 20th century.

2.3.1 Sea circulation theories

According to Stommel’s theory, the momentum created by the turbulence of the northern currents, is offset by the currents presented at the western limits. Stommel (1961), uses the turbulence equation, without taking into account inertial factors. According to this theory, the dissolution of the flow takes place due to the friction at the bottom. The weaknesses of this theory is that no friction is introduced into the flowing currents, the friction at the bottom does not actually exist, and the rebound currents are completely ignored.

According to Stewart (2008) Munk’s theory (1950), also uses the turbulence equation and ignores inertial factors. Munk states that it is the diffusion that balances the changes of planetary turbulence and the flows in the boundaries are also balanced (Sverdrup equilibrium) by the creation of rebound currents. Dissolution of the flow is a result of the lateral friction. The creation of weaker, that the real, rebound currents is the weakness of this theory.

Charney (1947), using stream functions and ignoring boundary flows, argues that total turbulence is conservative. The weakness of this theory is that there is no term describing the wind momentum. However, this theory applies (only) to internal flows.

Moore’s theory allows for the creation of Rossby waves, takes no account of boundary conditions, is based on flow functions, and considers lateral viscosity as a repressive (dissolving) factor. It seems to work only in external flows.

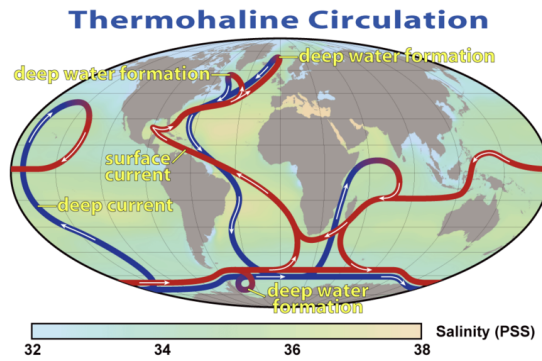


Figure 2.3: Thermohaline circulation: The largest volume flows in Antarctica over a period of about 600 years (Toggweiler and Samuels 1998).

Finally, the theory of Fofonof, use only non-forced inertial moments, ignoring all other factors and can create flow in every direction. Weakness in the asymmetric gyres presence makes this theory totally unrealistic.

Most theories developed or presented just after the end of World War II, and still used today for 'holistic' descriptions of conditions in the marine environment, or for the development of basic conditions for experimental numerical simulations.

2.4 Spatial and Temporal scales

The motions at sea are turbulent and cover a large range of spatial and temporal scales. To adequately reproduce the phenomenology of the study area, it is essential to use the correct scales and thus to select the mechanisms that should be parameterized and those that should not be taken into account.

As mentioned, circulation at sea is a complex result of the density gradients occurred due to different water masses mixing, the heat exchange between the atmosphere and the sea surface, the induced by the atmosphere momentum (wind action), and by the astronomical forces (tides).

The sea surface response covers wide temporal and spatial scales (from less than a hour to over-decade and from a few kilometers to planetary range). Until nowadays there are still efforts to fully understand the sea response, mainly due to the lack of enough data. The basic equations of motion in conjunction with the application of numerical methods for solving them, help in further research.

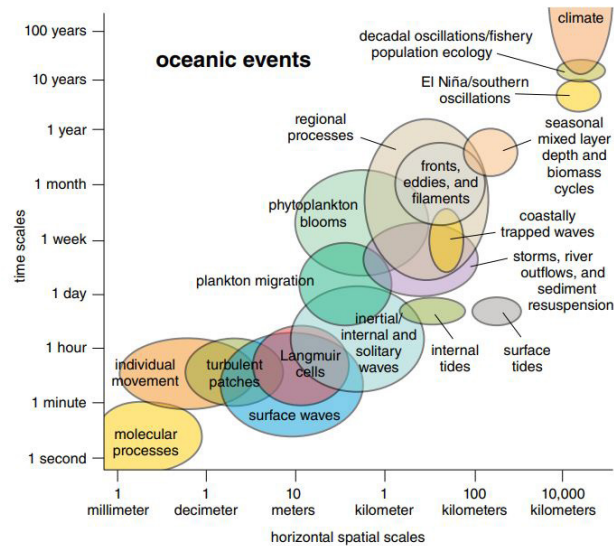


Figure 2.4: Spatial and temporal scales in marine sciences.(Based on Kantha and Clayson 2000).

On timescales of a few minutes and spatial scales between few centimeters to several tens of meters (microscale) the processes are associated with the turbulent motions, that are the least well understood physical mechanisms in the sea and atmosphere.

On time scales of a few hours and spatial scales 1–100 *km* dominant phenomena are the internal waves and astronomical tides with periods of 12 and 24 hours (Figure 2.4).

The internal waves generated at interfaces of the sea water column, are particularly important for the internal structure of the oceans and the vertical velocities caused by them often attract prognostic interest. Tidal motions, caused by the gravitational pull of the sun and moon on the sea are important for coastal areas of large oceans. These motions affect both the sea level and the current field, especially in shallow and narrow areas. Tidal motion influence is less important for semi-enclosed basins such as the Mediterranean sea.

On time scales of a few days dominating mechanism is the effect of weather changes which accompany atmospheric systems (short or synoptic range). The response of the sea to the wind shear stress and the effect of atmospheric pressure (inverse barometer) are the two main mechanisms of interest since they affect sea level and surface currents.

A number of processes, especially concerning vertical exchanges in the upper-ocean occurs at "sub-mesoscale" (i.e. features less than 25 km in size).

The mesoscale circulation is defined as a class of energetic phenomena of spatial scales ranging from about ten to several hundred kilometers and time scales ranging from

a few days to several months.

On timescales of a few months mesoscale formations (mesoscale eddies) are encountered, with spatial scales of the order of 100 km. These formations are generated by instabilities of large-scale circulation and the interaction of the topography or direct action of the wind. They are particularly important for the open sea circulation producing lateral flows with current velocities that may exceed 100 cm · s⁻¹. They also affect the biochemistry of the area with the strong upward or downward flows in their center, thus helping the surface to deeper layers material exchange.

Timescales of years and spatial scales of thousands of kilometers are dominated by Rossby waves and oceanic large-scale formations. The importance of these formations is high as they affect the climate of many areas of the planet by conveying hot and cold water masses over long distances (Gulf Stream, El-Nino) and also affect atmospheric circulation mainly through evaporation and heat exchange.

Finally in even larger temporal and spatial scales the focus is on the thermohaline ocean circulation based on the creation of deep waters in selected areas of the globe. In the following section the special characteristics of the Mediterranean basin circulation with an emphasis on the Levantine Sea region presented.

Other dimension scales include the *rotational timescale* f^{-1} (where f is the Coriolis parameter), the gravity wave speed, $c = \sqrt{gH}$, (where g is the gravity acceleration and H the depth), and the *Rossby radius of deformation*, $R_d = \sqrt{gH}f^{-1}$ for the horizontal scale.

The deformation radius is the distance a gravity wave can travel in the timescale f^{-1} , and sets the dominant horizontal scale for rotating flow (Hetland 2012).

2.5 Morphology and circulation of the Mediterranean Sea

2.5.1 Morphology

The Mediterranean basin extends between latitude 30° 00.00' North to 45° 00.00' North and longitude between 6° 00.00' West and 35° 00.00' East (Figure 2.5).

The Mediterranean basin is a semi-enclosed basin, connected to the Atlantic Ocean

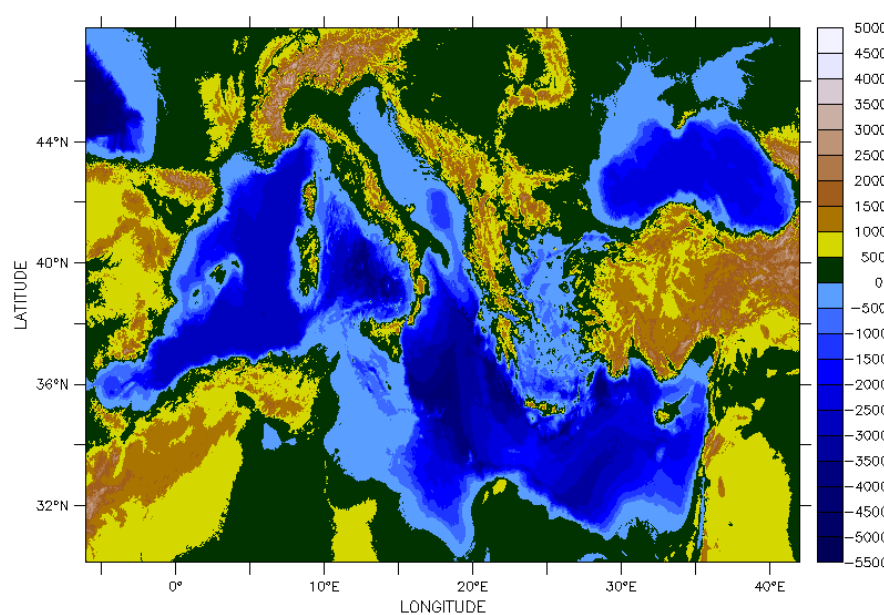


Figure 2.5: Bathymetry and Topography of the Mediterranean Sea in resolution of 100 *m* (Source: Ryan, Carbotte, Coplan, O’Hara, Melkonian, Arko, Weissel, Ferrini, Goodwillie, and Nitsche 2009).

through Gibraltar Strait, having a width of 13 *km* and a maximum depth of 300 *m*. The minimum depth is 10 *m* to the west end. The Mediterranean Sea is connected with the Black Sea by the Dardanelles / Sea of Marmara / Bosphorus system. The sea is bounded by Europe to the north, by Africa to the south and by Asia to the east. It presents narrow coastal zone with many small and large bays.

The Mediterranean Sea covers approximately surface $2.5 \times 10^6 \text{ km}^2$, which is 0.82% of the area of the world ocean surface, and contains 0.32% of the volume of the world’s water. The shore extend is approximately $46 \times 10^3 \text{ km}$ and the average depth is 1.5 *km*. The maximum depth in the Ionian Sea is 5.1 *km*. The passage (narrow, sill) Sicily – Tunisia, with 400 *m* depth, divides the Mediterranean basin into two major discrete sub-basins, western and eastern, and acts as a geographical and hydrological boundary.

The western basin of the Mediterranean includes the Alboran Sea in the extreme western zone between Spain and Morocco and the Balearic Sea next to the coast of Algeria extending to the north, to the Gulf of Lions. There are also the Ligurian Sea and the Tyrrhenian Sea in the north and east of the SW basin, respectively. With the exception of the Gulf of Lions, the continental shelf of the western basin is narrow. The Tyrrhenian Sea, between the Italian peninsula and the islands of Sardinia and Corsica, is the deepest

part of the western basin, about 3500 *m* deep, and is connected with the rest of the basin to the south, with a wide opening between Sardinia and Sicily.

The eastern Mediterranean basin is more complicated in comparison with the western. Four (4) distinct sub-basins are identified: the Ionian Sea, the Levantine Sea, the Adriatic Sea and the Aegean Sea.

The Ionian Sea located between Italy and Greece to the north, and Libya and Tunisia to the south, has a maximum depth of about 5000 *m* near southern Greece.

The Levantine Sea occupies part of the central and all of the east area of eastern basin. The Levantine Sea has depths of the order of 2500–3000 *m* in the center and a maximum depth of 4500 *m* on a fault located southeast of Rhodes.

Adriatic is the most continental basin in the Mediterranean and is enclosed between two mountain ridges (Apennine and Balkan). It is connected to the Ionian Sea with the Otranto narrow passage, whose width is approximately 75 *km* with average depth of about 800 *m*.

The Aegean Sea connects with the Levantine Sea through various passages that lie between Greece, Turkey, Crete and Rhodes, with a maximum depth of about 1500 *m* and many multifarious, irregular coasts and topography.

2.5.2 Circulation

The Mediterranean Sea is a water system in which various temporal and spatial scales (basin, sub-basin and average mesoscale) interact to form an extremely complex and variable circulation (Horton, Clifford, Schmitz, and Kantha 1997). It is one of the few places in the world where deep transfer and formation of water masses takes place. Because of these phenomena, it can be used for the research of the interaction between physical and other dynamic processes of the environment.

The Mediterranean is also an important marginal basin connected with the North Atlantic. It produces very salty waters, the outflow of which through the Strait of Gibraltar, is likely to support the deep circulation of the North Atlantic. Incoming sea water masses are changing because of increased evaporation of the basin, and are cooled during their

100-year trip before they return to the ocean. (El-Geziry and Bryden 2010)

The circulation is driven by the deficit of the balance of water and the heat flows between the sea and the atmosphere. The sea water deficit, caused by the evaporation and by the rivers runoff, is balanced by the influx of water from the Atlantic through the Strait of Gibraltar and the contribution of water from the Black Sea through the Straits of Dardanelles. The heat exchange with the atmosphere, leading to cooling and subsequent sinking of surface water, leads to the creation of thermohaline circulation.

According to the European Environment Agency (EEA/UNEP 1999) the Mediterranean Sea contains three (3) main water masses (Figure 2.6):

- (1) the Modified Atlantic Water (MAW) in the surface layer, with a thickness of 50–200 *m* and salinity 36.2 *psu* near Gibraltar and 38.6 *psu* in Levantine basin.
- (2) the Levantine Intermediate Water (LIW), formed in the Levantine basin, in a depth between 200 and 800 *m*, characterized by temperatures of 13–15.5 °C, with salinities 38.4 – 39.1 *psu*.
- (3) the Mediterranean Deep Water (MDW), formed both, in western and eastern basins. Western Mediterranean Deep Water (WMDW) is characterized by temperatures near to 12.7 °C and salinities of 38.4 *psu*, while the Eastern Mediterranean Deep Water (EMDW) is characterized by temperatures of 13.6 °C and salinities of 38.7 *psu*.

The incoming Atlantic water (MAW) is modified by the interactions with the atmosphere and the mixing of the surface and subsurface waters. During its course, it is heated or cooled depending on the seasonal period, increasing the salt load and becomes denser.

During autumn, the MAW remains on the northern coast of the Mediterranean basin. In winter the dry and cold air masses cause intense evaporation and cooling, resulting in significant densification and water mass sinking. This sinking takes place in specific zones, generally located in the northern part of the basin, and causes the formation of deep waters. Part of these masses in the western basin forms the Western Mediterranean Deep Water (WMDW).

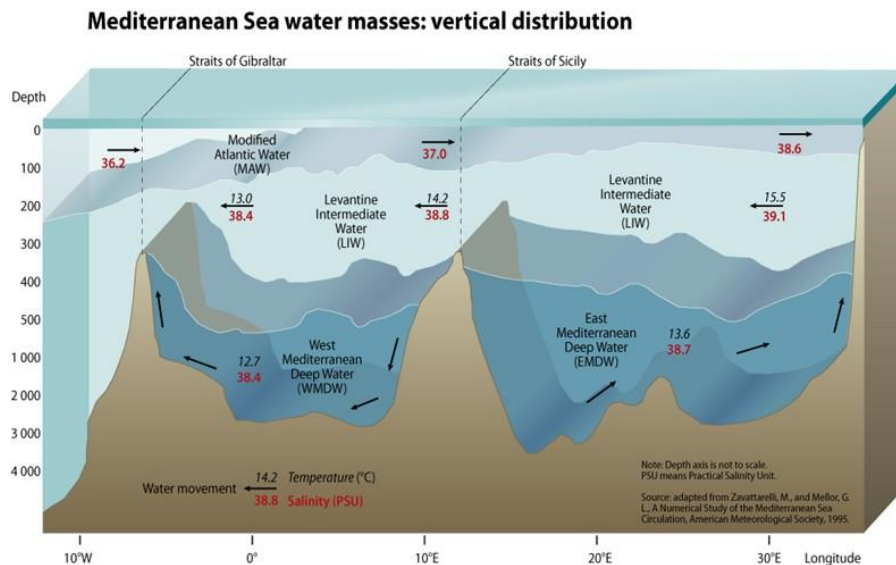


Figure 2.6: Vertical distribution of Mediterranean water masses. (Source: UNEP/MAP 2012).

Winter cold winds that occur between Rhodes and Cyprus and between the northern and central Adriatic, are responsible for the formation of LIW (Levantine Intermediate Water Levantine Intermediate Water). LIW is the warmest and denser intermediate water, and the largest in volume. Because of its characteristics and its quantity, the LIW is more or less detected throughout the Mediterranean. Due to its relatively low density, it is just below the MAW, and it mixes it with it as soon as the MAW begins to sink.

The total percentage of intermediate and deep water formed in the Mediterranean is estimated to be about 90% of Atlantic water entering Gibraltar (10% is estimated to evaporate). About three quarters of the intermediate and deep waters formed in the eastern Mediterranean basin. The estimated water residence time in the Mediterranean is quite high, about 50–100 years (Millot and Taupier-Letage 2005), with significant impact on recycling and export of pollutants.

According to the Millot and Taupier-Letage (2005) the large-scale Mediterranean circulation is evidenced by the basin outflow and the mesoscale circulation by cyclones interconnected and bounded by the currents and eddies (jets) with strong seasonal and annual variability. The general circulation is strongly influenced by the physiography of coastal areas, resulting in creation of local small scale currents.

Research results presented by Zodiatis et al.(2013), shown that the main characteristic

of the circulation in the Eastern Mediterranean Levantine Basin is a general cyclonic flow following more or less the coastline, with several persistent eddies in the open sea. The interaction between all of these dynamical features produces a complicated flow pattern with strong spatial variability on a synoptic, seasonal and inter-annual scales. It was found that for the period 1995–2012, three dominating flow features exist in the South Eastern Levantine Basin: The two warm core eddies, i.e. the Cyprus and Shikmona, and the open sea flow jet of the Mid Mediterranean. This research performed, based on the Cyprus Basin Oceanography (CYBO) cruises, along with Argo float drifters, satellite and glider collected data. The Cyprus warm core eddy appeared to be the most influential flow feature in the area, with significant fluctuations in time and space.

CHAPTER 3

NUMERICAL MARINE DYNAMICS MODELING

In this Chapter a synoptic description of the numerical modeling of the sea is provided. Also, a suggested definition of the term *numerical marine dynamics model* is introduced, followed by descriptions of the specific implementation of such a model over the Levantine and the Cyprus sea.

3.1 Introduction

The examination of the characteristics of the marine environment using *in-situ* measurements show the clear advantage of the accuracy of the observed data, but also come with considerable disadvantages. *In-situ* data are usually spatially and temporally limited providing a very precise but limited time snapshot of the state of the physical system. Problems that have to do with the spatial coverage of measurements often leads to weaknesses in identifying phenomena smaller than the distance between the selected observation stations, while time discretization of the measurements does not allow full understanding of the phenomenon evolution (Blumberg and Mellor 1987).

The critical difference between the sea and the atmosphere is the cause of their motion.

The atmosphere is heated primarily from below although a small heating percentage appeared in the upper part of the troposphere. Solar radiation penetrates the atmosphere and heats the land and the sea, which in turn heats the atmosphere. The heating differences of various continents and oceans is causing the general circulation of the atmosphere. Evaporation and precipitation are also important heat and water exchange factors and affect significantly to the dynamics of the atmosphere. The sea has no corresponding mechanisms. The main cause of the sea motion is the wind and the flows of heat and water on the surface.

Also, the time scales of the sea are much higher than in the atmosphere and this led to the saying that the sea has some kind of "memory".

At high latitudes spatial scales in the sea are much smaller than those in the atmosphere. The Rossby radius, that is used for the definition of typical spatial scales, is 1000 *km* in the atmosphere and 40 *km* in the sea (for the first baroclinic radius, Rossby 1959, Chelton, DeSzoeker, Schlax, El Naggar, and Siwertz 1998). Finally, another major difference between atmosphere and sea is the existence of topographic barriers between the oceans (the continents) something that does not exist to the atmosphere.

Due to the necessity of spatial and temporal information, the development and use of mathematical simulations (models) to predict and describe the phenomena became apparent very early, both for the atmosphere and the sea (Masumoto, Sasaki, Kagimoto, Komori, Ishida, Sasai, Miyama, Motoi, Mitsudera, and Takahashi 2004).

Numerical hydrostatic and hydrodynamic models applied to different spatial and temporal scales. Models of the large oceans or the entire globe is mainly focused on describing the large-scale thermohaline circulation and the mechanisms that hold it steady (dense water generation etc.).

The time scales considered vary with the simulation goals. In cases where phenomena ranging between a decade and a hundred years are studied, a special attention is given to the exchanges with the atmosphere. The general rule in these simulations is the coupling of sea-atmosphere models that will fully describe the exchanges and feedback mechanisms, focusing on climate change issues. It is well known that due to the high heat capacity (the upper 2.5 *m* of the oceans are equivalent to the entire troposphere) the sea is an important climate regulator.

The oceans also contain large amounts of CO₂ (60 times more than the atmosphere) and exchanges with the atmosphere are a key factor in the development of the greenhouse effect. The numerical models that describe these mechanisms are important tools of understanding and forecasting future climate changes.

The numerical simulation of the dynamic regional seas and semi-enclosed basins present different but equally important problems. For open basins (eg, Mexico Bay, Bengal Sea) where there is a very strong dependence on the open ocean, it is usually preferable to study them with models of the wider region. To increase the resolution in the area of

interest the best method is the use of successive models with increasing spatial resolution (Oey 2006).

For the semi-enclosed basins with fewer exchanges with the oceans (eg Mediterranean, Baltic) commonly used limited area models products and the ocean interaction are parameterized in some way.

A similar approach is used in local offshore applications (eg. Levantine) or coastal regions (eg. the southeast coast of Cyprus). The phenomenology of an area determines in many cases the weight that will be given in the description of the sea–atmosphere interaction. In ocean-scale applications it is important to sufficiently describe the heat exchange between atmosphere and sea water. The same applies to smaller basins also, when we have deep water formation phenomena. In coastal applications, it is often enough to describe the wind action and to put the weight on the open sea and to the tidal influence.

3.2 Marine dynamics models: A critical review

According to McGuffie and Henderson-Sellers (2014), a general circulation model (GCM) employs a mathematical model of the general circulation of a planetary atmosphere or ocean. It uses the Navier–Stokes equations on a rotating sphere with thermodynamic terms for various energy sources (radiation, latent heat). These equations are the basis for computer programs used to simulate the Earth’s atmosphere or oceans. Atmospheric and oceanic GCMs (AGCM and OGCM) are the distinct types of such models.

The term ocean general circulation models (OGCMs) is appointed to a particular kind of general circulation model describing physical and thermodynamical processes in oceans. The oceanic general circulation depict the sea motion using a three-dimensional grid that include active thermodynamics. A hierarchy of OGCMs have been developed that include varying degrees of spatial coverage, resolution, geographical realism, process detail, etc. The OGCM predicts the evolution of ocean horizontal and vertical velocity, temperature, and salinity fields over the full water column (Bryan 1987, Madec 2015).

With the evolution of these models new quantities were included (mostly incorporated) into the solution process of the system, such as biogeochemical processes. This

Table 3.1: z -, ρ -, σ - and hybrid vertical coordinate models

z-models	Documentation
MIT/MIT model	Marshall et al. (1997a,b)
Modular Ocean Model/GFDL	Pacanowski and Griffes (1999)
Parallel Ocean Program/Los Alamos	Smith et al. (1992)
<hr/>	
ρ-models	
HIM/Hallberg Isopycnal Model	Hallberg (1995, 1997)
MICOM/Miami Isopycnal Coordinate Ocean Model	Bleck et al. (1992)
POSEIDON/Center for Ocean, Land, and Atmosphere	Schopf and Lough (1995)
<hr/>	
σ-models	
POM/Princeton Ocean Model	Blumberg and Mellor (1987)
ROMS/Regional Ocean Model System	Shchepetkin et al. (2005)
<hr/>	
hybrid-models	
HYCOM/HYbrid Coordinate Ocean Model	Halliwell (2004)
NEMO/Nucleus for European Modelling of the Ocean	Madec (2015)

fact extends the prediction abilities over not only the circulation, but over all the dynamic structure of the ocean / sea area under investigation.

Taking account of all the above, a suggested **numerical marine dynamics model** definition, is that, it is a numerical ocean general circulation model that also includes biogeochemical processes (e.g. sediment transport and chlorophyll concentration).

3.2.1 Model categories

In the last decade, three main categories of numerical marine dynamics models (Table 3.1, σ -, ρ - and z -coordinates), including and the so called *hybrid*-coordinates, (which usually is a combination of ρ - and z -coordinates), are used worldwide, characterized by the vertical coordinate system they use (Griffies, Böning, Bryan, Chassignet, Gerdes, Hasumi, Hirst, Treguer, and Webb 2000). Each of these models has some particular characteristics and comparative advantages that make it suitable for specific applications, but none is able to cover the whole range of applications. The type of numerical schemes employed, the mode of discretization in the vertical plane (e.g. sigma coordinates, zeta, isopycnic), the calculation of turbulent diffusion and the use or not of the hydrostatic approximation are some of the differences of the models and the corresponding targets of their continuous development.

As forecasting applications are constantly increasing, the data assimilation is one of the most important research areas that is expected to significantly improve the current predictive ability. Significant improvement is also expected from the continuous increase in available computational power that will allow development of increased resolution (higher resolution) models. The circulation forecasting models are among the most demanding in computing power and often require the use of super-computers.

3.2.2 Horizontal coordinates and grids

Geophysical flows usually are represented with spherical orthogonal curvilinear coordinates. However, the convergence of the meridians and the associated polar singularity leads to many numerical problems with the CFL (Courant–Friedrichs–Lewy) condition. Hence, spherical coordinates require either, taking small time steps based on the very small zonal grid spacing near the pole, or using polar altering or finite impulse response altering within some region around the pole, in order to remove small zonal scale structures.

The first option is often prohibitively computational expensive. Thus, many have chosen to filter, with filters based largely on those used by atmospheric modellers. The main computational problem with polar filters in the ocean is related to the complicated land–sea boundaries, making each latitude row consist of numerous broken ocean segments, consisted of only a few ocean points. In contrast, grid–point atmospheric models, which are commonly based on a σ –coordinate systems, arrive to no meridional boundaries.

Separate filtering of each ocean segment is the only option, since otherwise water properties could be transported through land–sea boundaries via the action of the filter. This approach sometimes cause computational over– or under–flows. Additionally, filters have been found to introduce noises, for example to the vertical velocity, because when filtering the prognostic variables, pressure gradients are included.

Filtering the dynamic and thermodynamics fields separately can destroy geostrophic and thermodynamic balances. Therefore, polar filtering eliminates an important physical component to a simulation.

For this reason, marine dynamics modellers have chosen to generalize the spherical grid to allow arbitrary orthogonal curvilinear coordinates in a scheme, that the coordinate singularity can be moved from the ocean domain and placed over land (e.g., Haidvogel et al., 1991; Smith et al., 1995; Mellor, 1996).

3.2.3 Regarding the CFL criterion

CFL is a necessary condition for convergence while solving certain partial differential equations numerically. The CFL condition dictates that the distance that any information travels during the time-step length within a grid must be lower than the distance between grid elements. In other words, information from a given grid cell element must propagate only to its immediate neighbors (Courant, Friedrichs, and Lewy 1967).

With properly defined spatial coordinates, spatial dimension of the problem and time, the CFL condition is commonly prescribed for those terms of the finite-difference approximation of general partial differential equations that model the advection phenomenon.

The CFL condition make sure that the full numerical domain of dependence, contain the physical domain of dependence.

In one-dimensional case, the CFL has the form

$$C = \frac{\mathbf{u}\Delta t}{\Delta x} \leq C_{\max} \quad (3.1)$$

where, C is the Courant number, \mathbf{u} is the velocity magnitude (with dimensions length/time), Δx is the length interval and Δt is the time-step. The value of C_{\max} changes with the method used to solve the discretised equation, depending on whether the method is explicit or implicit. If an explicit (time-marching) solver is used, then typically $C_{\max} = 1$. Implicit (matrix) solvers are usually less sensitive to numerical instability and so larger values of C_{\max} may be tolerated.

The general CFL condition for the n -dimensional case is

$$C = \Delta t \left(\sum_{i=1}^n \frac{u_{x_i}}{\Delta x_i} \right) \leq C_{\max} \quad (3.2)$$

The interval length is not required to be the same for each spatial variable $\Delta x_i, i = 1, \dots, n$. This "degree of freedom" can be used to somewhat optimize the value of the time step for a particular problem, by varying the values of the different interval to keep it not too small.

3.3 Cyprus–Levantine numerical marine dynamics model implementation

3.3.1 Model overview

Regional Ocean Modeling System (ROMS) is an evolution of the σ -coordinate Rutgers University Model (SCRUM) described by Song and Haidvogel (1994). The initial model version was expanded to include a variety of new features:

- high-order advection-schemes; accurate pressure gradient algorithms; several subgrid-scale parameterizations ;
- atmospheric, oceanic and benthic boundary layers; biological modules ;
- radiation boundary conditions and
- data assimilation.

Currently ROMS does not designate a single model, but a variety of versions developed in an open mode by different institutions. The numerical aspects of the ROMS model are described in detail by Shchepetkin and McWilliams (2005).

The specific version of ROMS used, is known as "Roms–Agrif version 3.1.1, 07 July 2014" and is publicly available at the Internet ¹.

It is open-source code with sophisticated numerical techniques, including a split–explicit time–stepping scheme that treats the fast barotropic (2D) and slow baroclinic (3D) modes separately for improved efficiency.

ROMS provides the ability to resolve very fine scales (especially in the coastal area), and their interactions with larger scales. It contains the AGRIF method for real–time grid down-scaling (Debreu, Vouland, and Blayo 2008) with 1– and 2–way interaction.

¹[http://www.croco-ocean.org/download/roms_agrif-project/](http://www.croco-ocean.org/download/roms_agrif_project/)

Table 3.2: Variables used in the description of the numerical model.

Variable	Description
D_u, D_v, D_T, D_S	diffusive terms
F_u, F_v, F_T, F_S	forcing terms
f	Coriolis parameter
t	time
g	gravity acceleration
h	bottom depth
ν, κ	horizontal viscosity and diffusivity
K_m, K_T, K_S	vertical viscosity and diffusivity
$P \simeq -\rho_0 g z$	total pressure
$\phi(x, y, z, t)$	dynamic pressure $\phi = (P/\rho_0)$
$\rho_0 + \rho(x, y, z, t)$	total <i>in-situ</i> density
$S(x, y, z, t)$	Salinity
$T(x, y, z, t)$	potential temperature
u, v, w	the (x, y, z) components of the \vec{u} vector velocity
x, y	horizontal coordinates
z	vertical coordinate
$\zeta(x, y, z)$	surface elevation
s	stretched vertical coordinates
H_z	vertical gradient in s coordinates ($H_z = \partial z / \partial s$)
$\Omega(x, y, s, t)$	vertical velocity in s coordinates

3.3.2 Horizontal curvilinear coordinates

Sometimes the simulated flow fields include areas where boundary currents or fronts occupy a small fraction of the physical domain. In such cases, the efficiency of the results can be improved by placing more computational resolution over the specific areas. With the introduction of a suitable orthogonal coordinate transformation the construction of a boundary following coordinate system can be obtained (Hedström 2000; Hedström 2009).

With respect to the Table 3.2, let the new coordinates be $\xi(x, y)$ and $\eta(x, y)$, where the relationship of horizontal arc length to the differential distance is given by

$$(ds)_\xi = \frac{1}{m} d\xi \quad (3.3)$$

$$(ds)_\eta = \frac{1}{n} d\eta \quad (3.4)$$

Here $m(\xi, \eta)$ and $n(\xi, \eta)$ are scale factors which relate the differential distance $(\Delta\xi, \Delta\eta)$ to the actual (physical) arc lengths.

The u velocity component is

$$\frac{\partial u}{\partial t} - fv + \vec{u} \cdot \nabla u = -\frac{\partial \phi}{\partial x} - \left(\frac{g\rho}{\rho_0}\right) \frac{\partial z}{\partial x} - g \frac{\partial \zeta}{\partial x} + \mathcal{F}_u + \mathcal{D}_u \quad (3.5)$$

In the new coordinates system, the u and v velocity components defined to be

$$\vec{u} \cdot \xi = u \quad (3.6)$$

$$\vec{u} \cdot \eta = v \quad (3.7)$$

Hence the equation (3.5) of u velocity, after the transformation become

$$\begin{aligned} \frac{\partial}{\partial t} \left(\frac{H_z u}{mn} \right) + \frac{\partial}{\partial \xi} \left(\frac{H_z u^2}{n} \right) + \frac{\partial}{\partial \eta} \left(\frac{H_z uv}{m} \right) + \frac{\partial}{\partial s} \left(\frac{H_z u \Omega}{mn} \right) \\ - \left\{ \left(\frac{f}{mn} \right) + v \frac{\partial}{\partial \xi} \left(\frac{1}{n} \right) - u \frac{\partial}{\partial \eta} \left(\frac{1}{m} \right) \right\} H_z v = \\ - \left(\frac{H_z}{n} \right) \left(\frac{\partial \phi}{\partial \xi} + \frac{g\rho}{\rho_0} \frac{\partial z}{\partial \xi} + g \frac{\partial \zeta}{\partial \xi} \right) + \frac{H_z}{mn} (\mathcal{F}_u + \mathcal{D}_u) \end{aligned} \quad (3.8)$$

Similarly, the v velocity component that is

$$\frac{\partial v}{\partial t} + fu + \vec{u} \cdot \nabla v = -\frac{\partial \phi}{\partial y} - \left(\frac{g\rho}{\rho_0}\right) \frac{\partial z}{\partial y} - g \frac{\partial \zeta}{\partial y} + \mathcal{F}_v + \mathcal{D}_v \quad (3.9)$$

after the transformation to the new coordinate system will be

$$\begin{aligned} \frac{\partial}{\partial t} \left(\frac{H_z v}{mn} \right) + \frac{\partial}{\partial \xi} \left(\frac{H_z uv}{n} \right) + \frac{\partial}{\partial \eta} \left(\frac{H_z v^2}{m} \right) + \frac{\partial}{\partial s} \left(\frac{H_z v \Omega}{mn} \right) \\ - \left\{ \left(\frac{f}{mn} \right) + v \frac{\partial}{\partial \xi} \left(\frac{1}{n} \right) - u \frac{\partial}{\partial \eta} \left(\frac{1}{m} \right) \right\} H_z u = \\ - \left(\frac{H_z}{n} \right) \left(\frac{\partial \phi}{\partial \eta} + \frac{g\rho}{\rho_0} \frac{\partial z}{\partial \eta} + g \frac{\partial \zeta}{\partial \eta} \right) + \frac{H_z}{mn} (\mathcal{F}_v + \mathcal{D}_v) \end{aligned} \quad (3.10)$$

Equations (3.8) and (3.10) express the transformed momentum balance in x - and y -directions respectively. The advective–diffusive equations are

$$\frac{\partial T}{\partial t} + \vec{u} \cdot \nabla T = \mathcal{F}_T + \mathcal{D}_T \quad (3.11)$$

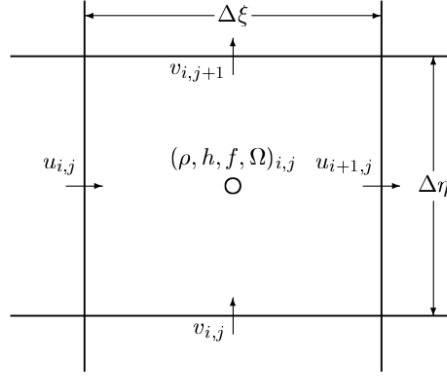


Figure 3.1: Numerical model's variable placement over an Arakawa–C grid.

and

$$\frac{\partial S}{\partial t} + \vec{u} \cdot \nabla S = \mathcal{F}_S + \mathcal{D}_S \quad (3.12)$$

Equations (3.11) and (3.12) will be transformed to

$$\frac{\partial}{\partial t} \left(\frac{H_z T}{mn} \right) + \frac{\partial}{\partial \xi} \left(\frac{H_z u T}{n} \right) + \frac{\partial}{\partial \eta} \left(\frac{H_z v T}{m} \right) + \frac{\partial}{\partial s} \left(\frac{H_z \Omega T}{mn} \right) = \frac{H_z}{mn} (\mathcal{F}_T + \mathcal{D}_T) \quad (3.13)$$

and

$$\frac{\partial}{\partial t} \left(\frac{H_z S}{mn} \right) + \frac{\partial}{\partial \xi} \left(\frac{H_z u S}{n} \right) + \frac{\partial}{\partial \eta} \left(\frac{H_z v S}{m} \right) + \frac{\partial}{\partial s} \left(\frac{H_z \Omega S}{mn} \right) = \frac{H_z}{mn} (\mathcal{F}_S + \mathcal{D}_S) \quad (3.14)$$

In Figure 3.1, the horizontal arrangement of the variables is shown. The Arakawa–C grid (Arakawa and Lamb 1977), is generally accepted as a good choice for problems with horizontal resolution that is fine compared to the first radius of deformation.

3.3.3 Vertical stretched sigma–coordinates

Typically, the σ –coordinates are defined to be

$$\sigma = \frac{z - \eta}{H + \eta} \quad (3.15)$$

where H is the topography, η the sea surface elevation and z the position depth (vertical coordinate). The $\sigma = 0$ when $z = \eta$ and $\sigma = -1$ when $z = H$ (Blumberg and Mellor 1987; Mellor 1998).

In ROMS model, the vertical coordinate z is defined (Song and Haidvogel 1994 ; Shchepetkin and McWilliams 2005)

$$z = \zeta(1 + \sigma) + h_c\sigma + (h - h_c)C(\sigma), \quad -1 \leq \sigma \leq 0 \quad (3.16)$$

where h_c is a depth above the which more resolution required. The quantity $C(\sigma)$, according Song and Haidvogel 1994, is defined to be

$$C(\sigma) = (1 - b)\frac{\sinh(\theta\sigma)}{\sinh(\theta)} + b\frac{\tanh[\theta(\sigma + \frac{1}{2})] - \tanh(\frac{1}{2}\theta)}{2\tanh(\frac{1}{2}\theta)} \quad (3.17)$$

where b and θ are bottom and surface control coefficients respectively, with ranges between $0 < b < 1$ and $0 < \theta < 20$. Equation (3.16) for $\sigma = 0$ produces $z = \zeta$ and for $\sigma = -1$, $z = h$.

This coordinate system has the following characteristics

- Setting $\theta = 0$ and using the L'Hospital's rule:

$$z = (\zeta + h)(1 + \sigma) - h \quad (3.18)$$

which is the σ -coordinate.

- It is linearly depended on ζ and infinitely differentiable to σ .
- Increasing the value of θ , increases the resolution above the h_c depth.
- For $b = 0$, the surface resolution increased in analogy to the θ value.

The equation (3.17) is known *vertical stretch function Type-1*. Since 1995, three more types have been developed², with most significant the *Type-2* (Shchepetkin and McWilliams 2005), where

$$C(\sigma) = \mu C_{srf}(\sigma) + (1 - \mu)C_{bot}(\sigma) \quad (3.19)$$

²More details on all types of the vertical stretch functions can be found in Shchepetkin and McWilliams 2005 and Warner, Sherwood, Signell, Harris, and Arango 2008.

In the equation (3.19),

$$\mu = (\sigma + 1)^a \left[1 + \frac{a}{b} (1 - (\sigma + 1)^b) \right]$$

where a and b are coefficients of local bed slope (Warner, Sherwood, Signell, Harris, and Arango 2008), and

$$C_{srf}(\sigma) = \frac{1 - \cosh(\theta_{srf}\sigma)}{\theta_{srf} - 1}, \quad \theta_{srf} > 0$$

$$C_{bot}(\sigma) = \frac{\sinh[\theta_{bot}(\sigma + 1)]}{\sinh(\theta_{bot})} - 1, \quad \theta_{bot} > 0$$

Stretch function Type–2, is using \cosh in the hyperbolic part of the equation (3.19), instead of the \tanh of Type–1 equation (3.17) and also provides

$$\frac{\partial C(\sigma)}{\partial \sigma} \rightarrow 0, \text{ when } \sigma \rightarrow 0$$

3.3.4 Time stepping

The momentum equations (3.8) and (3.10) and the temperature and salinity equations (3.13) and (3.14) are advanced in time, without computation of the vertical viscosity.

Numerical time stepping uses a discrete approximation to

$$\frac{\partial \phi(t)}{\partial t} = \mathcal{F}(t) \tag{3.20}$$

where, ϕ stands for any of u, v, S, T or ζ and \mathcal{F} represents all the right–hand–side terms (Hedström 2000; Hedström 2009; Shchepetkin and McWilliams 2005; Arango 2019)

According Arango 2019 and Hedström 2009 the simplest approximation is the *Euler* time–step:

$$\frac{\phi(t + \Delta t) - \phi(t)}{\Delta t} = \mathcal{F}(t) \tag{3.21}$$

where the future value of ϕ is predicted based only on the current field values. This

method is accurate to first order of Δt and has been found unconditionally unstable with respect to advection.

The *Leapfrog* time–step

$$\frac{\phi(t + \Delta t) - \phi(t - \Delta t)}{2\Delta t} = \mathcal{F}(t) \quad (3.22)$$

has been found accurate to $O(\Delta t^2)$ but it is also unconditionally unstable with respect to diffusion. The even and odd time steps tend to diverge in a computational mode. This is corrected by inserting a *trapezoid* correction on every step. The right–hand–side term of this correction is denoted by $\mathcal{F}^*(t + \Delta t)$. The *Leapfrog – trapezoid* (LF–TR) time–step is then

$$\frac{\phi(t + \Delta t) - \phi(t)}{\Delta t} = \frac{1}{2} [\mathcal{F}(t) + \mathcal{F}^*(t + \Delta t)] \quad (3.23)$$

This LF–TR time–step is stable with respect to diffusion but the right-hand-side terms are computed twice per time step. This time–step method is used for all the 2–D variables of the model.

The *third order Adams–Bashforth* (AB3) time–step is used for all the 3–D variables:

$$\frac{\phi(t + \Delta t) - \phi(t)}{\Delta t} = \alpha \mathcal{F}(t) + \beta \mathcal{F}(t - \Delta t) + \gamma \mathcal{F}(t - 2\Delta t) \quad (3.24)$$

where the coefficients α , β and γ are chosen to obtain a third–order estimate of $\phi(t + \Delta t)$. According to Hedström 2009 and to Arango 2019, $\alpha = 23/12$, $\beta = -4/3$, and $\gamma = 5/12$. With this method, the model carries one time level for the physical variables and three time levels for the right-hand-side terms, that are not stored. An *Euler* time–step is used for the first two steps for initialization.

3.3.5 The AGRIF nesting capability

Interactions between offshore and near-shore dynamics is a known challenge of marine modelling. The Adaptive grid refinement in Fortran (AGRIF, Debreu, Vouland, and Blayo 2008; Debreu, Marchesiello, Penven, and Cambon 2012) offers a method to face this problem with the inclusion of adaptive mesh refinement features within a finite difference

numerical model.

AGRIF package consists by a model-independent Fortran90 procedures containing the different operations in the time integration of grid hierarchy, clustering, interpolations, updates, etc. The model-dependent part of the code is based on an entry file written by the user. The basic idea of AGRIF is to make use of Fortran90 pointers to successively address the variables of the different grids, providing the re-gridding process. As pointers can be used exactly like other (static) variables in Fortran, most of the original code can remain unchanged.

One of the major advantages of AGRIF is that it can manage an arbitrary number of fixed grids and an arbitrary number of embedding levels in static-grids. This way, one or more finer resolution grids can be embedded and dynamically updated during the model's execution. Children grids can even contain nested grids ('telescopic' grids). Resulted conditions can focus only on the children grids (1-way mode) or update the parent grid also (2-way mode).

The time evolution for the child grids during every time-step is managed by a recursive integration procedure. For each parent time step the child is advanced using a time step divided by a refinement coefficient as many times, as necessary to reach the time of the parent, in order to preserve the CFL criterion.

For simple 2-level embedding, the procedure is as follows (Cambon, Penven, Marchesiello, and Debreu 2011):

1. Advance the parent grid by one parent time step.
2. Arrive to the proper boundary conditions of the child grid by interpolating the relevant parent variables in space and time.
3. Advance the child grid by as much child time steps as necessary to reach the new parent model time.
4. If the 2-way embedding has been selected, update point by point the parent model by averaging the more accurate values of the child model.

AGRIF³ package has been included into ROMS model since 2006 (Penven, Debreu, Marchesiello, and McWilliams 2006) and it is a semantic point of difference between this specific ROMS version and the rest of them. The 2-way mode was introduced and incorporated sometime later (Debreu, Marchesiello, and Penven 2010).

3.3.6 Preprocessing

The requirements for the proper use and initialization of the AGRIF package into the model's code, are dictated as rules in the model's definition code files, and with the implementation of a specific entry file. This option has been highly simplified by the ROMSTOOLS MATLABTM package (Penven and Tan 2003; Penven, Marchesiello, Debreu, and Lefèvre 2008; Penven, Cambon, Tan, Marchesiello, and Debreu 2010).

The ROMS-AGRIF schematic implementation is shown in figure 3.2.

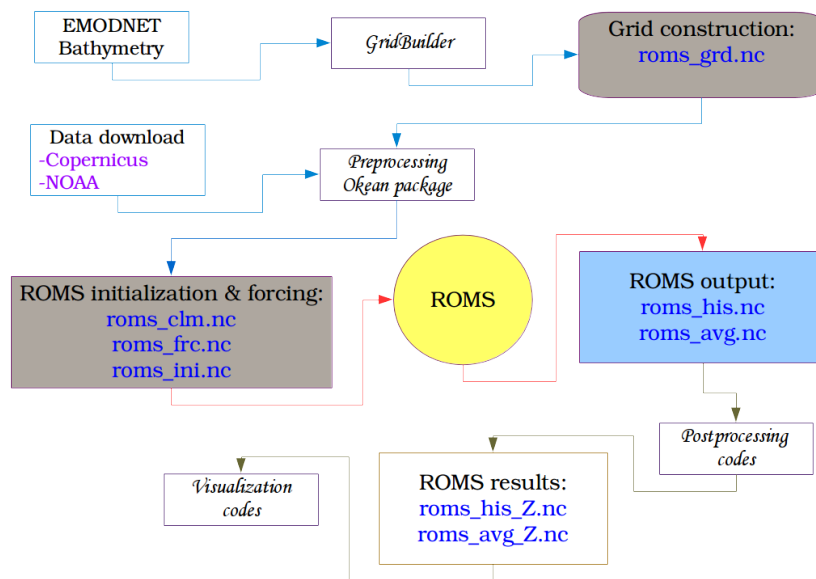


Figure 3.2: ROMS-AGRIF model implementation.

To perform a regional simulation using ROMS, the modeler needs to provide several data files like horizontal grid, bottom topography, surface forcing, lateral boundary conditions. These data files should be available in binary netcdf format.

Specifically the required files are

³ AGRIF details and code, are available at <http://www-ljk.imag.fr/MOISE/AGRIF/index.html>

- roms_grd.nc, the bathymetry file
- roms_clm.nc, the climatology file
- roms_frc.nc, the surface forcing file
- roms_ini.nc, the initialization file

The information required for the construction of these files, can be obtained from various (but limited) sources of geophysical data, freely available on the web. In this case the bathymetry obtained from the EMODNET portal, the hydrological climatology from the Copernicus marine portal and the atmospheric data (radiation fluxes and winds) from the NOAA Global Forecast System (GFS) portal.

ROMSTOOLS have been introduced as a collection of ready-made tools aimed to cover every aspect of initialization and preprocessing requirements. However, practice shown that much better results can be obtained by the use of some additional software applications.

The most important data file is the bathymetry one, that contains the spatial information over which all the data should be interpolated (Table 3.3). The *GridBuilder* MATLABTM toolbox (Austides-Consulting 2014), has been used to generate this file for the Cyprus – Levantine model.

The climatology, surface forcing and initialization data files, has been produced based on the Python *ocean* package (Marta-Almeida, Ruiz-Villarreal, Otero, Cobas, Peliz, Nolasco, Cirano, and Pereira 2011; Marta-Almeida 2018), after significant code changes, in the ROMS handling sources.

Data download and AGRIF nesting were applied based on the ROMSTOOLS, again after modifications to the download codes, extending them to include access to the Copernicus marine portal and fixing the NOAA GFS sites according their recent specifications.

In appendix (A) a detailed description of the configuration files and their meaning is provided. Furthermore, *post-processing* procedures, targeting to the visualization and the interpretation of the model's results are included.

Table 3.3: Bathymetry data 2-D variables used by ROMS-AGRIF model.

Variable	Description and units
angle(eta_rho, xi_rho)	angle between xi axis and east [degrees]
h(eta_rho, xi_rho)	Final bathymetry at RHO-points [m]
hraw(bath, eta_rho, xi_rho)	Working bathymetry at RHO-points [m]
alpha(eta_rho, xi_rho)	Weights between coarse and fine grids at RHO-points [-]
f(eta_rho, xi_rho)	Coriolis parameter at RHO-points [s^{-1}]
pm(eta_rho, xi_rho)	curvilinear coordinate metric in XI [m^{-1}]
pn(eta_rho, xi_rho)	curvilinear coordinate metric in ETA [m^{-1}]
dndx(eta_rho, xi_rho)	xi derivative of inverse metric factor pn [m]
dmde(eta_rho, xi_rho)	eta derivative of inverse metric factor pm [m]
x_rho(eta_rho, xi_rho)	x location of RHO-points [m]
x_u(eta_u, xi_u)	x location of U-points [m]
x_v(eta_v, xi_v)	x location of V-points [m]
x_psi(eta_psi, xi_psi)	x location of PSI-points [m]
y_rho(eta_rho, xi_rho)	y location of RHO-points [m]
y_u(eta_u, xi_u)	y location of U-points [m]
y_v(eta_v, xi_v)	y location of V-points [m]
y_psi(eta_psi, xi_psi)	y location of PSI-points [m]
lon_rho(eta_rho, xi_rho)	longitude of RHO-points [degrees east]
lon_u(eta_u, xi_u)	longitude of U-points [degrees east]
lon_v(eta_v, xi_v)	longitude of V-points [degrees east]
lon_psi(eta_psi, xi_psi)	longitude of PSI-points [degrees east]
lat_rho(eta_rho, xi_rho)	latitude of RHO-points [degrees north]
lat_u(eta_u, xi_u)	latitude of U-points [degrees north]
lat_v(eta_v, xi_v)	latitude of V-points [degrees north]
lat_psi(eta_psi, xi_psi)	latitude of PSI-points [degrees north]
mask_rho(eta_rho, xi_rho)	mask on RHO-points [0=land, 1=water]
mask_u(eta_u, xi_u)	mask on U-points [0=land, 1=water]
mask_v(eta_v, xi_v)	mask on V-points [0=land, 1=water]
mask_psi(eta_psi, xi_psi)	mask on PSI-points [0=land, 1=water]

CHAPTER 4

ROMS-AGRIF NUMERICAL OCEAN MODEL APPLICATION OVER EASTERN MEDITERRANEAN AND LEVANTINE SEA.

In this chapter it is presented a case study of implementation of the ROMS-AGRIF marine dynamics numerical model over the Levantine and Cyprus sea.

4.1 Introduction

The Mediterranean Sea covers an area of approximately $2.5 \times 10^6 \text{ km}^2$, which is 0.82% of the surface area of the world's oceans, and contains 0.32% of the volume of global water. The coast extends to approximately 4700 km and the average depth is 1.5 km. The maximum depth in the Ionian Sea is 5.1 km. The passage (narrow, sill) Sicily Tunisia, with 400 m depth, divides the Mediterranean basin into two major discrete sub-basins, western and eastern, and acts as a geographical and hydrological boundary.¹

The Eastern Mediterranean basin contains four (4) distinct sub-basins: the Ionian Sea, the Levantine Sea, the Adriatic Sea and the Aegean Sea. The Levantine Sea occupies part of the central and eastern region of the eastern basin. The Levantine Sea has depths of 2500-3000 m in its center and a maximum depth of 4500 m in a fault located southeast of Rhodes.

Since 2002 the oceanographic processes of the Eastern Mediterranean Levantine Basin, which covers the coastal and open sea of Cyprus, Cilician and Lattakian basins and the Eastern Levantine Base, have been examined by means of Cyprus Coastal Ocean Forecasting and Observing System (CYCOFOS, Zodiatis, Lardner, Georgiou, Demirov, Manzella, and Pinaridi 2003; Zodiatis, Lardner, Hayes, and Georgiou 2006; Zodiatis, Lardner, Hayes, Georgiou, Sofianos, Skliris, and Lascaratos 2008), a sub-regional forecasting system, based on Princeton Ocean Model (POM, Blumberg and Mellor 1987),

¹This chapter has been presented during the Seventh International Conference on Remote Sensing and Geoinformation of Environment, held on 18–21 March, 2019 in Cyprus. Also presented as a poster in the EGU General Assembly 2019, in Austria on 7–12 April 2019.

The Oceanography Center of the University of Cyprus, maintains a web page, with the daily results of the model publicly available².

ROMS-AGRIF (Regional Ocean Model System, Adaptive Mesh Refinement In Fortran; Shchepetkin and McWilliams, 2005; Penven et al, 2006; Debreu et al., 2011) is a free surface, hydrostatic primitive equations ocean model with terrain-following vertical coordinates that allow differential stretching (Shchepetkin and McWilliams, 2005; Haidvogel et al., 2008). It is an open source parallel Fortran code coupled to several models including biogeochemistry, waves, sediments, bio-optical and sea ice. It offers great flexibility for configuration and is widely used by the scientific community for a diverse range of applications.

The objective of the present work is to use for the first time the ROMS-AGRIF over the same area and make comparisons with the CYCOFOS model.

Both models are using initial and boundary conditions from Marine Copernicus Portal data and surface fluxes from NOAA Global Forecast System.

4.2 Methodology

4.2.1 The CYCOFOS model

CYCOFOS ocean forecasting system has been described in detail by Zodiatis et al., 2003; 2005; 2008. It is a well-known and mature ocean model that has been proved reliable and accurate for many years. Until recent days, is successfully following the developments of numerous European research projects (such as the MFSTEP, ECOOP, MyOcean, etc) developing and promoting the operational oceanography, and it is also related to operational oceanographic initiatives, such as EuroGOOS, MONGOOS, MedGLOSS and Copernicus-GMES.

In general the model has a free surface and a split time step. The external mode portion of the model is two-dimensional and uses a short time step based on the Courant-Friedrich-Levy (CFL) condition and the external wave speed. The internal mode is three-dimensional and uses a long time step based on the CFL condition and the internal wave

²(<http://www.oceanography.ucy.ac.cy/cycofos/bulletin.html>)

speed. It contains a turbulence closure sub-model (Mellor - Yamada 2.5; Mellor, 1998) to provide vertical mixing coefficients, based on Princeton Ocean Model Blumberg and Mellor 1987.

The horizontal grid, constructed of 374 x 355 cells with a resolution of 1852 m (1 nautical mile), uses curvilinear orthogonal coordinates and an "Arakawa C" differencing scheme. The vertical coordinate system is scaled on the water column depth, in a terrain following sigma coordinate system of 30 levels.

4.2.2 The ROMS model

The Regional Ocean Modeling System (ROMS) is a split-explicit, free-surface oceanic model, which solves the Primitive Equations (momentum equations, hydrostatic continuity, tracer conservation and the equation of state), using the Boussinesq approximation and the hydrostatic vertical momentum balance. Following the Hedström (2000) notation, and with $\rho_0 = 1025 \text{ kg m}^{-3}$ as reference density, Du, Dv, DT, DS are the diffusive terms, Fu, Fv, FT, FS are the forcing terms, $f(x, y)$ is the *Coriolis* term, $g = 9.81 \text{ m s}^{-2}$, is the gravity acceleration, $h(x, y)$ is the bottom depth, $P = -\rho_0 g z$ is the hydrostatic (total) pressure, $\phi = P/\rho_0$ is the dynamic pressure, S is the salinity term, T is potential temperature, t is time, u, v, w are the x, y, z components of the vector velocity, where x and y are the horizontal coordinates and z is the vertical coordinate. The equations of motion are described by the equations (4.1) to (4.7):

$$\frac{\partial u}{\partial t} + \vec{v} \cdot \nabla u - fv = \frac{-\partial \phi}{\partial x} + F_u + D_u \quad (4.1)$$

$$\frac{\partial v}{\partial t} + \vec{v} \cdot \nabla v + fu = \frac{-\partial \phi}{\partial y} + F_v + D_v \quad (4.2)$$

$$\frac{\partial T}{\partial t} + \vec{v} \cdot \nabla T = F_T + D_T \quad (4.3)$$

$$\frac{\partial S}{\partial t} + \vec{v} \cdot \nabla S = F_S + D_S \quad (4.4)$$

$$\rho = \rho(S, T, P) \quad (4.5)$$

$$\frac{\partial \phi}{\partial z} = \frac{-\rho g}{\rho_0} \quad (4.6)$$

$$\frac{\partial u}{\partial x} + \frac{\partial v}{\partial y} + \frac{\partial w}{\partial z} = 0 \quad (4.7)$$

In the above equations, u, v, T and S are prognostic and the w, P and ρ are diagnostic variables.

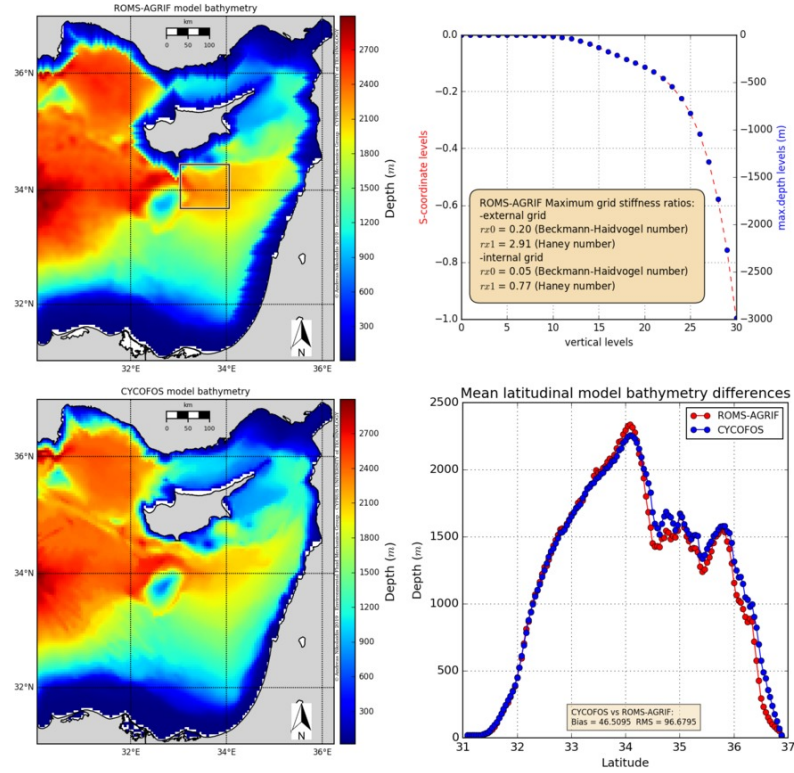


Figure 4.1: ROMS-AGRIF and CYCOFOS model bathymetries and their longitudinal differences (bottom right). On the top right is shown the ROMS vertical coordinate levels in S-coordinates and their analogy at the maximum depths. On the top left, the rectangular shows the internal higher resolution nested grid.

ROMS model, uses short 2-way time-averaging time steps to advance the ssh and the 2D barotropic momentum equations, while much larger time steps used for temperature, salinity, and the rest 3D variable equations of the baroclinic momentum. This is done with a discretized third-order accurate predictor (Leap-Frog) and corrector (Adams-Molton) time-stepping algorithm. Subgrid scale vertical mixing processes are solved with K-Profile Parameterization (KPP) boundary-layer scheme.

The horizontal grid is using curvilinear orthogonal coordinates and an "Arakawa C" differencing scheme. Vertical coordinates are terrain-following sigma coordinates, with a special smoothing scheme, based on Beckman-Haidvogel rx_0 and Haney rx_1 numbers

(Song and Haidvogel, 1994).

On this case, two grids were nested using the AGRIF algorithms for real-time down-scaling access, which are included the ROMS model. The horizontal external grid is constructed with 122 XI x 142 ETA cells in a resolution of 4558 to 4716 m for the external grid and on 62 XI x 56 ETA cells with resolution of 1537 to 1550 m for the internal. In both cases 30 sigma levels were used. Both CYCOFOS and ROMS models were developed over the area that is defined by the geographical coordinates, 30.05° E to 36.25° E longitude and 30.99° N to 36.96° N latitude.

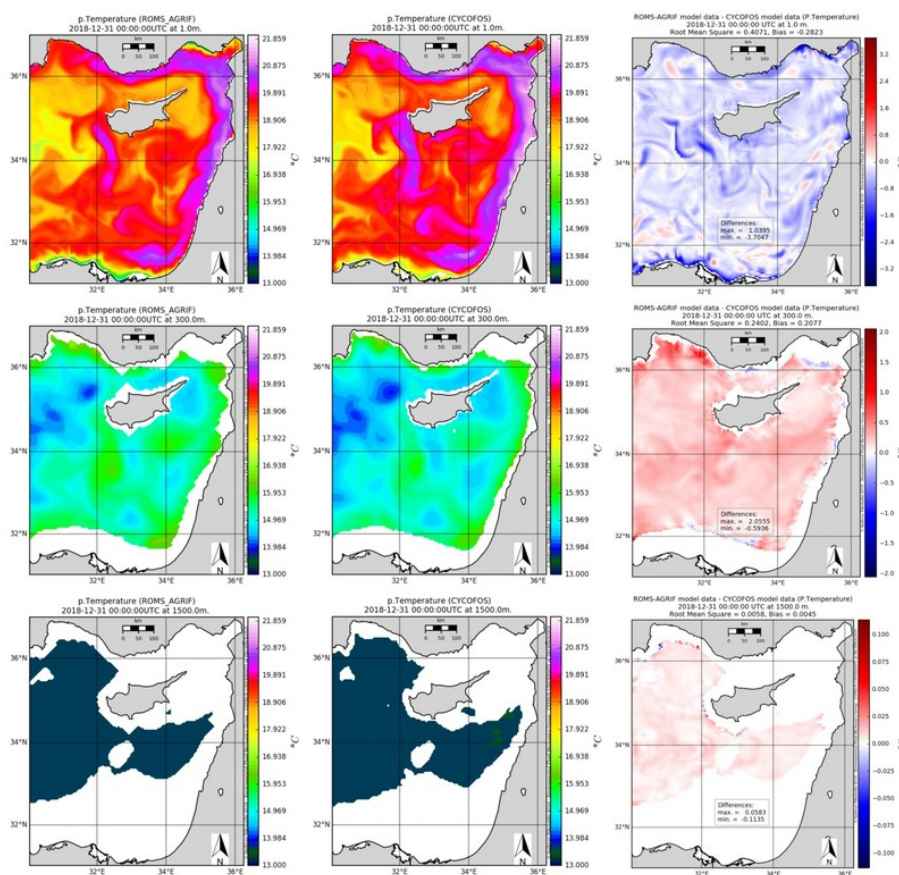


Figure 4.2: ROMS-AGRIF and CYCOFOS potential temperature results for the December 31st, 2018, at surface, 300 and 1500 m.

Figure 4.1 shows the model bathymetries with their differences. The differences were mainly caused by the smoothing preprocess. In future versions there will be an effort to reduce this effect. The bias and root mean square (RMS) statistical measures used are shown in equations (4.8), where x are the reference values and y the observed over a population of N values.

$$BIAS = \frac{1}{N} \sum_N (y - x) \quad RMS = \sqrt{\frac{1}{N} \sum_N (y - x)^2} \quad (4.8)$$

The model has been used for a duration of nine (9) days in forecast mode, starting from December 29, 2018 until January 6, 2019.

4.2.3 ROMS model setup and compilation

ROMS-AGRIF grid has been prepared with the aid of the MATLAB® *GridBuilder Toolbox* (freely provided by Austides Consulting). The internal grid contraction was made with the MMATLAB® ROMSTOOLS (Penven, 2003) *nestgui* utility. The pre-process and the production of the required initialization, climatological and forcing data were prepared with a modified version of the Python language ‘*ocean*’ package (ocean modelling and analysis tools; Marta-Almeida et al., 2011).

After some modifications to the original source code, the model was compiled with the Portland PGI Community Edition Version 18.10 (PGI, 2018) FORTRAN compiler, with shared memory parallelization (OpenMP) option enabled.

4.3 Results and comparison

4.3.1 CYCOFOS and ROMS-AGRIF

Comparisons on the results of CYCOFOS and ROMS-AGRIF model show that the observed differences between them vary, depending to the horizontal level and the time step. Such differences are shown in Figures 4.2, 4.3 and 4.4, for the potential temperature, salinity and current magnitude and direction respectively, for December 31st, 2018.

Potential temperature bias appeared to be between 0.4 in the surface to 0.005 and even less at depths below 1500 m. Salinity bias appeared to be between 0.002 in the surface to 0.0002 and less below the 1500 m and current magnitude bias is between 0.002 and 0.0002. RMS values appeared between -0.02 to 0.004 for surface potential temperature, 0.06 to 0.001 for salinity and 0.07 to 0.007 for current magnitude. Similar results were obtained for all the time steps. Figures 4.5, 4.6 and 4.7 show potential temperature at

1500 m, salinity at 650 m and surface currents for January 5th, 2019.

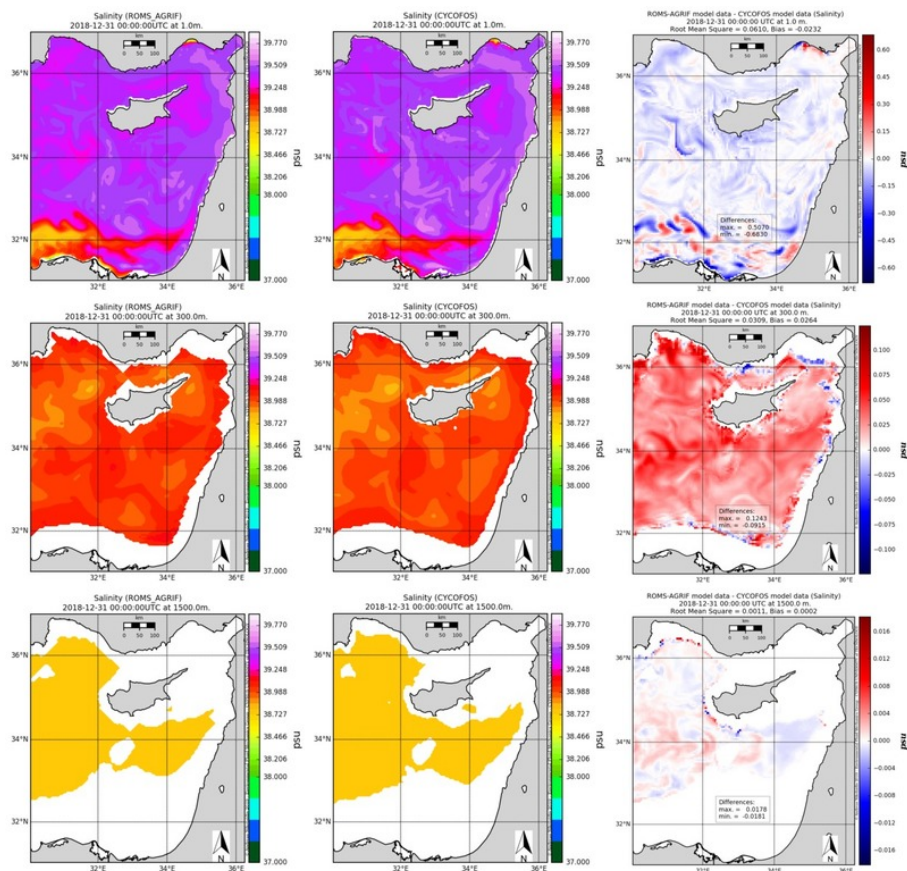


Figure 4.3: ROMS-AGRIF and CYCOFOS salinity results for the December 31st, 2018, at surface, 300 and 1500 m.

All comparisons were made using the average daily results. CYCOFOS results were projected on the lower resolution ROMS-AGRIF grid.

Using the package ‘*Goodness of Fit*’ (GoF; Holst, 2012) of the statistical processing software R, nineteen (19) statistical tests were performed over the time series of surface temperature and salinity for all the available period (Figure 4.8). Even though the various indicators like the Pearson’s correlation coefficient $r=0.97-0.98$ for both time series are in same levels, deviation appear to increase with time.

4.3.2 ARGO Floats profiles vs Model results

Publicly available data of ARGO Floats were obtained from USGODAE Argo GDAC Data repository. For the period under examination two (2) floats were operational. Float 6902770 provided data for December 31st, 2018 and float 6901773 for January 5th, 2019.

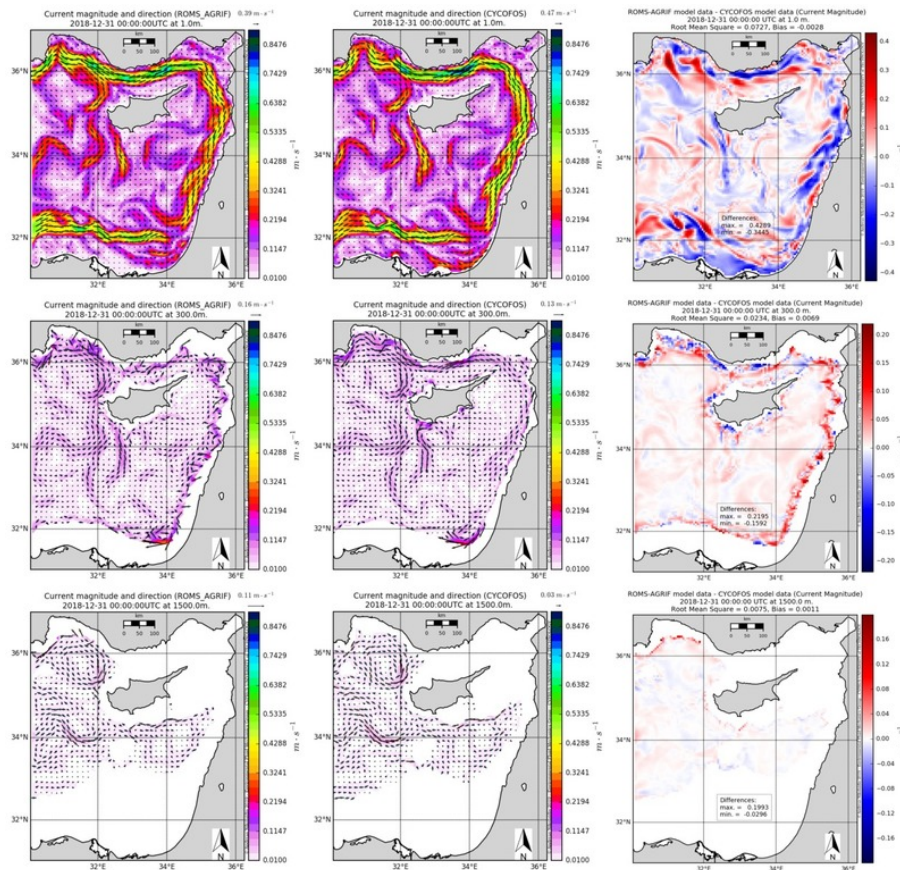


Figure 4.4: ROMS-AGRIF and CYCOFOS current magnitude and direction results for the December 31st, 2018, at surface, 300 and 1500 m.

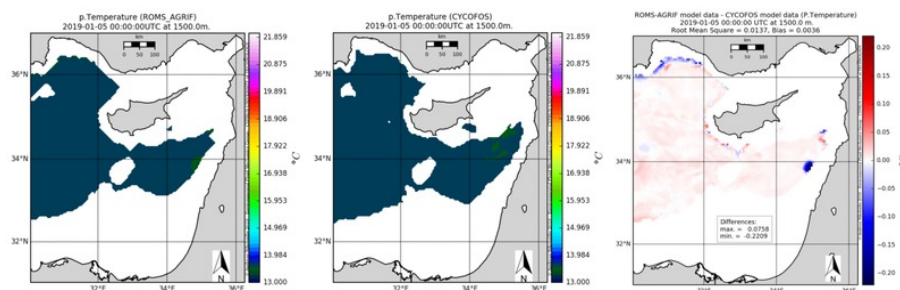


Figure 4.5: ROMS-AGRIF and CYCOFOS potential temperature results for the January 5th, 2019, at 1500 m.

Figure 4.9 shows the comparison between the model results and the in-situ reported data. It should be noted that the comparisons were made between the average daily profiles of the models and at the closest grid position.

The profiles of December 31st, 2018, indicate that the models overestimate the surface values of both temperature, by about $0.4\text{ }^{\circ}\text{C}$, and salinity, by about 0.06 psu , and below the 100 m of depth, start underestimation at the same value ranges. Below a depth of 650 m model values are almost identical and converge to the float profile results, with an

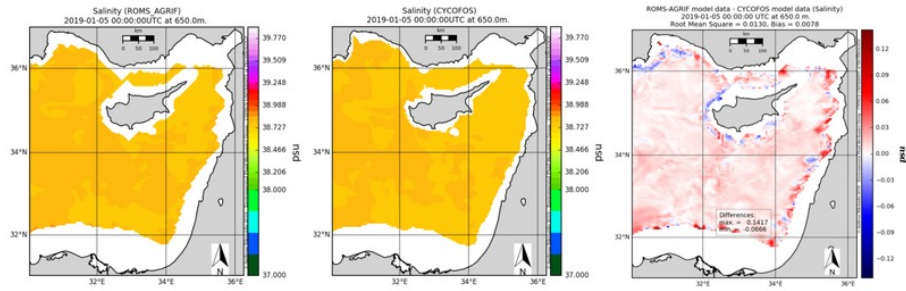


Figure 4.6: ROMS-AGRIF and CYCOFOS salinity results for the January 5th, 2019, at 650 m.

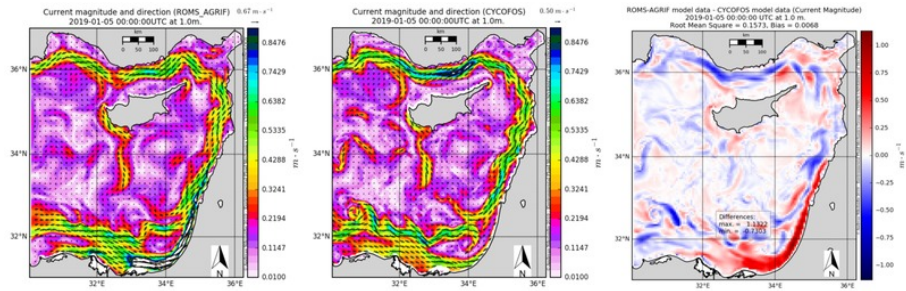


Figure 4.7: ROMS-AGRIF and CYCOFOS surface current magnitude and direction results for the January 5th, 2019.

exception of the temperature value at the maximum depth. ROMS-AGRIF values seem closer to the float's profile values.

The comparison of the results for January 5th, 2019 with the ARGO float data reveal that both models underestimate the surface temperature. The deviation was 0.6 °C for ROMS-AGRIF while CYCOFOS's deviation was 0.08 oC. However, below a depth of 150 m model profiles start to converge, with the ROMS-AGRIF values closer to the float's profile values.

Figures 4.10 and 4.11, shown the precise locations of the ARGO floats. In the included T-S diagrams the diapycnal mixing of the water masses is identified in all results, supporting their similarity.

4.4 Discussion and conclusions

The comparisons between ROMS-AGRIF and CYCOFOS models suggest that both models produce similar results. Differences were expected, mainly due to bathymetry divergence, however, the influence was not so strong. Although the ROMS-AGRIF model run on a lower resolution grid, the results obtained were almost identical with the results of

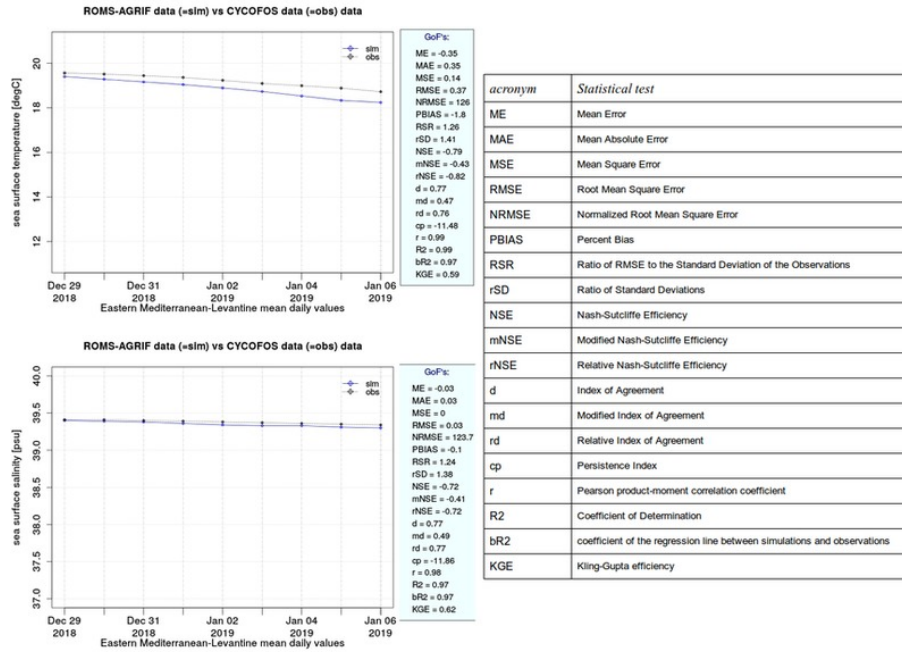


Figure 4.8: Surface Temperature and Salinity ‘Goodness of Fit’ (GoF) statistical tests (Holst, 2012) for the period December 29th, 2018 until January 6th, 2019.

the higher resolution CYCOFOS model. This implies that a grid of about 5 km resolution is accurate enough to describe the area circulation, since the Rossby radius of deformation in the Mediterranean is of the order of 10 to 15 km. However, higher resolution sometimes is required in order to describe small-scale spatial phenomena, such as small scale eddies. This can be obtained for specific areas, with nested grids in ROMS-AGRIF, without the requirement of finer grid over the full area and with the additional benefit of real time interaction on the boundary layers. Comparisons of ARGO float profile data with model profiles showed significant differences to the upper layers for both models. This can be attributed to the 4 to 9 hours difference between the chosen samples. More important are the water masses patterns shown in Figure 4.11, where the similarities are obvious. ROMS-AGRIF model results appeared to be closer to the in-situ profile values. For the above reasons it is suggested that the new ROMS-AGRIF model implementation can be used efficiently for operational oceanographic forecasts for the area of Eastern Mediterranean and the Levantine sea around Cyprus.

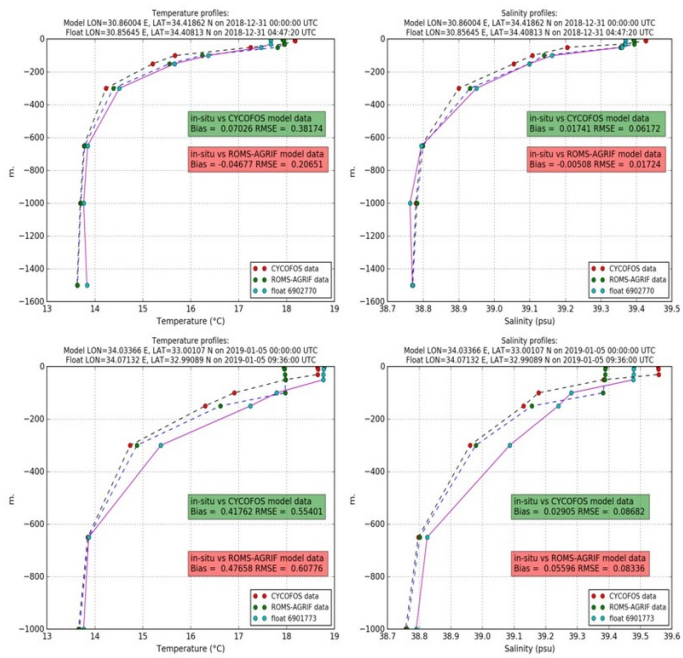


Figure 4.9: ARGO floats (in-situ), CYCOFOS and ROMS-AGRIF vertical temperature and salinity profile comparison.

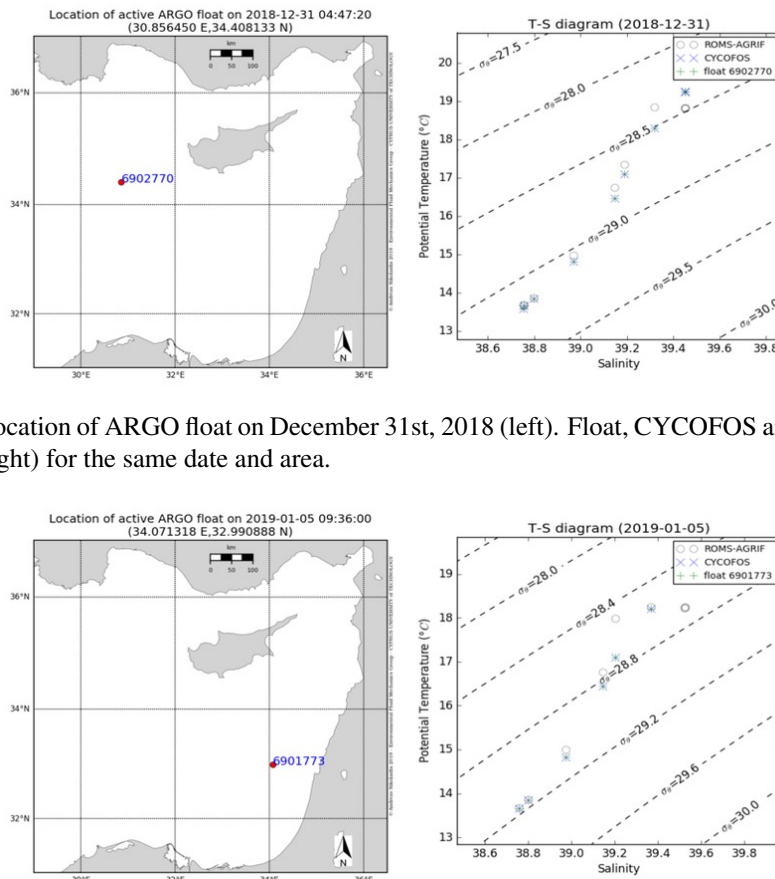


Figure 4.10: Location of ARGO float on December 31st, 2018 (left). Float, CYCOFOS and ROMS-AGRIF T-S diagram (right) for the same date and area.

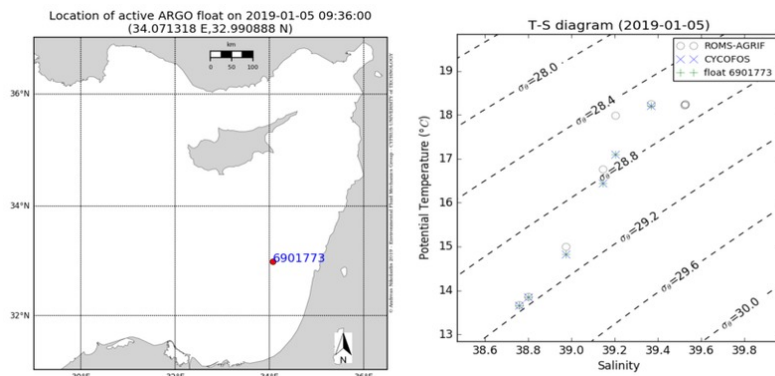


Figure 4.11: Location of ARGO float on January 5th, 2019 (left). Float, CYCOFOS and ROMS-AGRIF T-S diagram (right) for the same date and area.

CHAPTER 5
APPLYING A DINEOF ALGORITHM ON CLOUDY SEA-SURFACE
TEMPERATURE SATELLITE DATA OVER THE EASTERN
MEDITERRANEAN SEA

In this chapter it is presented the DINEOF algorithm. A case study of the algorithm implementation over Levantine is included.

5.1 Introduction

Let us consider a basin filled with water whose surface is oscillating. To describe this surface wave we should note the position of every water particle at every moment, which rapidly generates a huge amount of data. During the last decades there has been considerable effort to find simple (usually referred as '*empirical*') functions, describing satisfactorily such a system.¹

The most common approach is using a spatial function which gives the form of the wave at a given moment and a temporal function which characterizes the variation of the wave over time. Determining these functions then allows one to bypass severe data accumulation. In geophysics, a well known and used method (introduced by Lorentz at 50's) for this, is the geographically weighted *Principal Component Analysis (PCA)*, which normally is referred to, as *empirical orthogonal functions (EOFs)*.

Specifically, PCA is defined as an orthogonal linear transformation that maps the data to a new coordinate system such that the greatest variance by any projection of the data comes to lie on the first coordinate (called the first principal component), the second greatest variance on the second coordinate, and so on. EOFs can present different physical meanings, like coherent spatial patterns with maximum variance, modes of energy, even just convenient mathematical abstractions, depending on the nature of the problem.

¹This chapter has been published in 2014 to the Central European Journal of Geosciences, 6(1), pp.27-41.

Backers and Rixen (2003) demonstrated an innovative EOF method that does not need any a priori knowledge of a correlation function or correlation length, of the data. Due to the iterative nature of the algorithm, any inhomogeneity or non-isotropic behavior is automatically taken into account, generating an interpolation effect, hence the name *Data Interpolating Empirical Orthogonal Functions (DINEOF)*. An adaptation to handle the large data sets (typical of satellite imagery) can be found in Alvera-Azcárate et al. (2005).

Filling the gaps, generated by the existence of clouds, rain, or simply due to incomplete track coverage of upper atmospheric layers, is one of the most common problems, faced during the processing of satellite data. Many methods have been tested out over the years for solving this problem, with different results, regarding the field of application and the expertise of the scientists involved. Notable examples, are the *Data-Interpolating Variational Analysis (DIVA)* that allows the spatial interpolation of data (analysis) in an optimal way, and the optimal interpolation method Troupin et al. (2012). However, the DINEOF method is simply faster.

Optimal Interpolation (OI) is the best known and the most classical method. The main problem is the demanding calculating time. For a typical ensemble of data, DINEOF is an innovative method, 30 times faster than OI. This acceleration is a direct consequence of the different statistical methodology between the two different approaches. In particular DINEOF constitutes a procedure that fills gaps by iteratively decomposing the data field via *Singular Value Decomposition (SVD)* until a best solution is found as compared to a subset of reference values (non-gaps). This is done by progressively including more EOFs in the reconstruction of the missing locations until minimization of error converges.

In this section, we will describe the application of the DINEOF method in order to reconstruct a fully filled satellite derived sea surface temperature (SST) field, for the area of Eastern Mediterranean, Levantine sea and Cyprus coasts. SST is a physical parameter commonly used in most oceanographic and meteorological applications Giannakopoulos, Good, Law, Wang, Akylas, and Koussis 2004 and among others is a principal factor for relevant arithmetic model calibration, assimilation and initialization (Akylas, Tombrou, Lalas, and Zilitinkevich 2001, Akylas, Tsakos, Tombrou, and Lalas 2003, Akylas and

Tombrou 2005). DINEOF is applied for the first time over the specific area of Eastern Mediterranean Sea, a step which is crucial, both for the research as for the operational implementation of the method. The structure of this work is as follows. In subsection 5.2 a description of the DINEOF method and of the corresponding algorithm is given. Subsection 5.3 describes the application of the method in Eastern Mediterranean Sea. Finally in subsection 4 the results of the implementation are analyzed and discussed.

5.2 Description

By using the EOF method one is able to identify a set of orthogonal spatial modes, such that, when ordered, each successive eigenvector explains the maximum amount possible of the remaining variance in the data. Each eigenvector pattern is associated with a series of time coefficients that describe the time evolution of the particular spatial mode. The eigenvector patterns that account for a large fraction of the variance are, in general, considered to be physically meaningful and connected to important 'centers of action'.

The EOFs can be regarded as eigenvectors, which are aligned so that the leading EOFs describe the spatially coherent pattern that maximizes its variance Peixoto and Oort 1992. EOFs are often used as functional basis (a new set of axes or reference frame), providing a convenient method for studying the spatial and temporal variability of long time series of data, over large areas. The method splits the temporal variance of the data into orthogonal spatial patterns called empirical eigenvectors. The EOF analysis may be thought of as being analogous to data reconstruction based on Fourier transforms (FT), in the sense that both produce series (vectors) which form an orthogonal basis. In the following, we briefly summarize the mathematical principles of the algorithm.

5.3 PCA-SVD-EOF

Principal Component Analysis (**PCA**), tries to explore the question 'can our data set be expressed in one other basis which is a linear combination of our current basis?' The answer to the above identifies the existence of linearity, noises, and correlations of given data. In order to explain the way this method works, one may assume two data sets

$A = \{a_1, a_2, a_3, \dots, a_n\}$ and $B = \{b_1, b_2, b_3, \dots, b_n\}$, $n \in \mathbb{N}^*$. Their variances will be $\sigma_A^2 = \frac{1}{N} \sum_i^N (a_i - \mu_A)^2$ and $\sigma_B^2 = \frac{1}{N} \sum_i^N (b_i - \mu_B)^2$ respectively, where $\mu_A = \frac{1}{N} \sum_i^N a_i$ and $\mu_B = \frac{1}{N} \sum_i^N b_i$ are the mean values of the data sets. Hence the covariance between A and B sets will be $\sigma_{AB}^2 = \frac{1}{N} \sum_i^N (a_i - \mu_A)(b_i - \mu_B)$. The covariance matrix is a measure of the degree of linear relationship between two variables. In other words, it is a measure of the proportion of the variance of a set that can be explained, through a linear relation, from the respective variance of the other one. A large positive value indicates positively correlated data. On the other hand a large negative value denotes negatively correlated data. The absolute magnitude of the covariance measures the degree of redundancy between the data sets.

If σ_{AB} is zero, then sets A and B are uncorrelated. The equality $\sigma_{AB}^2 = \sigma_A^2 = \sigma_B^2$ holds if and only if, $A = B$. All the methods applied here yield a finite number of modes that represent the covariance matrix of the data. Its rows and columns indicate the covariance (or correlation) between the time-series at a given station or grid-point of one field and the time-series at all stations or grid-points of the other field. Singular-Value Decomposition (**SVD**) analysis offers the same types of normalizing and scaling options as EOF analysis (e.g., it can be based on either the covariance matrix or the correlation matrix.). Each mode in the analysis is identified by an eigenvalue (a positive definite number which defines its rank and relative importance in the hierarchy of modes), an eigenvector or Empirical Orthogonal Function (**EOF**, a linear combination of the input variables in the domain of the structure), and a principal component (PC) which documents the amplitude and polarity of that structure in the domain of the sampling. It should be noted that a common measurement of the feasibility of the PCA application is the *Signal-To-Noise* (**SNR**) ratio. SNR is defined as $SNR = \frac{\sigma_{signal}^2}{\sigma_{noise}^2}$ which in practice is the ratio of the variances. A high SNR ($SNR \gg 1$) indicates a high precision measurement, while a low SNR indicates very noisy data (Shlens, 2009). If PCA is made by using Singular Value Decomposition (SVD) then the output consists of the eigenvalues plus two rectangular matrices. Which one should be labeled the Empirical Orthogonal Function (EOF) matrix and which one the Principal Components (PC) matrix depends upon the context of the

analysis.

5.4 The algorithm

Recalling the description given by Alvera-Azcarate et al. (2009), we consider a $M \times N$ matrix X , M being the spatial size and N the temporal size. Anomalies are computed and the missing data are initialized to the mean (i.e. to a zero anomaly). Initially the most dominant EOF mode of this matrix is obtained, and the missing data are calculated by means of

$$X_{m,n} = U \cdot S \cdot V^T \quad (5.1)$$

where $m = 1, \dots, M$ and $n = 1, \dots, N$. U is a $M \times R$ matrix representing the spatial EOF nodes, the spatial EOF modes, V^T is a $N \times R$ matrix containing the temporal modes, and S is a $R \times R$ matrix containing singular values. The value $R \leq \min(m, n)$ is the *rank* of the X matrix. For the reconstruction of X , only the most significant spatial and temporal EOF is used. The new estimation of X for the missing data is reintroduced in the data matrix, and the EOF mode calculation is repeated. This process is continued in a successive way until the convergence of the missing values, and then the EOF modes calculated are increased to two, then to three, etc. The EOF mode calculation is succeeded using a Lanczos solver provided by the **ARPACK** free software Lehoucq, Sorensen, and Yang 1997. A major improvement of the latest DINEOF version, is the ability of outlier detection, provided by the ratio between the analysis residuals and their expected standard deviation,

$$O_i = \frac{X_i^a - X_i^o}{\Delta_i} \quad (5.2)$$

for non-missing X_i^o , where $i = 1, \dots, M$ is the spatial index, X_i^a is the new value, as created by DINEOF, X_i^o is the original given value, and Δ_i is the expected misfit, calculated by

$$\Delta_i = \sqrt{\mu_{eff}^2 - \sum_{i,k} E_{i,k}^2} \quad (5.3)$$

In the above, $i = 1, \dots, N$ is the number of EOFs used from the algorithm for the reconstruction, while $k \ll N$ are all the used modes. Parameter is an estimation of the average

noise of the initial field, obtained as a cross-validation error. The expected error E_{ik} of each i -position is calculated by

$$E = L_p S_c \text{ with correlation matrix } C = S_c S_c^T \quad (5.4)$$

where L_p is constructed by $m \times N$ columns of the spatial EOFs multiplied by the corresponding singular values and S_c is the $N \times N$ *Cholesky factorization* of the C correlation matrix. More details on the mathematical procedure can be found in Alverta-Azcarate et al. (2011). In Figure 5.1, the outline of the implementation of the DINEOF algorithm is presented.

The optimal number of EOFs needed to calculate the missing is determined by cross-validation: a small percentage of valid data (typically 1% of the total data) is initially set apart and flagged as missing. Once convergence is reached for a given number of EOF modes, a root mean square error is calculated between the newly obtained estimate and the initial data set. The number of modes that minimizes this error is considered as optimal. It is notable that not all modes need to be calculated, as one can observe that when the error increases steadily for three (3) consecutive modes, a minimum has been reached Alverta–Azcarate et al. (2012). The optimal number of EOF modes retained are calculated by cross-validation (i.e., a few valid data are set aside and the error of the reconstruction is assessed by comparing the reconstructed data to these cross-validation data).

For an extended description of DINEOF, and similar developments, the reader is referred to Beckers and Rixen (2003), Alverta-Azcarate et al. (2005,2007), and Beckers et al. (2006.)

5.5 Application

The DINEOF algorithm is successfully implemented over the Western Mediterranean in a continuous basis by the GeoHydrodynamics and Environment Research, a research group of the University of Liège, producing daily cloud-free SST for that area Alverta–Azcarate et al. (2011). The scope of the present work is the extension of the DINEOF algorithm

application over the Eastern Mediterranean Sea. Until now there is no known procedure which, on a systematic basis and for the full area covering the Levantine Sea and the Cyprus coasts, recovers missing data from satellite images. However, cloud-generated noise is frequent, especially during winter and spring, resulting in incomplete information, which is important for many applications. The present application aims at recovering missing SST data from sparsely covered satellite images. The data refer to SST measured twice per day at 10:00 am and 20:00 pm GMT and cover the area from southern Italy to Middle East (Figure 5.2). The data are collected collaboratively by Meteo-France and the Norwegian Meteorological service (DNMI) just 2 hours after the last satellite data acquisition. This data is available on the IFREMER Medspiration site with a 24 hour delay. The same type of data, L3 from MERIS satellite products, is used for the aforementioned Western Mediterranean project.

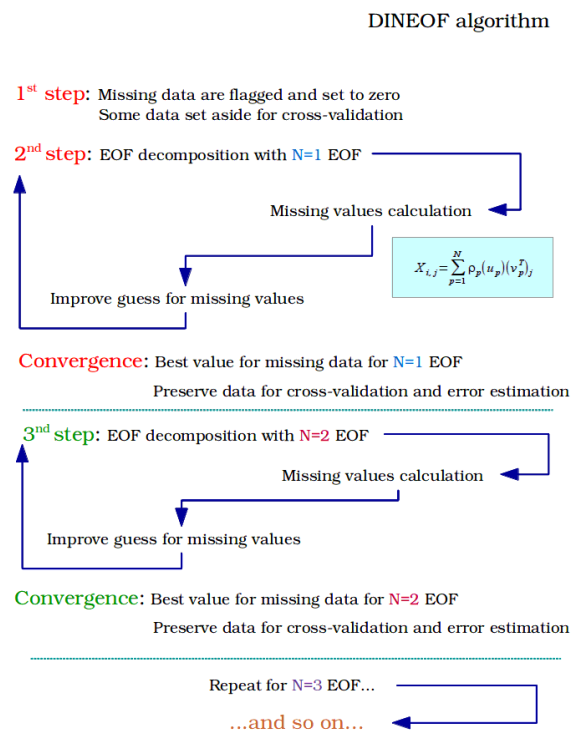


Figure 5.1: DINEOF algorithm iterative scheme (based on Alvera-Azcárate et al., 2011).

A typical example of initially incomplete data is shown in Figure 5.2(left), for the 11th of January 2013. In order to recover the missing information, DINEOF code version 3.0,

provided by GHER web site, has been used. Although in the case of the Eastern Mediterranean the application is based on a long term sample collection, in this work we have chosen to perform the experiment only in a 4 days period from 9th to 12th January 2013 (Figure 5.3). It is suggested that the induction of the sample size, accelerates markedly the procedure without affecting seriously the accuracy. The effectiveness of the application can be more clearly shown, if one separates a rather “empty” input image, and provides the corresponding result in Figure 5.2 right). The explanation of the regeneration is the fact that all the available steps have been taken into account in order to reproduce the area coverage. It is suggested that the longer the time-series available, the better results can be obtained, in relation to the covered area Alvera–Azcarate et al. (2009). However, a question regarding the quality and the validity of the generated results and their dependence on the sampling size still remains. In our opinion, the reduction of the sampling size in terms of its dependence on the long-past data offers, a less biased reproduction of rapid local changes. Nevertheless, a “first-guess” information exists, where no information was appeared. That is, at least, a strong evidence of the dominant factors around the area of interest. The results of the present application on a 12-hour basis from 9th to 12th January 2013 are given in Figure 5.3. It should be underlined that heavily cloudy data, between 11th and 12th of January could easily led to extreme values and corruptions to the sea-surface temperature field. The accuracy obtained with the DINEOF application, as it will be shown, is mainly due to two reasons: the filtering of spikes on the temporal EOFs, and the standard number of EOFs that were retained in the Eastern Mediterranean Sea. For the current application the same model set-up parameters have been used for all the cases. After several different runs and continuous testing it has been concluded that calculations keeping five (5) EOF modes using the application’s default threshold (10-8), without modifying the existing data (at the original satellite images) and without normalization of the results, rendered the most satisfactory results. The results were obtained by using the five first EOFs in the area under consideration, which implies that this is the best choice allowing for a reconstruction and capturing even the small scale variability. It is known, that the higher order EOFs do not only contain small-scale information, but

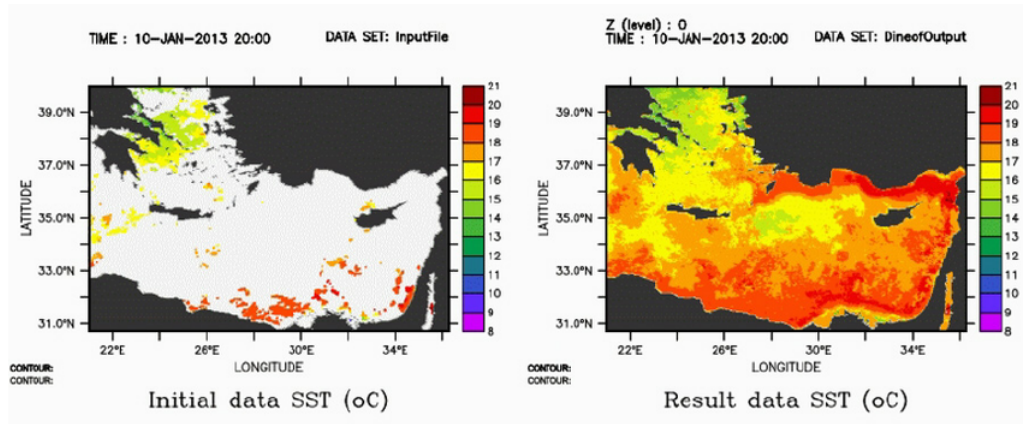


Figure 5.2: A typical example of cloud-covered area during the data collection (left), and its recovered information (right) over the area of application.

also noise, so forcing DINEOF to retain a higher number of EOFs than what is calculated with the cross-validation method is not to be done without caution, as it might degrade the overall quality of the reconstruction.

5.6 Validation of the Results and discussion

In order to estimate and test the successful implementation of the presented application, a comparison of the recovered results against the outputs of oceanographic models providing regional now-casting real time information is further performed. Two of the most important relevant models, are:

1. the ROMS-AGRIF (Nikolaidis, Stylianou, Georgiou, Hadjimitsis, and Akylas 2019), a marine dynamics numerical model, providing very accurate data in high-resolution around Cyprus and in the Levantine sea, and
2. the U.S. Navy Coastal Oceanographic Model (NCOM, NOAA/PMEL 2013), which covers a wider area, at a lower resolution.

In Figure 5.2, we outline the testing procedure; (a) the initially cloudy image is regenerated with DINEOF; (b) as explained, the respective model's output for the same time is selected; (c) the differences between (b) and (c) at all points are computed; and (d) the same procedure is followed for each time step for both models.

Firstly, we present the comparison against the less detailed model US NCOM, in Figure 5.4. The deviation of the model from the recovered SST values is illustrated. For all

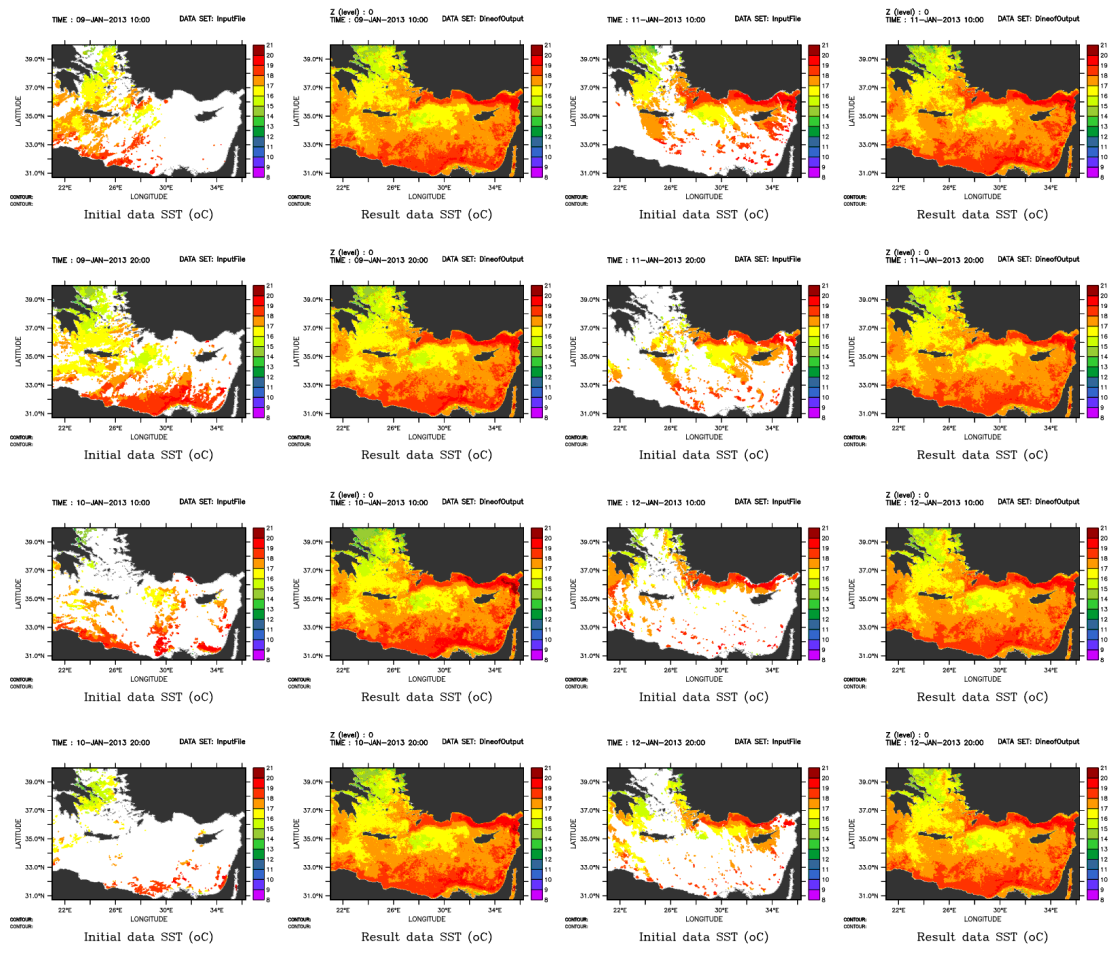


Figure 5.3: Original and reconstructed SST data for the Eastern Mediterranean, for the period from 9/1/2013 to 12/1/2013.

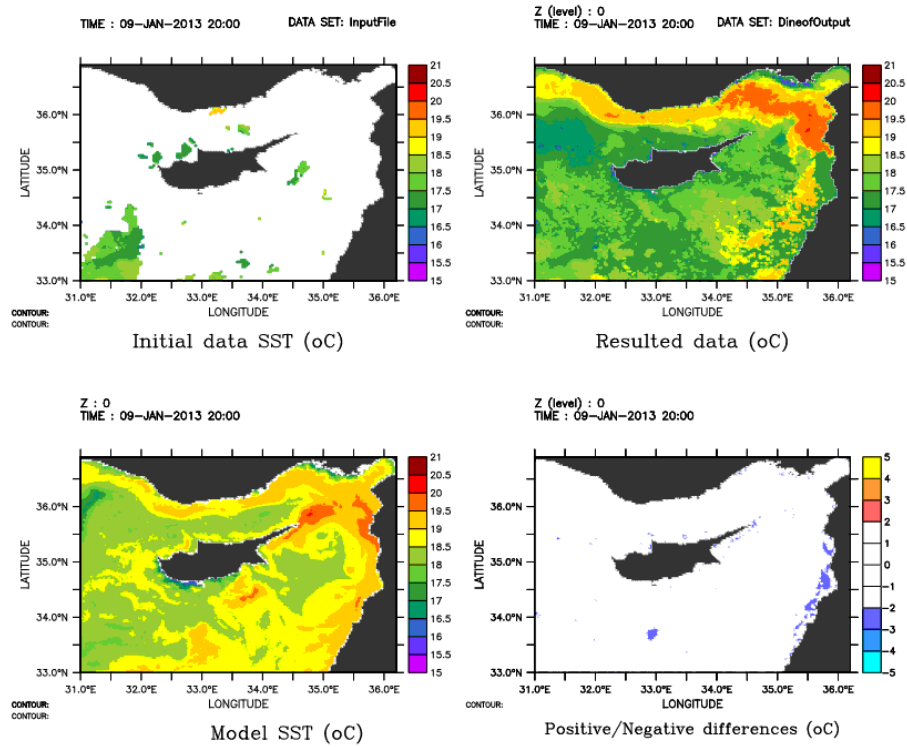


Figure 5.4: Outline of the validation procedure for an arbitrary time-step of Eastern Mediterranean SST data.

the time-steps, it is evident that the recovered data are partially overestimated compared to the model. Although over most of the studied area, the differences remained relatively small, (less than $1^{\circ}C$), near the Eastern Mediterranean coastal area the difference peaks around $4^{\circ}C$. This difference could be intuitively attributed to the fact that the specific area lacks original SST information as shown in Figure 5.3. In other words this difference could be due to DINEOF's inaccuracies. However, this is not true. The US NCOM model, covers the specific area in low resolution resulting in less accurate results. In fact Figure 5.4, which focus in the vicinity of Cyprus through the ROMS-AGRIF operational model, proves the high level of agreement between the model results and the DINEOF outcomes. As mentioned, ROMS-AGRIF is a source of very accurate data, given in high-resolution for Cyprus coasts and Levantine sea. The observed agreement, with absolute differences of less than $1^{\circ}C$, is further verified by respective in-situ measurements from Paphos tide-gauge station, revealing the same behavior.

In Figure 5.4, the detailed SST fields from ROMS-AGRIF model and the respective ones from the application of the DINEOF procedure are illustrated. This illustration is

crucial, in order to test the basic pattern and the main physical characteristics of the recovered SST fields. As noted, a clear general difference of the order of one Celsius degree for all the period is observed between the two cases, with the DINEOF to estimate lower SST values. This difference is considered acceptable, especially since the comparison is done against modeled and not necessarily real values. In fact, observing in detail the DINEOF results one may identify some remarkable features. The high temperature values that appear near the Asia Minor coast are a good indicator of the consistency of the reconstructed values with the reality, with respect to historical climatologic SST values of the specific area. Furthermore, the profound concentrations of colder water that appear in the North West area, in agreement with the known cold water formations near the Ierapetra gyro, is a further indication of success. Finally the existence of remarkably lower temperature patterns near the Palestinian coasts could naturally have been the result of the impact of the Cyprus gyro Robinson, Leslie, Theocharis, and Lascaratos 2001. The above comments show that all the information obtained by the reprocessed satellite data constitutes a good, acceptable representation of the known conditions and of the impact of the main physical mechanisms that influence the studied area, concerning SST. The resulting DINEOF representation could even prove more detailed and accurate compared to the ROMS-AGRIF model. For instance DINEOF application results to lower SST values (around $16^{\circ}C$) at the western Cyprus coast compared to the $17 - 18^{\circ}C$ estimation of the model. The in situ measurements from Paphos tide-gauge station for the same period vary between $15^{\circ}C$ and $16^{\circ}C$, showing a better agreement with the DINEOF results. The overall success suggests the existence of a strong basis available for further testing and application, including more sophisticated procedures, in the direction of successfully implementing a continuous recovery of SST data from satellite images over Eastern Mediterranean. It is expected, that in a future step such results could serve as input for assimilation processes and model calibrations.

5.7 Conclusions

Data Interpolating Empirical Orthogonal Functions is a special technique, for the reconstruction of missing data from satellite images. It is an innovative method, especially useful for filling in missing data from geophysical fields. SST is a physical parameter commonly used in most oceanographic and meteorological applications and among others is a principal factor for relevant arithmetic model calibration, assimilation and initialization. Past works reported successful implementation of DINEOF in recovering missing SST data over the Western Mediterranean area. The DINEOF method has been applied in order to recover a fully filled satellite derived sea surface temperature field, for the first time over Eastern Mediterranean, Levantine sea and Cyprus coasts. This is a crucial step, for the operational implementation of the method. The results are really impressive, recovering data from very cloudy images with remarkable efficiency. The comparison against widely used highly accurate simulations, revealed close agreement with differences not exceeding one oC. The same quantitative agreement holds also against in-situ measurements from Paphos tide-gauge station. It should be pointed out that this agreement is in favor of the DINEOF reconstructed results more than of those produced by the detailed ROMS-AGRIF model. The overall success suggests the existence of a strong basis available for further testing and application.

Besides the impressive results of the DINEOF algorithm in recovering SST data, the application of the method is not restricted to satellite processing. Travis et al. (2009) using DINEOF studied the relations between the surface wind and the SST and Chl-a variations in South Atlantic during 2003. Sirjacobs et al. (2011), effectively applied the DINEOF method to study the case of suspended matter in the North Sea. In addition, similarly to the present application, daily DINEOF cloud-free SSTs for the Western Mediterranean Sea and for the Canary-Madeira region are produced on an operational basis (GHER group of the University of Liège). There exists also a simplified R-project package, specially designed for adoption into this statistical environment. Due to the simplicity of the method, and to the good quality of the results, it is easy to guess a rapid propagation of the DINEOF usage, guiding to better quality of reconstructed results on data with missing

values, from any source. This could be effectively achieved through a combined solution with parallel use of special dedicated geo-statistical tools, like those included in a GIS, for further optimizations of the results. This direction is a main topic for future research.

CHAPTER 6

IMPLEMENTATION OF DINEOF ARCGIS TOOLBOX: CASE STUDY OF RECONSTRUCTION OF CLOROPHYLL-A MISSING DATA OVER THE MEDITERRANEAN USING MYOCEAN SATELLITE DATA PRODUCTS.

In this chapter is presented a case study of DINEOF algorithm implementation over Mediterranean sea, using chlorophyll-a satellite derived data.

6.1 Introduction

Investigation¹ of georeferenced information, provided by Research Centers around the globe, is today essential for many critical decisions on almost every aspect of human activities. In the same sense, lack of relevant information is considered a major problem requesting a valid solution. Since the development of the Geographical Information Systems (GIS) and furthermore of Geomatics and of their rapid adaption on studies concerning the sea environment, spatial analysis of satellite products is of primary interest. DINEOF (Data Interpolating Empirical Orthogonal Functions), considered among the methods that had proved effective in applying the missing data caused by cloudiness or other noise sources, over the satellite signals.

This study is aimed at presenting the availability of this algorithm into a GIS system, providing a method for fast data reconstruction, plus, the added value of the separated produced raster files, that can be used for additional applications. The case study of Chlorophyll-a data missing data filling over the Mediterranean sea, is an example of the potential provided with the toolbox, than a specific 'in-depth' study of the matter. A similar study for Chlorophyll-a, concerning the area of Bohai and Yellow sea, was presented recently by Yequi and Liu, (2014), and constitutes one more evidence of the suitability of the algorithm usage for similar applications. In the past, DINEOF has been applied also

¹Note: This chapter has been presented and published in Second International Conference on Remote Sensing and Geoinformation of the Environment (RSCy2014) 2014 Aug 12 (Vol. 9229, p. 922919) of the International Society for Optics and Photonics.

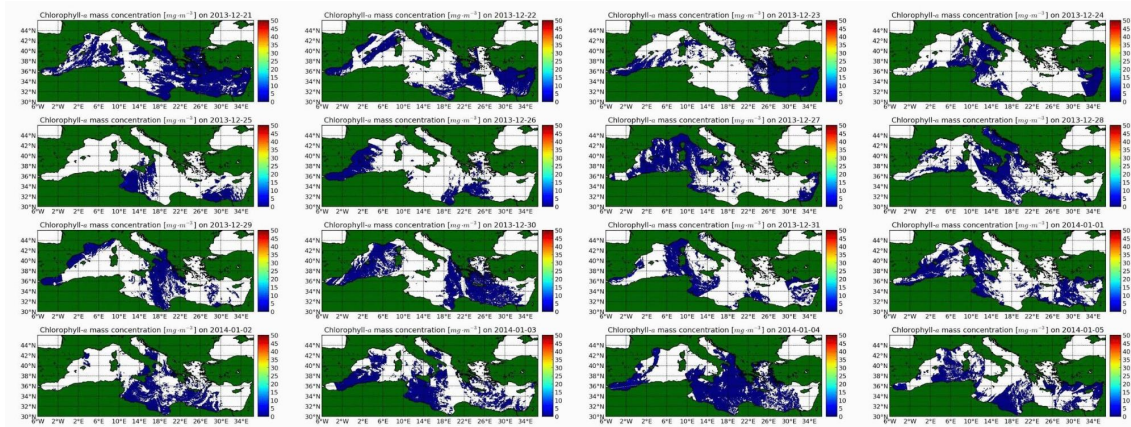


Figure 6.1: Chlorophyll-a L3 MODIS Aqua data coverage of Mediterranean sea from December 21st,2013 to January 5th,2014.(16 time-steps).

on studies of sea surface temperature (SST) around Corsican Island (Beckers, Barth, and Alvera-Azcárate 2006), and for eastern Mediterranean Sea (Nikolaidis, Georgiou, Hadjimitsis, and Akylas 2013; Nikolaidis, Georgiou, Hadjimitsis, and Akylas 2014), and of Total Suspended Matter (Nechad, Alvera-Azcárate, Ruddick, and Greenwood 2011).

By the use of Global Monitoring for Environment and Security program (GMES) project MyOcean 2, satellite data are available to researchers, mainly in binary (netcdf) format. For this case, data used, were gathered by Gruppo di Oceanografia da Satellite (Nardelli, Tronconi, Pisano, and Santoleri 2013) of the Institute of Atmospheric Sciences and Climate (ISAC) of the Italian National Research Council (CNR). The source was Moderate Resolution Imaging Spectroradiometer (MODIS) Aqua (EOS PM) satellites, covering Mediterranean sea with 1 Km resolution. Level 3 daily products, for sixteen days, starting from December 21st, 2013 and finishing on January 5th, 2014, were selected, consisting a characteristic sample of winter season Chlorophyll-a conditions over Mediterranean sea. All time steps, presented 73% of missing data (6.1).

6.2 Methodology

Data INterpolating Empirical Orthogonal Function (DINEOF) is a method to fill in missing data from geophysical fields. This is achieved by providing a spatial data set with missing values in successive time steps. Initially the mean temporal spatial value is subtracted and the missing data set to zero. The EOF decomposition is computed by the

singular value decomposition (SVD) method, obtaining the spatial EOFs(U), the singular values matrix (S) and the temporal EOFs(V).

Successive repetitions (iterations) of the formula performed, until the predefined convergence criterion reached. This criterion, constructed during the initialization process where a randomly selected set of data (3%), set aside for progressive cross-validation, examines when the root mean square error (RMSE) at the cross-validation points is stabilized. Stability is defined by a threshold value of 1.0×10^{-5} between the current and the previous iteration. During each iteration, the number of EOFs (p) increased by one. The optimal number of EOFs retained when the minimum RMSE is obtained. When the optimal number of EOFs achieved, the entire process repeated with the inclusion of the cross-validation points, producing the final results.

DINEOF method is described with details at Alvera-Azcárate et al. (2009), Beckers et al. (2003,2006), Beckers and Rixen (2003), Nikolaidis et al. (2013,2014) and can be downloaded separately from the GeoHydrodynamics and Environment Research Internet page of the University of Liège (GHER) .

6.3 Implementation

The process of applying the algorithm is guided mainly by the ability of the software to handle netcdf binary files. The initial data given to the application, were constructed in such a manner to contain all time step data in a single file (with NaNs [“Not a Number”] for missing value flag) and a “mask” file, containing ones (1) for the valid points and zeroes (0) everywhere else. In order to overcome the memory limitations of the operating system and in order to reduce the execution time, the application is able to automatically divide the initial data in parts of sizes up to 200Kb each.

The implementation of the toolbox, can be described as a ‘wrapper’ of the program provided by GHER. Since, the program allows additional options that influence the overall performance of the algorithm, the toolbox also provides this ability.

The options presented in Table (1) can be used for the construction of a configuration/initialization file of the application, required for the execution. The original program

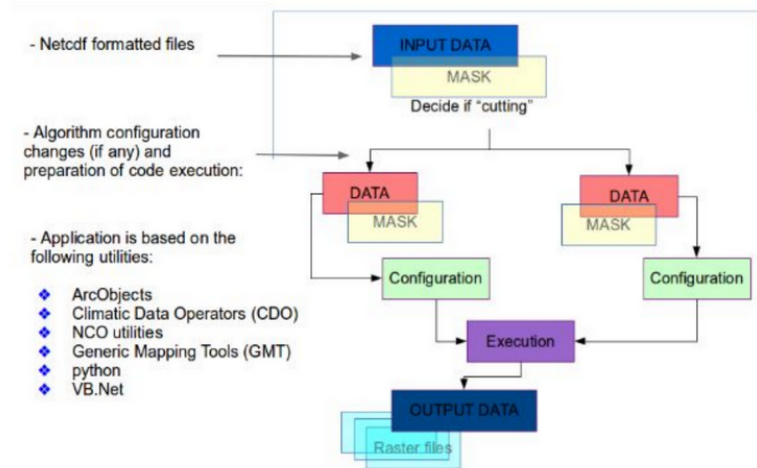


Figure 6.2: Schematic DINEOF toolbox flowchart.

however, provides more options than those available by the application in the direct user interface. This limitation can be overcome by manually adding any additional parameters required, into the configuration file, produced during the preprocess step. Further option addition and handling, along with additional products, will be a matter of a future version of the toolbox.

At the DINEOF site (GHER group of the University of Liège 2011) a complete list of options with their descriptions is available.

Application framework is the VB.Net ® (Microsoft 2017) combined with **python** programming language (Van Rossum and Drake Jr 1995) with the aid of *ArcObjects* (Palladini 2004). Climate Data Operators (**CDO**) (Schulzweida, Kornblueh, and Quast 2004) and NCO utilities (Zender 2008) have been used, as well as utilities from Generic Mapping Tools (**GMT**) (Wessel and Smith 1998). This combination of utilities was necessary, both, for the division and the final merging of large files and for the raster (.tiff)².

The raster files production is one of the main targets of the toolbox, since these type of files provide the essential basis for many further applications with the ArcGIS ® aid.

There are a lot of open source or free utility programs that take place in the proper preparation of the results. In Figure 6.2, a design of the flowchart of the application is shown.

The initialization procedure that takes place when the application starts, consists of the

²Tagged Image File Format, is a computer file format for storing raster graphics images data production.

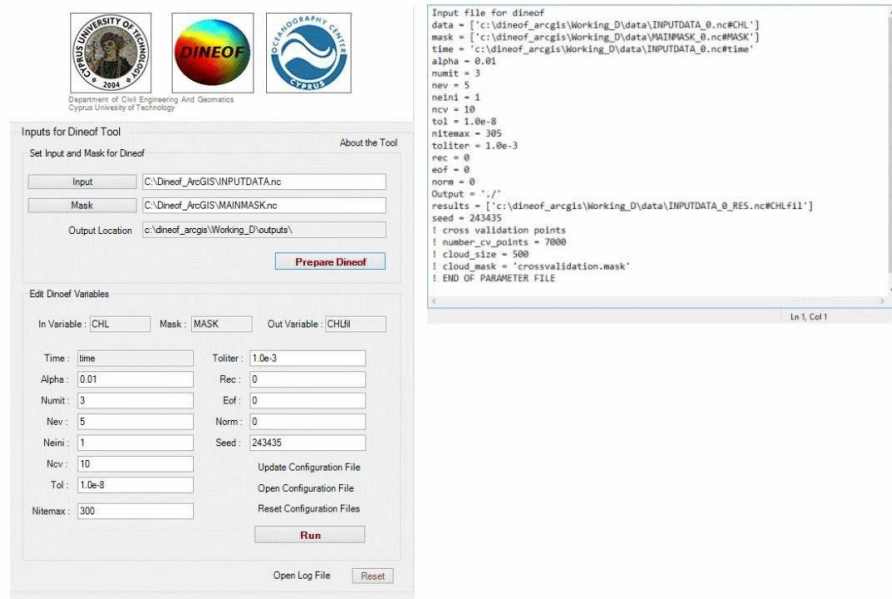


Figure 6.3: Left: DINEOF toolbox user interface options. Right: Configuration file contents example. Lines beginning with the (!) symbol, are considered as comments.

input data file selection and the automatic generation of the configuration files, in response to the selections made. Further changes, additions or omissions can be made through the initialization by the ‘Open Configuration File’ option, provided in the user interface. On-the-fly simple help documentation is also provided by the ‘About the Tool’ option. The ‘Reset Configuration Files’ option, provides a way of canceling all previous selections, and setting all initialization configuration parameters to their default values. All the messages produced during every step of the execution of the application, are available through the ‘Open Log File’ option (Figure 6.3).

GHER version 3.0 of DINEOF application, contains an additional module for results cross validation, that it was not included in this implementation. That explains the comments in the end of the configuration initialization file. It is scheduled for future versions to contain this ability also, depending on the scientific community response.

6.4 Installation and execution

The toolbox installation is accomplished as a typical Windows [<http://windows.microsoft.com/en-us/windows/home>] software application installation. The toolbox is provided as a 21 M Bytes binary (.msi) file. After this process applied a new desktop image will appeared on

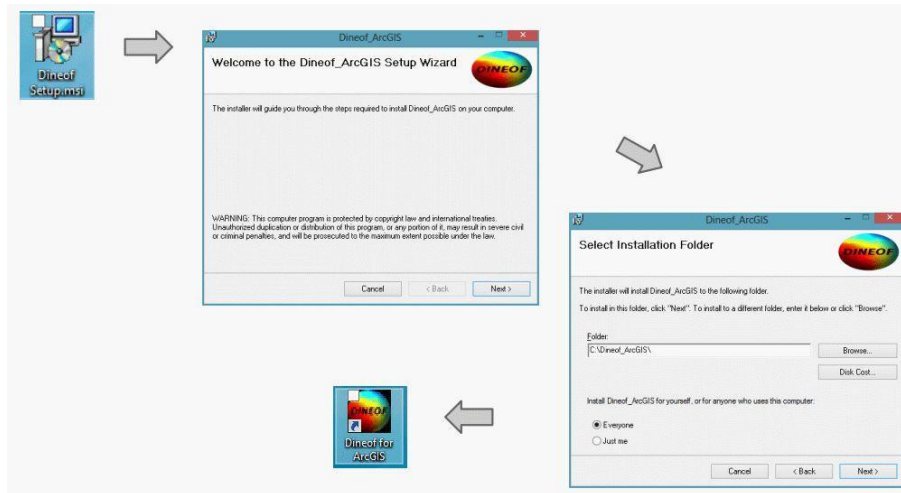


Figure 6.4: Installation process of the toolbox. There is an option of selection of the destination folder, according to the user's choice. A new icon will appeared on desktop after the task finished.

desktop, that enables the automatic application loading (Figure 6.4), inside the ArcMap [®] environment.

Figure 6.5 shows the new toolbar that appeared, containing besides the main execution key, some additional options for measuring distances, copy and paste items, pan and zoom of areas, and area re-positioning options.



Figure 6.5: DINEOF toolbar in ArcMap. Button icons description (from left to the right): Main process button, distance measure button, information button, copy and paste buttons, zoom and pan buttons, view entire region button.

When the application is running the initial screen contains the ArcMap interface including the new toolbar (Figure 6.6). The application will start functioning after the selection (point and click with mouse) of the main process button. This action will bring forth the actual interface, where all the further process will take place.

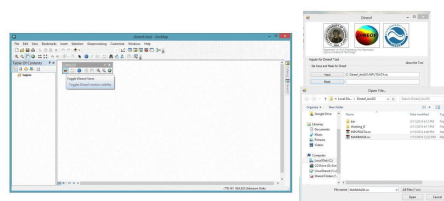


Figure 6.6: DINEOF toolbox interface initial appearance (left). Example of input file selection in the application's interface (right).

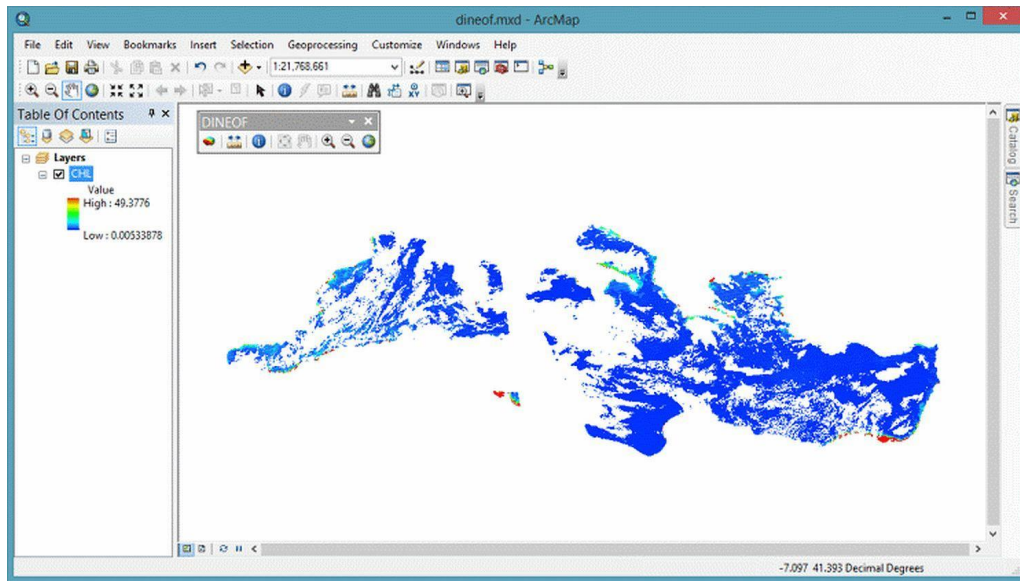


Figure 6.7: Input data appearance after the file selection. Empty (blank) space denotes the missing data.

The netcdf input file selection is the mandatory step that will provide the necessary information for the execution of the application.

There may be many time steps included in the input file. All input data appeared as one rasterized data set, providing the given total area coverage, independent to the time (Figure 6.7). If inspection of a specific time step is required, that can be done using the ArcMap layer options, appeared with right-click on the Table of Contents catalog, over the selected layer name.

During the data loading, the preprocess action will determine the need of further input data separation in smaller files, with respect to the size of the input data. An upper limit of 200 Mb is defined experimentally as an indicator of splitting to smaller areas. All selected options, described in Implementation section, will be preserved and delegated to the new files. The new areas are separated only horizontally taking account of the longitudes, while at the same time the vertical sizes, the latitudes, remain unchanged. In the current case, there was a division of the initial file with size of 319 Mb to two parts.

File splitting actions will preformed, after the ‘Prepare Dineof’ button selection (Figure 6.3) producing results that are stored into the application’s execution log file, along with the algorithm performance and execution messages (Figure 8). Through the ‘Open Log File’ button (Figure 6.3) those messages are visible at any time.

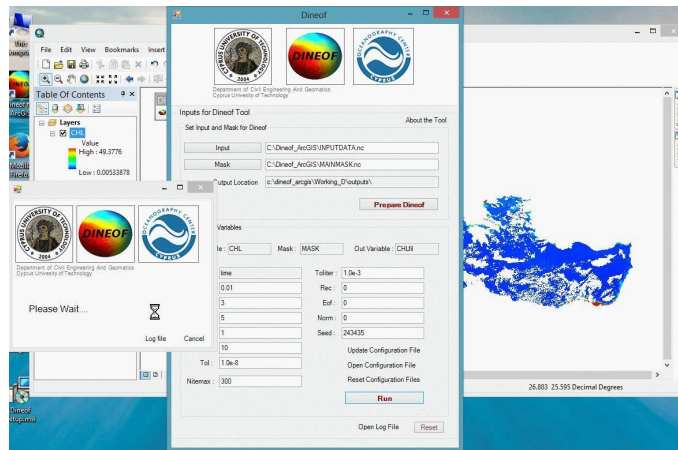


Figure 6.8: DINEOF application appearance during execution. A new window indicates the process.

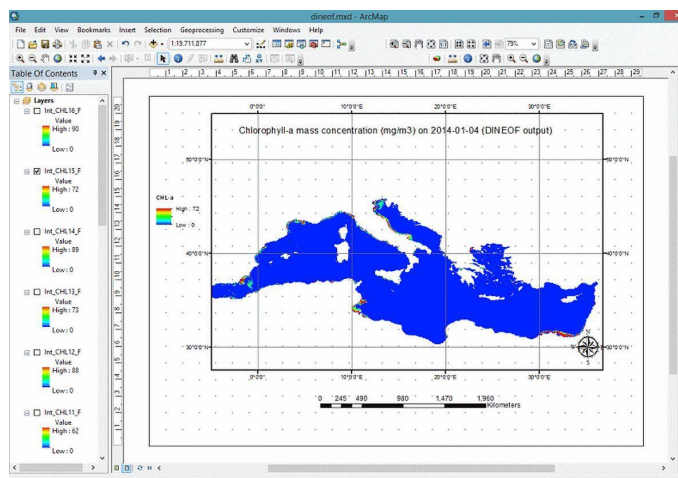


Figure 6.9: Application results: Under the Table of Contents section, all time steps included as separated layers.

The algorithm itself will be executed with the selection of ‘Run’ button (Figure 6.3), that is activated only when the preprocess action have been terminated successfully. It will produce a new window on screen, that will disappeared with the termination of the execution.(Figure 6.8)

After the algorithm execution finish, results will be merged in one file and the Table of Contents catalog, will contain all the time steps, in separated layers, rasterized in Tagget Image File (.tiff) format. (Figure 6.9). Additionally, the results will be placed into a new netcdf output file, that will be stored, along with all the raster files, under the output subdirectory (subfolder) that will be created, under the installation folder.

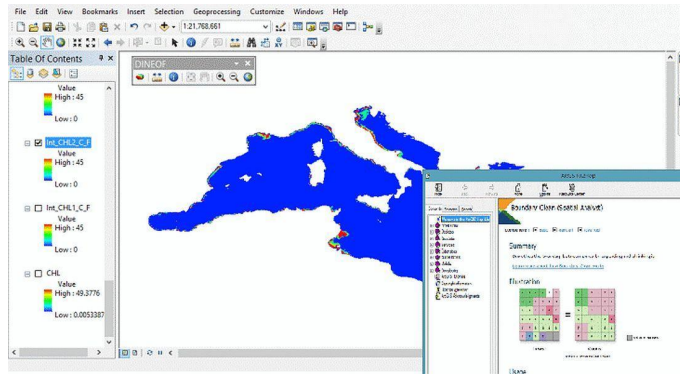


Figure 6.10: Spatial Analyst’s Boundary Clean algorithm application on the DINEOF results.

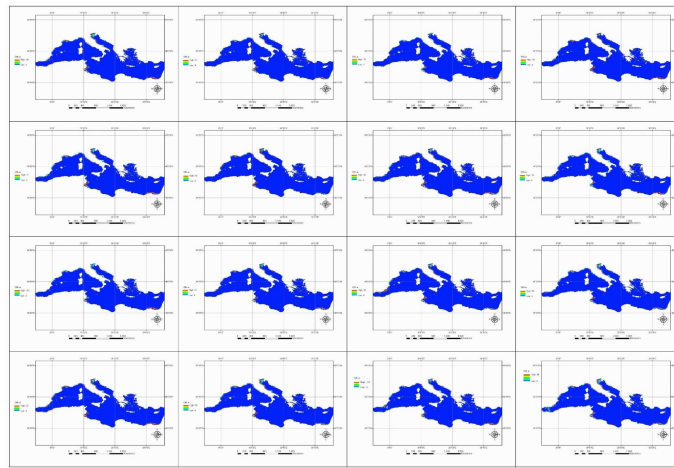


Figure 6.11: Filling 16 time steps of chlorophyll-a concentration over Mediterranean sea, after DINEOF and Boundary Clean algorithm application.

6.5 Conclusions

The chlorophyll-a satellite data over the Mediterranean sea for a period of 16 days after the DINEOF algorithm process produced results covering all the time steps of the area without any missing data. Stepping forward, an additional process was performed with the aid of Boundary Clean algorithm, provided by the ArcGIS³ Spatial Analyst library (Figure 6.10).

The result (Figure 6.11) was an effective ‘smoothing of the edges’ that produce a more physically appeared impression of the existing conditions over the area.

Concluding it should be noted that: Generated raster data, can be further processed by

³Legal notice: Maps and images of various sections of this document were created using ArcGIS® software by Esri. ArcGIS® and ArcMap™ are the intellectual property of Esri and are used herein under license. Copyright © Esri. All rights reserved. Windows 8® is trademark of Microsoft Company. All the rest software tools included and described herein were under GNU open source license or freely available.

various methods, providing the source of previously non-existent information. In this case study a Boundary Clean Spatial Analysis algorithm was applied, for smoothing existing 'rough' edges. This tool applies a new platform in a well known GIS environment, for future similar experiments.

It is expected that the toolbox and the methodology described above to be used as a leverage for further similar studies. For the future it is scheduled the inclusion of additional options, as cloudiness for example, already included in the current software version, but not yet fully applied in the graphic user interface.

CHAPTER 7

CONCLUSIONS AND RECOMMENDATIONS FOR FUTURE WORK

This chapter summarises the basic conclusions of this work and proposes directions of further research and development based on the achieved results.

7.1 ROMS-AGRIF application

ROMS-AGRIF version 3.1.1 (2014) has been applied effectively for the first time on Eastern Mediterranean and, specifically, over the Levantine and Cyprus Seas. The model run in operational prognostic mode, producing results every six hours, for a period of ten days, with daily averages included. Comparisons of the results with the CYCOFOS system (Cyprus Coastal Ocean Forecasting and Observing System, Zodiatis, Lardner, Georgiou, Demirov, Manzella, and Pinardi 2003; Zodiatis, Lardner, Hayes, and Georgiou 2006; Zodiatis, Lardner, Hayes, Georgiou, Sofianos, Skliris, and Lascaratos 2008) and with ARGOS float profiles showed compliance and very high accuracy. The new ROMS-AGRIF model implementation can be used efficiently for operational oceanographic forecasts for the area of Eastern Mediterranean and the Levantine sea around Cyprus.

7.2 DINEOF operational implementations

The Data Interpolating Empirical Orthogonal Functions innovative method for the reconstruction of missing data from satellite images, has been applied in order to recover a fully filled satellite derived sea surface temperature field, for the first time over Eastern Mediterranean, Levantine sea and Cyprus coasts. The results were impressive, recovering data from very cloudy images with remarkable efficiency. The comparison against widely used highly accurate simulations, revealed close agreement with differences not exceeding one °C. Due to the simplicity of the method, and to the good quality of the results, it is easy to guess a rapid propagation of the DINEOF usage, guiding to better quality of reconstructed results on data with missing values, from any source. This could

be effectively achieved through a combined solution with parallel use of special dedicated geo-statistical tools, like those included in a GIS, for further optimizations of the results.

7.3 DINEOF application on chlorophyll-a data

ArcGIS ® is a well known standard on Geographical Information Systems, used over the years for various remote sensing procedures.

As mentioned above the DINEOF method, applied with relative success in various experimental trials (Wang and Liu, 2013; Nikolaidis et al., 2013;2014), and tends to be an effective and computationally affordable solution, on the problem of data reconstruction, for missing data from geophysical fields, such as chlorophyll-a, sea surface temperatures or salinities and geophysical fields derived from satellite data. Implementation of this method inside a GIS system provide with a more complete, integrated approach, permitting the expansion of the applicability over various aspects.

For this purpose, a new GIS toolbox implemented and present that aims to automate the usage of the algorithm, incorporating the DINEOF codes provided by GHER (GeoHydrodynamics and Environment Research Group of University of Liege) into the ArcGIS ®. A case-study of filling the chlorophyll-a missing data in the Mediterranean Sea area, for a 18-day period is analyzed, as an example for the effectiveness and simplicity of the usage of this toolbox. All the daily chlorophyll-a MODIS satellite data products with an initial level of only 27% data coverage were successfully reconstructed, without any missing data. Stepping forward, an additional process was performed with the aid of Boundary Clean algorithm, provided by the ArcGIS Spatial Analyst library. The result was an effective ‘smoothing of the edges‘ that produce a more physically appeared impression of the existing conditions over the area.

It is expected that the toolbox and the methodology described above to be used as a leverage for further similar studies.

7.4 Future work

Regarding the GIS DINEOF toolbox, for the future it is scheduled the inclusion of additional options, as cloudiness for example, already included in the current software version, but not yet fully applied in the graphic user interface.

Regarding the marine dynamics modeling, what shown up to now, focus in the ability of ROMS-AGRIF model to present high quality results for the sea temperature, salinity, surface height and sea current velocities. Additionally, the model can provide information for the

- dissolved oxygen, nutrients, chlorophyll-a,
- sediment transport,
- floating objects orbits and transects,
- specific location condition changes, in execution time.

Further more, it can be coupled with atmospheric and wave models (Du, Larsén, and Bolaños 2015; Sikiric, Roland, Janekovic, Tomazic, and Kuzmic 2013), providing a holistic view of the area of interest.

As a future work, it is expected to extend the current marine dynamics numerical model so, that to be able to provide all the available information for the Levantine and Cyprus sea.

Also, all the non-complete geophysical data that will be used for the model's forcing, is planed to be filled with the application of the DINEOF algorithm.

The results that will be received after the construction of such a complete system, will be a significant step in the understanding of the marine environment and in the scientific research.

Appendices

APPENDIX A
CYPRUS – LEVANTINE NUMERICAL MARINE DYNAMICS MODEL
CONFIGURATION

A.1 Introduction

In this appendix is provided the description of the specific ROMS-AGRIF configuration files for the construction of the Cyprus – Levantine model.

ROMS-AGRIF source code is written in C-preprocessor Fortran code which generates the Fortran 90 source code. The C-preprocessor code, is consisted by a series of rules that builds the application according the indicated conditions. These conditions are given by two text files:

- the *param.h*, which contains the grid and array dimensions, including parallelization options,
- the *cppdefs.h*, which contains the methods for the application of boundary conditions, and of the various physical and biogeochemical procedures.

The MATLAB based preprocessing is driven by the code provided by the *romstools_param.m* script. The code execution during the model’s run is guided by the *roms.in* rule text file.

The following sections contain the relevant rules and codes.

A.1.1 param.h configuration file

```
!  
!-----  
! ROMS_AGRIF is a branch of ROMS developped at IRD and INRIA, in France  
! The two other branches from UCLA (Shchepetkin et al)  
! and Rutgers University (Arango et al) are under MIT/X style license.  
! ROMS_AGRIF specific routines (nesting) are under CeCILL-C license.  
!  
! ROMS_AGRIF website : http://www.romsagrif.org  
!-----  
!  
! Dimensions of Physical Grid and array dimensions:  
! =====  
! LLm,MMm Number of the internal points of the PHYSICAL grid.  
!           in the XI- and ETA-directions [physical side boundary
```

```

!           points and peroodic ghost points (if any) are excluded].
!
! Lm,Mm    Number of the internal points [see above] of array
!           covering a Message Passing subdomain. In the case when
!           no Message Passing partitioning is used, these two are
!           the same as LLm,MMm.
!
! N        Number of vertical levels.
!
integer LLm,Lm,MMm,Mm,N, LLm0,MMm0
#if defined AGRIF
integer LLmm2, MMmm2
integer LLmm3, MMmm3
#endif
#if defined BASIN
parameter (LLm0=60, MMm0=50, N=10)
#elif defined CANYON_A
parameter (LLm0=65, MMm0=48, N=16)
#elif defined CANYON_B
parameter (LLm0=66, MMm0=48, N=16)
#elif defined EQUATOR
parameter (LLm0=40, MMm0=32, N=32) ! 100 km resolution
#elif defined GRAV_ADJ
! parameter (LLm0=32, MMm0=4, N=10) ! 2 km resolution
parameter (LLm0=128, MMm0=4, N=40) ! 500 m resolution
! parameter (LLm0=512, MMm0=4, N=160) ! 125 m resolution
#elif defined INNERSHELF
parameter (LLm0=200, MMm0=3, N=60)
#elif defined INTERNAL
! parameter (LLm0=120, MMm0=10, N=40) ! 10 km resolution
! parameter (LLm0=800, MMm0=4, N=40) ! 1.5 km resolution
parameter (LLm0=1600, MMm0=4, N=40) ! .75 km resolution
#elif defined OVERFLOW
parameter (LLm0=4, MMm0=128, N=10)
#elif defined RIVER
parameter (LLm0=40, MMm0=80, N=20)
#elif defined SEAMOUNT
parameter (LLm0=64, MMm0=64, N=20)
#elif defined SHELFROnt
parameter (LLm0=4, MMm0=40, N=10)
#elif defined SOLITON
parameter (LLm0=96, MMm0=32, N=10)
#elif defined UPWELLING
parameter (LLm0=16, MMm0=64, N=16)
#elif defined VORTEX
! parameter (LLm0=360, MMm0=360, N=10) ! 5 km resolution
! parameter (LLm0=180, MMm0=180, N=10) ! 10 km resolution
! parameter (LLm0=90, MMm0=90, N=10) ! 20 km resolution
parameter (LLm0=60, MMm0=60, N=10) ! 30 km resolution
#elif defined JET
# ifdef ANA_JET
! parameter (LLm0=250, MMm0=1000,N=100) ! 2 km resolution
! parameter (LLm0=100, MMm0=400, N=80) ! 5 km resolution
! parameter (LLm0= 50, MMm0=200, N=60) ! 10 km resolution
parameter (LLm0= 25, MMm0=100, N=40) ! 20 km resolution
# else
! parameter (LLm0=300, MMm0=500, N=30) ! 2 km resolution
! parameter (LLm0=120, MMm0=200, N=30) ! 5 km resolution
! parameter (LLm0=60, MMm0=100, N=30) ! 10 km resolution
parameter (LLm0=30, MMm0=50, N=30) ! 20 km resolution

```

```

# endif
#elif defined SHOREFACE
    parameter (LLm0=59, MMm0=7, N=20) ! Planar Beach 20m
#elif defined RIP
# ifdef BISCA
    parameter (LLm0= 86, MMm0= 92, N=20) ! 10 m Bisca Rip
# else
!   parameter (LLm0=256, MMm0=256, N=20) ! 3 m resolution
!   parameter (LLm0= 96, MMm0= 96, N=20) ! 8 m resolution
    parameter (LLm0= 48, MMm0= 48, N=20) ! 16 m resolution
# endif
#elif defined THACKER
    parameter (LLm0=199, MMm0=199, N=5 ) ! 1 km resolution
#elif defined REGIONAL
# if defined USWC0
    parameter (LLm0=62, MMm0=126, N=40) ! US_West grid15 L0
# elif defined USWC1
    parameter (LLm0=60, MMm0=96, N=40) ! US_West grid15 L1
# elif defined USWC2
    parameter (LLm0=60, MMm0=120, N=40) ! US_West grid15 L2
# elif defined USWC155
    parameter (LLm0=83, MMm0=168, N=20) ! US_West USWC155 L1
# elif defined CANARY
!   parameter (LLm0=97, MMm0=159, N=32) ! Canary
# elif defined FINISTERE
    parameter (LLm0=78, MMm0=100, N=16) ! Finistere
# elif defined RIA
    parameter (LLm0=77, MMm0=96, N=28) ! RIA
# elif defined PERU
    parameter (LLm0=39, MMm0=32, N=20) ! Peru test
# elif defined SAFE
    parameter (LLm0=111, MMm0=96, N=32) ! SAFE
# elif defined PACIFIC
    parameter (LLm0=170, MMm0=60, N=30) ! Pacific
# elif defined CORAL
    parameter (LLm0=81, MMm0=77, N=32) ! CORAL sea
# elif defined BENGUELA_LR
    parameter (LLm0=41, MMm0=42, N=32) ! BENGUELA_LR
# elif defined BENGUELA_HR
    parameter (LLm0=83, MMm0=85, N=32) ! BENGUELA_HR
# elif defined BENGUELA_VHR
    parameter (LLm0=167, MMm0=170, N=32) ! BENGUELA_VHR
# elif defined LEVANTINE
    parameter (LLm0=122, MMm0=142, LLmm2=60, MMmm2=54, N=30) ! LEVANTINE SEA (1)
# else
    parameter (LLm0=94, MMm0=81, N=40)
# endif
#else
    parameter (LLm0=xx, MMm0=xx, N=xx)
#endif

#ifdef AGRIF
    common /scrum_physical_grid/ LLm, Lm, LLmm2, MMm, Mm, MMmm2
#else
    parameter (LLm=LLm0, MMm=MMm0)
#endif

!
! MPI related variables
! === =====

```

```

!
integer Lmmpi,Mmmpi,iminmpi,imaxmpi,jminmpi,jmaxmpi
common /comm_setup_mpi/ Lmmpi,Mmmpi,
&
iminmpi,imaxmpi,jminmpi,jmaxmpi

!
! Domain subdivision parameters
! =====
!
! NPP          Maximum allowed number of parallel threads;
! NSUB_X,NSUB_E Number of SHARED memory subdomains in XI- and
!
!                      ETA-directions;
! NNODES      Total number of MPI processes (nodes);
! NP_XI,NP_ETA Number of MPI subdomains in XI- and ETA-directions;
!
integer NSUB_X, NSUB_E, NPP
#ifdef MPI
integer NP_XI, NP_ETA, NNODES
parameter (NP_XI=1, NP_ETA=4, NNODES=NP_XI*NP_ETA)
parameter (NPP=1)
parameter (NSUB_X=1, NSUB_E=1)
#elif defined OPENMP
parameter (NPP=8)
# ifdef AUTOTILING
common/distrib/NSUB_X, NSUB_E
# else
parameter (NSUB_X=1, NSUB_E=NPP)
# endif
#else
parameter (NPP=1)
# ifdef AUTOTILING
common/distrib/NSUB_X, NSUB_E
# else
parameter (NSUB_X=1, NSUB_E=NPP)
# endif
#endif

!
! Derived dimension parameters
! =====
!
integer stdout, Np, padd_X,padd_E
#ifdef AGRIF
common/scrup_deriv_param/padd_X,padd_E
#endif
parameter (stdout=6, Np=N+1)
#ifdef AGRIF
# ifdef MPI
parameter (Lm=(LLm+NP_XI-1)/NP_XI, Mm=(MMm+NP_ETA-1)/NP_ETA)
# else
parameter (Lm=LLm, Mm=MMm)
# endif
parameter (padd_X=(Lm+2)/2-(Lm+1)/2)
parameter (padd_E=(Mm+2)/2-(Mm+1)/2)
#endif

#if defined AGRIF || defined AUTOTILING
integer NSA, N2d,N3d,N1dXI,N1dETA
parameter (NSA=28)
common /scrup_private_param/ N2d,N3d,N1dXI,N1dETA

```



```

#else
    integer NSA, N2d,N3d, size_XI,size_ETA
    integer se,sse, sz,ssz
    parameter (NSA=28)
# ifdef ALLOW_SINGLE_BLOCK_MODE
    parameter (size_XI=6+Lm, size_ETA=6+Mm)
# else
    parameter (size_XI=7+(Lm+NSUB_X-1)/NSUB_X)
    parameter (size_ETA=7+(Mm+NSUB_E-1)/NSUB_E)
# endif
    parameter (sse=size_ETA/Np, ssz=Np/size_ETA)
    parameter (se=sse/(sse+ssz), sz=1-se)
    parameter (N2d=size_XI*(se*size_ETA+sz*Np))
    parameter (N3d=size_XI*size_ETA*Np)
#endif

!
! Number maximum of weights for the barotropic mode
! =====
!
!
    integer NWEIGHT
    parameter (NWEIGHT=137)

!
! Tides, Wetting-Drying, Point sources, Floast, Stations
! =====
!
!
#if defined SSH_TIDES || defined UV_TIDES
    integer Ntides          ! Number of tides
    parameter (Ntides=8)   ! =====
#endif
#if defined WET_DRY
    real Dcmin, Dcmax      ! Critical Depth for Drying cells
    parameter (Dcmin=0.20) ! =====
    parameter (Dcmax=0.20)
#endif
#if defined PSOURCE || defined PSOURCE_NCFILE
    integer Msrc           ! Number of point sources
    parameter (Msrc=10)   ! =====
#endif
#if defined FLOATS
    integer Mfloats        ! Maximum number of floats
    parameter (Mfloats=32000) ! =====
#endif
#if defined STATIONS
    integer NS              ! Number of output stations
    parameter (NS=5)       ! =====
    integer Msta            ! Maximum number of stations
    parameter (Msta=1000)  ! =====
#endif

!
! Number of tracers and tracer identification indices
! =====
!
!
#if defined SOLVE3D
    integer NT, itemp
    & , ntrc_salt, ntrc_pas, ntrc_bio, ntrc_sed
    & , ntrc_diats, ntrc_diauv, ntrc_diabio
# ifdef BIOLOGY

```

```

        &          , itrc_bio
# endif
# ifdef SEDIMENT
        &          , itrc_sed
# endif
# ifdef SALINITY
        &          , isalt
# endif
# ifdef PASSIVE_TRACER
        &          , itpas
# endif
# ifdef BIOLOGY
#   ifdef PISCES
        &          , iDIC_ , iTAL_ , iOXY_ , iCAL_ , iPO4_
        &          , iPOC_ , iSIL_ , iPHY_ , iZOO_ , iDOC_
        &          , iDIA_ , iMES_ , iBSI_ , iFER_
        &          , iBFE_ , iGOC_ , iSFE_ , iDFE_ , iDSI_
        &          , iNFE_ , iNCH_ , iDCH_ , iNO3_ , iNH4_
#   endif
#   ifdef DIAGNOSTICS_BIO
#     ifdef key_trc_dia3d
        &          , Nhi , Nco3 , Naksp , Netot , Nprorca
        &          , Nprorca2 , Npronew , Npronew2
        &          , Nprorca3 , Nprorca4 , Nprorca5
        &          , Ngraztot1 , Ngraztot2 , NnitriFo2
        &          , Npronewo2 , Nprorego2 , Nremino2
        &          , Nmicroo2 , Nmesoo2 , Nfixo2
#     endif
#     ifdef key_trc_diaadd
        &          , Nfld , Nflul6 , Nkgco2 , Natcco2 , Nsinking
        &          , Nsinking2 , Nsinkfer , Nsinkfer2 , Nsinksil
        &          , Nsinkcal , Nzmeu , Nirondep , Nnitrpot
#     endif
#   endif
        &          , NumFluxTerms , NumVSinkTerms , NumGasExcTerms
# elif defined BIO_NChlPZD
        &          , iNO3_ , iChla , iPhy1 , iZool
        &          , iDet1
#   ifdef OXYGEN
        &          , iO2
#   endif
        &          , NFlux_NewProd , NFlux_Grazing , NFlux_SlopFeed
        &          , NFlux_Pmort , NFlux_Zmetab , NFlux_Zmort , NFlux_Remind
        &          , NumFluxTermsN
#   ifdef OXYGEN
        &          , OGain_NewProd , OLoss_Zmetab
        &          , OLoss_Remind , NumFluxTermsO , OFlux_GasExc
        &          , NumGasExcTerms , NumFluxTerms
#   else
        &          , NumGasExcTerms
        &          , NumFluxTerms
#   endif
        &          , NFlux_VSinkP1 , NFlux_VSinkD1
        &          , NumVSinkTerms
# elif defined BIO_N2ChlPZD2
        &          , iNO3_ , iNH4_ , iChla , iPhy1 , iZool
        &          , iDet1 , iDet2
        &          , NFlux_NewProd
        &          , NFlux_RegProd
        &          , NFlux_Nitrific
        &          , NFlux_Grazing

```

```

& , NFlux_SlopFeed
& , NFlux_Pmort
& , NFlux_Zmetab
& , NFlux_Zmort
& , NFlux_Remind1, NFlux_Remind2
& , NumFluxTermsN, NumFluxTerms, NumGasExcTerms
& , NFlux_VSinkP1
& , NFlux_VSinkD1, NFlux_VSinkD2
& , NumVSinkTerms

# elif defined BIO_BioEBUS
& , iNO3_, iNO2_, iNH4_, iPhyl, iPhy2, iZool, iZoo2
& , iDet1, iDet2, iDON, iO2
# ifdef NITROUS_OXIDE
& , iN2O
# endif
& , NFlux_lightlimitP1, NFlux_lightlimitP2
& , NFlux_templimitP1, NFlux_templimitP2
& , NFlux_NO3limitP1, NFlux_NO2limitP1
& , NFlux_NH4limitP1, NFlux_NO3limitP2
& , NFlux_NO2limitP2, NFlux_NH4limitP2
& , NFlux_ProdNO3P1, NFlux_ProdNO3P2
& , NFlux_ProdNO2P1, NFlux_ProdNO2P2
& , NFlux_Nitrif1, NFlux_Nitrif2, NFlux_ProdNH4P1
& , NFlux_ProdNH4P2, NFlux_P1Z1Grazing
& , NFlux_P2Z1Grazing, NFlux_P1mort, NFlux_P2mort
& , NFlux_P1Z2Grazing, NFlux_P2Z2Grazing
& , NFlux_Z1Z2Grazing, NFlux_Z1metab, NFlux_Z1mort
& , NFlux_Z2metab, NFlux_Z2mort, NFlux_Hydro1D1
& , NFlux_ReminOxyD1, NFlux_Denitr1D1
& , NFlux_Denitr2D1
& , NFlux_Hydro1D2, NFlux_ReminOxyD2
& , NFlux_Denitr1D2, NFlux_Denitr2D2
& , NFlux_ReminOxyDON
& , NFlux_Denitr1DON, NFlux_Denitr2DON
& , NFlux_NO2anammox
& , NFlux_NH4anammox, O2Flux_GasExc, NumFluxTermsN
# ifdef NITROUS_OXIDE
& , NFlux_paramN2O, N2OFlux_GasExc
# endif
& , NumFluxTerms, NumGasExcTerms
& , NFlux_VSinkP2, NFlux_VSinkD1
& , NFlux_VSinkD2, NumVSinkTerms

# endif
/*-----*/
# endif /* BIOLOGY */

# ifdef SEDIMENT
& , isand, isilt
& , NST, NLAY
# endif

parameter (itemp=1)
# ifdef SALINITY
parameter (ntrc_salt=1)
parameter (isalt=itemp+1)
# else
parameter (ntrc_salt=0)

```

```

#endif
# ifdef PASSIVE_TRACER
    parameter (ntrc_pas=1)
    parameter (itpas=itemp+ntrc_salt+1)
# else
    parameter (ntrc_pas=0)
# endif

!
! ===== BIOLOGY =====
!
# ifdef BIOLOGY
#   ifdef PISCES
        parameter (ntrc_bio=24,itrc_bio=itemp+ntrc_salt+ntrc_pas+1)
        parameter (iDIC_=itrc_bio, iTAL_=iDIC_+1,
&         iOXY_=iDIC_+2, iCAL_=iDIC_+3, iPO4_=iDIC_+4,
&         iPOC_=iDIC_+5, iSIL_=iDIC_+6, iPHY_=iDIC_+7,
&         iZOO_=iDIC_+8, iDOC_=iDIC_+9, iDIA_=iDIC_+10,
&         iMES_=iDIC_+11, iBSI_=iDIC_+12, iFER_=iDIC_+13,
&         iBFE_=iDIC_+14, iGOC_=iDIC_+15, iSFE_=iDIC_+16,
&         iDFE_=iDIC_+17, iDSI_=iDIC_+18, iNFE_=iDIC_+19,
&         iNCH_=iDIC_+20, iDCH_=iDIC_+21, iNO3_=iDIC_+22,
&         iNH4_=iDIC_+23)
#   ifdef key_trc_dia3d
        parameter (Nhi      = 1,
&         Nco3      = 2,
&         Naksp     = 3,
&         Netot     = 4,
&         Nprorca   = 5,
&         Nprorca2  = 6,
&         Npronew   = 7,
&         Npronew2  = 8,
&         Nprorca3  = 9,
&         Nprorca4  = 10,
&         Nprorca5  = 11,
&         Ngraztot1 = 12,
&         Ngraztot2 = 13,
&         NnitriFo2 = 14,
&         Npronewo2 = 15,
&         Nprorego2 = 16,
&         Nremino2  = 17,
&         Nmicroo2  = 18,
&         Nmesoo2   = 19,
&         Nfixo2    = 20,
&         NumFluxTerms = Nfixo2)
#   else
        parameter (NumFluxTerms = 0)
#   endif
#   ifdef key_trc_diaadd
        parameter (Nfld      = 1,
&         Nflul6     = 2,
&         Nkgco2     = 3,
&         Natcco2    = 4,
&         Nsinking   = 5,
&         Nsinking2  = 6,
&         Nsinkfer   = 7,
&         Nsinkfer2  = 8,
&         Nsinksil   = 9,
&         Nsinkcal   = 10,
&         Nzmeu      = 11,

```

```

&         Nirondep = 12,
&         Nnitropot = 13,
&         NumGasExcTerms = 0,
&         NumVSSinkTerms = Nnitropot)
# else
    parameter (NumGasExcTerms = 0, NumVSSinkTerms = 0)
# endif
# elif defined BIO_NChlPZD
# ifdef OXYGEN
    parameter (ntrc_bio=6, itrc_bio=itemp+ntrc_salt+ntrc_pas+1)
# else
    parameter (ntrc_bio=5, itrc_bio=itemp+ntrc_salt+ntrc_pas+1)
# endif
    parameter (iNO3_=itrc_bio, iChla=iNO3_+1,
&         iPhyl=iNO3_+2,
&         izoo1=iNO3_+3,
&         iDet1=iNO3_+4)
# ifdef OXYGEN
    parameter (iO2=iNO3_+5)
# endif
    parameter (NFlux_NewProd = 1,
&         NFlux_Grazing = 2,
&         NFlux_SlopFeed = 3,
&         NFlux_Pmort = 4,
&         NFlux_Zmetab = 5,
&         NFlux_Zmort = 6,
&         NFlux_Remind = 7,
&         NumFluxTermsN = 7,
# ifdef OXYGEN
&         OGain_NewProd = 8,
&         OLoss_Zmetab = 9,
&         OLoss_Remind = 10,
&         NumFluxTermsO = 3,
&         OFlux_GasExc = 1,
&         NumGasExcTerms = 1,
&         NumFluxTerms = 10,
# else
&         NumGasExcTerms = 0,
&         NumFluxTerms = 7,
# endif
# endif
&         NFlux_VSinkP1 = 1,
&         NFlux_VSinkD1 = 2,
&         NumVSSinkTerms = 2)
# elif defined BIO_N2ChlPZD2
    parameter (ntrc_bio=7, itrc_bio=itemp+ntrc_salt+ntrc_pas+1)
    parameter (iNO3_=itrc_bio, iNH4_=iNO3_+1, iChla=iNO3_+2,
&         iPhyl=iNO3_+3,
&         izoo1=iNO3_+4,
&         iDet1=iNO3_+5, iDet2=iNO3_+6)
    parameter (NFlux_NewProd = 1,
&         NFlux_RegProd = 2,
&         NFlux_Nitrific = 3,
&         NFlux_Grazing = 4,
&         NFlux_SlopFeed = 5,
&         NFlux_Pmort = 6,
&         NFlux_Zmetab = 7,
&         NFlux_Zmort = 8,
&         NFlux_Remind1 = 9,
&         NFlux_Remind2 = 10,
&         NumFluxTermsN = 10,

```

```

&      NumFluxTerms = 10,
&      NumGasExcTerms = 0,
&      NFlux_VSinkP1 = 1,
&      NFlux_VSinkD1 = 2,
&      NFlux_VSinkD2 = 3,
&      NumVSinkTerms = 3)
# elif defined BIO_BioEBUS

# ifdef NITROUS_OXIDE
  parameter (ntrc_bio=12,itrc_bio=itemp+ntrc_salt+ntrc_pas+1)
# else
  parameter (ntrc_bio=11,itrc_bio=itemp+ntrc_salt+ntrc_pas+1)
# endif

  parameter (iNO3=itrc_bio, iNO2=iNO3+1, iNH4=iNO3+2,
&      iPhy1=iNO3+3, iPhy2=iNO3+4,
&      iZoo1=iNO3+5, iZoo2=iNO3+6,
&      iDet1=iNO3+7, iDet2=iNO3+8,
&      iDON=iNO3+9, iO2=iNO3+10)

# ifdef NITROUS_OXIDE
  parameter (iN2O=iNO3+11)
# endif

  parameter( NFlux_lightlimitP1=1
&      , NFlux_lightlimitP2=2
&      , NFlux_templimitP1=3
&      , NFlux_templimitP2=4
&      , NFlux_NO3limitP1=5
&      , NFlux_NO2limitP1=6
&      , NFlux_NH4limitP1=7
&      , NFlux_NO3limitP2=8
&      , NFlux_NO2limitP2=9
&      , NFlux_NH4limitP2=10
&      , NFlux_ProdNO3P1=11
&      , NFlux_ProdNO3P2=12
&      , NFlux_ProdNO2P1=13
&      , NFlux_ProdNO2P2=14
&      , NFlux_Nitrif1=15
&      , NFlux_Nitrif2=16
&      , NFlux_ProdNH4P1=17
&      , NFlux_ProdNH4P2=18
&      , NFlux_P1Z1Grazing=19
&      , NFlux_P2Z1Grazing=20
&      , NFlux_P1mort=21
&      , NFlux_P2mort=22
&      , NFlux_P1Z2Grazing=23
&      , NFlux_P2Z2Grazing=24
&      , NFlux_Z1Z2Grazing=25
&      , NFlux_Z1metab=26
&      , NFlux_Z1mort=27
&      , NFlux_Z2metab=28
&      , NFlux_Z2mort=29
&      , NFlux_HydrolD1=30
&      , NFlux_ReminoxyD1=31
&      , NFlux_Denitr1D1=32
&      , NFlux_Denitr2D1=33
&      , NFlux_HydrolD2=34
&      , NFlux_ReminoxyD2=35
&      , NFlux_Denitr1D2=36

```

```

& , NFlux_Denitr2D2=37
& , NFlux_ReminoxyDON=38
& , NFlux_Denitr1DON=39
& , NFlux_Denitr2DON=40
& , NFlux_NO2anammox=41
& , NFlux_NH4anammox=42
# ifdef NITROUS_OXIDE
& , NFlux_paramN2O=43
& , NumFluxTermsN=NFlux_paramN2O
# else
& , NumFluxTermsN=NFlux_NH4anammox
# endif
& , NumFluxTerms=NumFluxTermsN
& , O2Flux_GasExc=1
# ifdef NITROUS_OXIDE
& , N2OFlux_GasExc=2
& , NumGasExcTerms=2
# else
& , NumGasExcTerms=1
# endif
& , NFlux_VSinkP2=1
& , NFlux_VSinkD1=2
& , NFlux_VSinkD2=3
& , NumVSinkTerms=3)
# endif /* ELODIE G */
/*-----*/

# if defined BIO_NChlPZD || defined BIO_N2ChlPZD2 || defined PISCES \
    || defined BIO_BioEBUS
# ifdef DIAGNOSTICS_BIO
parameter (ntrc_diabio=NumFluxTerms+
& NumGasExcTerms+NumVSinkTerms)
# else
parameter (ntrc_diabio=0)
# endif
# else
parameter (ntrc_diabio=0)
# endif
# else
parameter (ntrc_bio=0,ntrc_diabio=0)
# endif /* BIOLOGY */

!
! ===== SEDIMENTS =====
!
# ifdef SEDIMENT
!
! NST          Number of sediment (tracer) size classes
! NLAY        Number of layers in sediment bed
!
parameter (NST=2, NLAY=2)
parameter (ntrc_sed=NST,
& itr_c_sed=itemp+ntrc_salt+ntrc_pas+ntrc_bio+1)
parameter (isand=itr_c_sed, isilt=isand+1)
# else
parameter (ntrc_sed=0)
# endif

!

```

```

! === total number of tracers ===
!
    parameter (NT=itemp+ntrc_salt+ntrc_pas+ntrc_bio+ntrc_sed)

!
! === Diagnostics ===
!
# ifdef DIAGNOSTICS_TS
#   ifdef DIAGNOSTICS_TS_MLD
        parameter (ntrc_diats=15*NT)
#   else
        parameter (ntrc_diats=7*NT)
#   endif
# else
        parameter (ntrc_diats=0)
# endif
# ifdef DIAGNOSTICS_UV
        parameter (ntrc_diauv=16)
# else
        parameter (ntrc_diauv=0)
# endif
! I/O : flag for type sigma vertical transformation
! =====
# ifdef NEW_S_COORD
    real Vtransform
    parameter (Vtransform=2)
# else
    real Vtransform
    parameter (Vtransform=1)
# endif
# endif /*SOLVE3D */

```


APPENDIX B

POST-PROCESSING

B.1 Introduction

In this appendix is presented the code used for the sigma- to zeta vertical coordinates transformation and the visualization of the model's resulted data.

After a successful model's execution three new netcdf data files should generated:

- roms_avg.nc, containing instantaneous averages,
- roms_rst.nc, containing restart data, useful for model's future execution and
- roms_his.nc, which is the resulted data over every time-step.

The new data files are produced in sigma- vertical coordinates. In order to examine and to provide visual information for the included variables the sigma- coordinates should transformed to their 'physical' depth (zeta-) analogous.

For this purpose a new code has been developed in the NOAA FERRET¹ software, an interactive computer visualization and analysis environment designed mainly for oceanographers and meteorologists.

After the transformation procedure the new files

- roms_his_Z.nc, corresponding to roms_his.nc
- roms_avg_Z.nc, corresponding to roms_avg.nc,

will be available.

B.1.1 Sigma- to zeta- coordinates transformation codes

First part:

¹The author wish to acknowledge use of the Ferret program for analysis and graphics in this dissertation. Ferret is a product of NOAA's Pacific Marine Environmental Laboratory. (Information is available at <http://ferret.pmel.noaa.gov/Ferret/>)

```

! roms_sigma2z.jnl
! Ferret code
! Authorized by Andreas Nikolaidis, 2018
!
cancel mode upcase_out
set memory /size=790

use roms_his.nc ! <--1 (or roms_avg.nc)
use roms_grd.nc ! <--2

define axis/name=x1/units=degrees_east/from_data/x lon_rho[j=1,d=2]
define axis/name=y1/units=degrees_north/from_data/y lat_rho[i=1,d=2]
define axis/name=z1/units=m/from_data/z z[gz=s_rho] ! roms coordinate at rho point

define grid /x=x1/y=y1/z=z1 gridsq
let sg=z[g=gridsq]

let cs_rz=zsequence(cs_r[D=1])
let /title="Depth"/units="meters" depth = if mask_rho[D=1] then abs(h[D=2] * cs_rz)

define axis/z/unit=meters/depth zdepth={1,10,30,50,100,150,300,650,1000,1500,2500,2600}

let temperature=zaxreplace(temp[D=1],depth,z[gz=zdepth])

let salinity=zaxreplace(salt[D=1],depth,z[gz=zdepth])

let UonT=u[gxy=temp,D=1]
let u_vel=zaxreplace(UonT,depth,z[gz=zdepth])

let VonT=v[gxy=temp,D=1]
let v_vel=zaxreplace(VonT,depth,z[gz=zdepth])
!
set var/title="Velocity Zonal Component" /UNITS="m s-1" /BAD=-1.e+34 u_vel
set var/title="Velocity Meridional Component" /UNITS="m s-1" /BAD=-1.e+34 v_vel
set var/title="Temperature" /UNITS="degrees C" /BAD=-1.e+34 temperature
set var/title="Salinity" /UNITS="psu" /BAD=-1.e+34 salinity

let /title="Bottom Bathymetry" /units=m /BAD=-1.e+34 hb=if mask_rho[D=1] THEN h[GXY=temp[D=1],D=2]
let /title="Sea Level" /units=m /BAD=-1.e+34 eta_sl=if mask_rho[D=1] then zeta[GXY=temp[D=1],D=1]
!
say to z-levels
save/file=Z_file1.nc /nobounds u_vel,v_vel,temperature,salinity,hb,eta_sl
!
!cancel data/all
!go final_zeta

```

Second part:

```

! final_zeta.jnl
! Ferret code
! Authorized by Andreas Nikolaidis, 2018
!
cancel mode upcase_out
set memory /size=790

use Z_file1.nc ! <--1
use roms_grd.nc ! <--2
say to final file

```

```

define axis/name=x1/units=degrees_east/from_data/x lon_rho[j=1,d=2]
define axis/name=y1/units=degrees_north/from_data/y lat_rho[i=1,d=2]
define axis/t/units=hours/t=29-dec-2018:7-jan-2019:6 t1

define grid /x=x1/y=y1/t=t1 gridr

let temp=temperature[G=gridr@ASN,D=1]

let sal=salinity[G=gridr@ASN,D=1]

let u = u_vel[G=gridr@ASN,D=1]

let v = v_vel[G=gridr@ASN,D=1]
!
set var/title="Velocity Zonal Component" /UNITS="m s-1" /BAD=-1.e+34 u
set var/title="Velocity Meridional Component" /UNITS="m s-1" /BAD=-1.e+34 v
set var/title="Temperature" /UNITS="degrees C" /BAD=-1.e+34 temp
set var/title="Salinity" /UNITS="psu" /BAD=-1.e+34 sal

let /title="Bottom Bathymetry" /units=m /BAD=-1.e+34 h=hb[GXY=gridr@ASN,D=1]
let /title="Sea Level" /units=m /BAD=-1.e+34 zeta=eta_sl[GXY=gridr@ASN,D=1]
!
save/file=roms_his_Z.nc /nobounds u,v,temp,sal,h,zeta

```

REFERENCES

- [1] E. E. Agency, *State and pressures of the marine and coastal Mediterranean environment*. Office for Official Publ. of the European Comm., 1999.
- [2] E Akylas and M Tombrou, “Reconsidering and generalized interpolation between kansas-type formulae and free convection forms,” *Boundary-Layer Meteorol*, vol. 115, pp. 381–398, 2005.
- [3] E Akylas, M Tombrou, D Lalas, and S. Zilitinkevich, “Surface fluxes under shear-free convection,” *Quarterly Journal of the Royal Meteorological Society*, vol. 127, no. 574, pp. 1183–1197, 2001.
- [4] E Akylas, Y Tsakos, M Tombrou, and D. Lalas, “Considerations on minimum friction velocity,” *Quarterly Journal of the Royal Meteorological Society*, vol. 129, no. 591, pp. 1929–1943, 2003.
- [5] A. Alvera-Azcárate, A. Barth, J.-M. Beckers, and R. H. Weisberg, “Multivariate reconstruction of missing data in sea surface temperature, chlorophyll, and wind satellite fields,” *Journal of Geophysical Research: Oceans*, vol. 112, no. C3, 2007.
- [6] A. Alvera-Azcárate, A. Barth, M. Rixen, and J.-M. Beckers, “Reconstruction of incomplete oceanographic data sets using empirical orthogonal functions: Application to the adriatic sea surface temperature,” *Ocean Modelling*, vol. 9, no. 4, pp. 325–346, 2005.
- [7] A. Alvera-Azcárate, A. Barth, D. Sirjacobs, and J.-M. Beckers, “Enhancing temporal correlations in eof expansions for the reconstruction of missing data using dineof,” *Ocean Science*, vol. 5, no. 4, pp. 475–485, 2009.
- [8] A. Alvera-Azcárate, A. Barth, D. Sirjacobs, F. Lenartz, and J.-M. Beckers, “Data interpolating empirical orthogonal functions (dineof): A tool for geophysical data analyses,” *Mediterranean Marine Science*, vol. 12, no. 3, pp. 5–11, 2011.
- [9] A. Alvera-Azcárate, D. Sirjacobs, A. Barth, and J.-M. Beckers, “Outlier detection in satellite data using spatial coherence,” *Remote Sensing of Environment*, vol. 119, pp. 84–91, 2012.
- [10] J. D. Anderson and J Wendt, *Computational fluid dynamics*. Springer, 1995, vol. 206.
- [11] A Arakawa and V. Lamb, “Methods of computational physics,” *New York: Academic Press*, vol. 17, pp. 173–265, 1977.
- [12] H. G. Arango, *Model help:roms*, 2019.

- [13] Austides-Consulting, *GridBuilder MATLAB Toolbox*, Austides Consulting, 2014 <http://austides.com/downloads/>, (Accessed: December 2018), 2014.
- [14] J.-M. Beckers, A. Barth, and A. Alvera-Azcárate, “Dineof reconstruction of clouded images including error maps? application to the sea-surface temperature around corsican island,” *Ocean Science*, vol. 2, no. 2, pp. 183–199, 2006.
- [15] J.-M. Beckers and M Rixen, “Eof calculations and data filling from incomplete oceanographic datasets,” *Journal of Atmospheric and Oceanic Technology*, vol. 20, no. 12, pp. 1839–1856, 2003.
- [16] A. F. Blumberg and G. L. Mellor, “A description of a three-dimensional coastal ocean circulation model,” *Three-dimensional coastal ocean models*, pp. 1–16, 1987.
- [17] F. Bryan, “Parameter sensitivity of primitive equation ocean general circulation models,” *Journal of Physical Oceanography*, vol. 17, no. 7, pp. 970–985, 1987.
- [18] G. Cambon, P. Penven, P. Marchesiello, and L. Debreu, “Ocean model roms_agrif & processing-tools romstools,” *Practice presentation for ROMS_AGRIF*, vol. 0, 2011.
- [19] D. B. Chelton, R. A. DeSzoeke, M. G. Schlax, K. El Naggar, and N. Siwertz, “Geographical variability of the first baroclinic rossby radius of deformation,” *Journal of Physical Oceanography*, vol. 28, no. 3, pp. 433–460, 1998.
- [20] R. Courant, K. Friedrichs, and H. Lewy, “On the partial difference equations of mathematical physics,” *IBM journal of Research and Development*, vol. 11, no. 2, pp. 215–234, 1967.
- [21] L. Debreu, P. Marchesiello, and P. Penven, “Two ways embedding algorithms for a split-explicit free surface model,” *Ocean Modelling*, submitted, 2010.
- [22] L. Debreu, P. Marchesiello, P. Penven, and G. Cambon, “Two-way nesting in split-explicit ocean models: Algorithms, implementation and validation,” *Ocean Modelling*, vol. 49, pp. 1–21, 2012.
- [23] L. Debreu, C. Vouland, and E. Blayo, “Agrif: Adaptive grid refinement in fortran,” *Computers & Geosciences*, vol. 34, no. 1, pp. 8–13, 2008.
- [24] J. Du, X. G. Larsén, and R. Bolaños, “A coupled atmospheric and wave modeling system for storm simulations,” in *EWEA Offshore 2015 Conference*, European Wind Energy Association (EWEA), 2015.
- [25] P. Dyke, *Coastal and Shelf Sea Modelling*. Springer Science & Business Media, 2001, vol. 2.

- [26] T. El-Geziry and I. Bryden, “The circulation pattern in the mediterranean sea: Issues for modeller consideration,” *Journal of Operational Oceanography*, vol. 3, no. 2, pp. 39–46, 2010.
- [27] EuroGOOS, the European Global Ocean Observing System, *What is Operational Oceanography?* <http://eurogoos.eu/about-eurogoos/what-is-operational-oceanography/>, EuroGOOS, 2019.
- [28] GHER group of the University of Liège, *Daily DINEOF SST reconstruction in the Western Mediterranean*, http://www.dineof.net/DINEOF/dineof_all.html, GeoHydrodynamics and Environment Research group of the University of Liège, 2011.
- [29] C Giannakopoulos, P Good, K. Law, K.-Y. Wang, E Akylas, and A Koussis, “Rain-fall parameterization in an off-line chemical transport model,” *Atmospheric Science Letters*, vol. 5, no. 5, pp. 82–88, 2004.
- [30] S. M. Griffies, C. Böning, F. O. Bryan, E. P. Chassignet, R. Gerdes, H. Hasumi, A. Hirst, A.-M. Treguier, and D. Webb, “Developments in ocean climate modelling,” *Ocean Modelling*, vol. 2, no. 3-4, pp. 123–192, 2000.
- [31] K. S. Hedström, “Draft technical manual for a coupled sea-ice/ocean circulation model (version 2),” *US Department of the Interior Minerals Management Service Anchorage, Alaska (Contract No. M07PC13368)*, 2000.
- [32] ———, “Draft technical manual for a coupled sea-ice/ocean circulation model (version 3),” *US Department of the Interior Minerals Management Service Anchorage, Alaska (Contract No. M07PC13368)*, 2009.
- [33] R. Hetland, “*Coastal Ocean Dynamics*”. University of Texas A & M, May 2012.
- [34] C. Horton, M. Clifford, J. Schmitz, and L. H. Kantha, “A real-time oceanographic nowcast/forecast system for the mediterranean sea,” *Journal of Geophysical Research: Oceans*, vol. 102, no. C11, pp. 25 123–25 156, 1997.
- [35] L. H. Kantha and C. A. Clayson, *Numerical models of oceans and oceanic processes*. Elsevier, 2000, vol. 66.
- [36] R. Lehoucq, D. Sorensen, and C Yang, “Arpack users’ guide: Solution of large scale eigenvalue problems with implicitly restarted arnoldi methods.,” *Software Environ. Tools*, vol. 6, 1997.
- [37] G. Madec *et al.*, “Nemo ocean engine,” 2015.
- [38] J Marshall and R. Plumb, *Atmosphere, ocean, and climate dynamics: An introductory text*, vol. v. 93, 2008.

- [39] Marta-Almeida, *okean package*, okean Python package, 2018 <https://github.com/martalmeida/okean>, (Accessed: June 2018), 2018.
- [40] M. Marta-Almeida, M. Ruiz-Villarreal, P. Otero, M. Cobas, A. Peliz, R. Nolasco, M. Cirano, and J. Pereira, “Oof-e: A python engine for automating regional and coastal ocean forecasts,” *Environmental modelling & software*, vol. 26, no. 5, pp. 680–682, 2011.
- [41] Y. Masumoto, H. Sasaki, T. Kagimoto, N. Komori, A. Ishida, Y. Sasai, T. Miyama, T. Motoi, H. Mitsudera, K. Takahashi, *et al.*, “A fifty-year eddy-resolving simulation of the world ocean: Preliminary outcomes of ofes (ogcm for the earth simulator),” *J. Earth Simulator*, vol. 1, pp. 35–56, 2004.
- [42] K. McGuffie and A. Henderson-Sellers, *The climate modelling primer*. John Wiley & Sons, 2014.
- [43] G. L. Mellor, *Users guide for a three dimensional, primitive equation, numerical ocean model*. Program in Atmospheric and Oceanic Sciences, Princeton University Princeton, NJ, 1998.
- [44] Microsoft, *MICROSOFT Corporation, .NET*, <http://www.microsoft.com/net/>, Microsoft, 2017.
- [45] T. N. Miles, R. He, and M. Li, “Characterizing the south atlantic bight seasonal variability and cold-water event in 2003 using a daily cloud-free sst and chlorophyll analysis,” *Geophysical Research Letters*, vol. 36, no. 2, 2009.
- [46] C Millot and I Taupier-Letage, “Additional evidence of liw entrainment across the algerian subbasin by mesoscale eddies and not by a permanent westward flow,” *Progress in Oceanography*, vol. 66, no. 2-4, pp. 231–250, 2005.
- [47] B. B. Nardelli, C Tronconi, A Pisano, and R Santoleri, “High and ultra-high resolution processing of satellite sea surface temperature data over southern european seas in the framework of myocean project,” *Remote Sensing of Environment*, vol. 129, pp. 1–16, 2013.
- [48] B. Nechad, A. Alvera-Azcaràte, K. Ruddick, and N. Greenwood, “Reconstruction of modis total suspended matter time series maps by dineof and validation with autonomous platform data,” *Ocean Dynamics*, vol. 61, no. 8, pp. 1205–1214, 2011.
- [49] A. Nikolaidis, G. Georgiou, D. Hadjimitsis, and E. Akylas, “Applying dineof algorithm on cloudy sea-surface temperature satellite data over the eastern mediterranean sea,” in *First International Conference on Remote Sensing and Geoinformation of the Environment (RSCy2013)*, International Society for Optics and Photonics, vol. 8795, 2013, p. 87950L.
- [50] A. Nikolaidis, G. C. Georgiou, D. Hadjimitsis, and E. Akylas, “Filling in missing sea-surface temperature satellite data over the eastern mediterranean sea using the

- dineof algorithm,” *Central European Journal of Geosciences*, vol. 6, no. 1, pp. 27–41, 2014.
- [51] A. Nikolaidis, S. Stylianou, G. Georgiou, D. Hadjimitsis, and E. Akylas, “Application of roms-agrif over levantine and cyprus seas.” in *EGU General Assembly Conference Abstracts*, vol. 21, 2019, p. 13 889.
- [52] C. G. Nittis Konstantinos, *Introductory notes on Operational Oceanography*. University of Aegean, Department of Marine Science, 2005.
- [53] L.-Y. Oey, “An ogcm with movable land–sea boundaries,” *Ocean Modelling*, vol. 13, no. 2, pp. 176–195, 2006.
- [54] S. Palladini, “Arcobjects development in zone design using visual basic for applications,” in *International Conference on Computational Science and Its Applications*, Springer, 2004, pp. 1057–1068.
- [55] J. P. Peixoto and A. H. Oort, “Physics of climate, american institute of physics,” *New York*, p. 520, 1992.
- [56] P. Penven, G. Cambon, T.-A. Tan, P. Marchesiello, and L. Debreu, “Roms agrif/romstools user’s guide,” *Institut de Recherche pour le Developpement, Dunkerque*, 2010.
- [57] P. Penven, L. Debreu, P. Marchesiello, and J. C. McWilliams, “Evaluation and application of the roms 1-way embedding procedure to the central california upwelling system,” *Ocean Modelling*, vol. 12, no. 1-2, pp. 157–187, 2006.
- [58] P. Penven, P. Marchesiello, L. Debreu, and J. Lefèvre, “Software tools for pre- and post-processing of oceanic regional simulations,” *Environmental Modelling & Software*, vol. 23, no. 5, pp. 660–662, 2008.
- [59] P. Penven and T.-A. Tan, “Romstools user’s guide,” *Rapport techn., IRD and LPO/UBO, Laboratoire de Physique des Oceans, Universite de Bretagne Occidentale/UFR Sciences*, vol. 0, 2003.
- [60] N Pinardi and G Coppini, “Preface” operational oceanography in the mediterranean sea: The second stage of development”, *Ocean Science*, vol. 6, no. 1, pp. 263–267, 2010.
- [61] A. R. Robinson, W. G. Leslie, A. Theocharis, and A. Lascaratos, “Mediterranean sea circulation,” *Ocean currents: a derivative of the Encyclopedia of Ocean Sciences*, pp. 1689–1705, 2001.
- [62] C. Rossby, “The atmosphere and the sea in motion,” *Current problems in meteorology*, vol. 1959, pp. 9–50, 1959.

- [63] W. B. Ryan, S. M. Carbotte, J. O. Coplan, S. O'Hara, A. Melkonian, R. Arko, R. A. Weissel, V. Ferrini, A. Goodwillie, F. Nitsche, *et al.*, "Global multi-resolution topography synthesis," *Geochemistry, Geophysics, Geosystems*, vol. 10, no. 3, 2009.
- [64] A. Schiller and G. B. Brassington, *Operational oceanography in the 21st century*. Springer Science & Business Media, 2011.
- [65] A. Schiller, B. Mourre, Y. Drillet, and G. Brassington, "Overview of operational oceanography," *New Frontiers in operational oceanography*, pp. 1–26, 2018.
- [66] U Schulzweida, L Kornblueh, and R Quast, "Climate data operators," *Max-Planck-Institute for Meteorology, Hamburg and <http://www.mpimet.mpg.de/~cdo>*, 2004.
- [67] A. F. Shchepetkin and J. C. McWilliams, "The regional oceanic modeling system (roms): A split-explicit, free-surface, topography-following-coordinate oceanic model," *Ocean modelling*, vol. 9, no. 4, pp. 347–404, 2005.
- [68] M. D. Sikiric, A. Roland, I. Janekovic, I. Tomazic, and M. Kuzmic, "Coupling of the regional ocean modeling system (roms) and wind wave model," *Ocean Modelling*, vol. 72, pp. 59–73, 2013.
- [69] D. Sirjacobs, A. Alvera-Azcárate, A. Barth, G. Lacroix, Y. Park, B. Nechad, K. Ruddick, and J.-M. Beckers, "Cloud filling of ocean colour and sea surface temperature remote sensing products over the southern north sea by the data interpolating empirical orthogonal functions methodology," *Journal of Sea Research*, vol. 65, no. 1, pp. 114–130, 2011.
- [70] Y. Song and D. Haidvogel, "A semi-implicit ocean circulation model using a generalized topography-following coordinate system," *Journal of Computational Physics*, vol. 115, no. 1, pp. 228–244, 1994.
- [71] R. H. Stewart, *Introduction to physical oceanography*. Texas A & M University College Station, 2008.
- [72] L. D. Talley, *Descriptive physical oceanography: an introduction*. Academic press, 2011.
- [73] D Tillinger and A. Gordon, "Transport weighted temperature and internal energy transport of the indonesian throughflow," *Dynamics of Atmospheres and Oceans*, vol. 50, no. 2, pp. 224–232, 2010.
- [74] J. Toggweiler and B Samuels, "On the ocean's large-scale circulation near the limit of no vertical mixing," *Journal of Physical Oceanography*, vol. 28, no. 9, pp. 1832–1852, 1998.
- [75] C. Troupin, A. Barth, D. Sirjacobs, M. Ouberdous, J.-M. Brankart, P. Brasseur, M. Rixen, A. Alvera-Azcárate, M. Belounis, A. Capet, *et al.*, "Generation of analysis

- and consistent error fields using the data interpolating variational analysis (diva),” *Ocean Modelling*, vol. 52, pp. 90–101, 2012.
- [76] UNEP/MAP, *State of the mediterranean marine and coastal environment*, 2012.
- [77] G. Van Rossum and F. L. Drake Jr, *Python tutorial*. Centrum voor Wiskunde en Informatica Amsterdam, The Netherlands, 1995.
- [78] Y. Wang and D. Liu, “Reconstruction of satellite chlorophyll-a data using a modified dineof method: A case study in the bohai and yellow seas, china,” *International journal of remote sensing*, vol. 35, no. 1, pp. 204–217, 2014.
- [79] J. C. Warner, C. R. Sherwood, R. P. Signell, C. K. Harris, and H. G. Arango, “Development of a three-dimensional, regional, coupled wave, current, and sediment-transport model,” *Computers & Geosciences*, vol. 34, no. 10, pp. 1284–1306, 2008.
- [80] P. Wessel and W. H. Smith, “New, improved version of generic mapping tools released,” *Eos, Transactions American Geophysical Union*, vol. 79, no. 47, pp. 579–579, 1998.
- [81] C. S. Zender, “Analysis of self-describing gridded geoscience data with netcdf operators (nco),” *Environmental Modelling & Software*, vol. 23, no. 10, pp. 1338–1342, 2008.
- [82] V Zervakis, *Introduction to Dynamic Oceanography – Part A*. University of Aegean, Lecture notes, Apr. 2007.
- [83] V. Zervakis, *Introduction to Hydrodynamics with Oceanographic applications*. University of Aegean, Lecture notes, Oct. 2005.
- [84] G Zodiatis, R Lardner, D. Hayes, G Georgiou, S Sofianos, N Skliris, and A Lascaratos, “Operational ocean forecasting in the eastern mediterranean: Implementation and evaluation,” *Ocean Science (OS)*, vol. 4, no. 1, pp. 31–47, 2008.
- [85] G. Zodiatis, G. Galanis, G. Kallos, A. Nikolaidis, C. Kalogeri, A. Liakatas, and S. Stylianou, “The impact of sea surface currents in wave power potential modeling,” *Ocean Dynamics*, vol. 65, no. 11, pp. 1547–1565, 2015.
- [86] G. Zodiatis, G. Galanis, A. Nikolaidis, C. Kalogeri, D. Hayes, G. C. Georgiou, P. C. Chu, and G. Kallos, “Wave energy potential in the eastern mediterranean levantine basin. an integrated 10-year study,” *Renewable energy*, vol. 69, pp. 311–323, 2014.
- [87] G. Zodiatis, D. Hayes, I. Gertman, P.-M. Poulain, M. Menna, and A. Nikolaidis, “On the main flow features of the se levantine (cybo cruises 1995-2012),” in *EGU General Assembly Conference Abstracts*, vol. 15, 2013.
- [88] G. Zodiatis, R. Lardner, G. Georgiou, E. Demirov, G. Manzella, and N. Pinardi, “An operational european global ocean observing system for the eastern mediter-

ranean levantine basin: The cyprus coastal ocean forecasting and observing system,” *Marine Technology Society Journal*, vol. 37, no. 3, pp. 115–123, 2003.

- [89] G. Zodiatis, R. Lardner, D. R. Hayes, and G. Georgiou, “An operational oceanographic forecasting and observing system for the eastern mediterranean levantine basin: The cyprus coastal ocean forecasting and observing system,” *European Operational Oceanography: Present and Future*, vol. 3, p. 591, 2006.